博士論文

A global assessment of solar photovoltaic resource and energy–water nexus for future sustainability

(太陽光発電資源の全球評価及び持続可能な将来に向けたエネルギー・水ネクサスに関する研究)

ムスタジャブ アリ

A global assessment of solar photovoltaic resource and energy–water nexus for future sustainability

(太陽光発電資源の全球評価及び持続可能な将来に向けたエネルギー・水ネクサスに関する研究)

Mustajab Ali

A dissertation submitted to the University of Tokyo in partial fulfillment of the requirements for the degree of Doctor of Philosophy

Examination Committee

Project Associate Professor Hyungjun Kim
Professor Taikan Oki
Professor Wataru Takeuchi
Project Professor Yoshihide Sekimoto
Project Professor Akiyuki Kawasaki
Associate Professor Shinichiro Fujimori

Department of Civil Engineering
Graduate School of Engineering
The University of Tokyo
Tokyo, Japan

March 2021

Abstract

A global assessment of solar photovoltaic resource and energy–water nexus for future sustainability

Mustajab Ali

Energy and water are among the essential needs of human beings and vital for sustainable development. Both energy and water are highly interconnected: we use water for energy and we need energy for water. Failure to consider the energy and water nexus (E–W nexus) may give rise to improper planning and resource allocation as constraints of one resource affects the other. The energy in the shape of solar photovoltaic (PV) is linked with the cooling water withdrawals (CWW), the water used to cool the Thermoelectric Power Plants (TEPPs) while generating the electricity. The actual solar PV resource is calculated to support the required electricity on a global scale which will potentially result in minimizing the usage of freshwater quantity for cooling TEPPs and overcoming the future freshwater scarcity under changing climate and socio–economic scenarios.

As discussed above, this study mainly consists of three parts, solar PV resource mapping, water withdrawals by TEPPS to generate electricity, and solar PV potential to support such demands on the CWW sides from 2015 to 2100. First, global solar PV resource maps under different environments are produced using the solar irradiance available near the earth's surface and all limiting factors (temperature, dust, and snow) acting together. Most of the previous studies considered just a single or few limiting factors without taking into account the individual or combined effects of meteorological factors that do affect the solar PV performances based on local climatic and environmental conditions. Some studies which included the combined negative effects from the above parameters are just for a small area or region for a certain period. Also, our solar PV resource maps are harmonized in terms of spatial–temporal resolution, datasets used, and approaches involved. Moreover, exploring the EW–nexus, considering solar PV as a vital energy resource has not yet been explored at a global scale. This global analysis is performed for 2050 and by the end of the 21st century by considering climate changes in terms of Representative Concentration Pathways (RCP2.6, RCP4.5, and RCP6.0) and novel socio–

economic scenarios, Shared Socioeconomic Pathways (SSP1, SSP2, and SSP3). Solar PV cost analysis for the present is also included for both centralized and decentralized schemes.

Second, this study deals with the freshwater used by TEPPs while generating electricity. This component is a vital part of industrial water withdrawals (IWW), in addition to the industrial manufacturing water. This extracted water is a kind of pressure on the available freshwater resources as most of it is not available to the downstream areas because of being polluted and raised temperatures. For this, country–wise electricity generation data for different sources (coal, oil, gas, nuclear, and biomass) are used to calculate regional electricity consumption. Then cooling technologies shares, once–through and wet tower type for each region are applied to the regional electricity values. These values are finally multiplied with water use intensity (WUI) to have the final water withdrawals. Some countries use seawater to cool the power plants, this share is subtracted from the total withdrawals to have the freshwater withdrawals. For future analysis, cooling technology like carbon capture and storage (CCS) which uses more water is also considered to avoid any underestimation. Such global analysis provides a bigger picture of freshwater withdrawals and it can be seen that which part of the world is using maximum or minimum water for electricity generation. Furthermore, future analysis will show the changes in CWW due to the technology shifts and efficiency changes for various SSP and RCP scenarios.

Lastly, solar PV resource maps are used to support the regional electricity demands, and to look for potential/additional water saved from cooling the TEPPs while generating the required electricity. Globally 17 regions are formed based upon the classifications available with the Asia–Pacific Integrated Model (AIM). In the beginning, three probable scenarios (2%, 3%, and 5%) for solar PV input to the total electricity are devised for the present to see how much area for the provision of solar PV in each region is needed to support such electricity demand scenarios. Later, based upon the country policy to decarbonizes and solar PV recent growth and technological development, three future scenarios LOW, MEDIUM, and HIGH are developed for 2050 and 2100 to see how much solar PV area is needed to support such electricity demand and how helpful it would be in achieving energy and freshwater sustainability in the future. Besides the provision of neat and clean electricity, such scenarios developed under the roof of EW–nexus will be helpful in saving a big population from explicit water scarcity. Finally,

considering the fact that megacities need the maximum electricity and are being able to offer sufficient roof–top area as well, solar electric footprints for world megacities are estimated.

This study looks for answering the following questions: What are the factors affecting the performance of solar PV yield and how much is the contribution of each individual or combines one? Which part of the world has the maximum and which one has the minimum solar PV resource available? How our model performances are in comparison to the observation and how uncertain are the results while considering various uncertainties involved from changes in fixation angles, material types, cell efficiencies, and data sets? What are the potential areas for centralized and decentralized solar PV schemes in the context of the demand and supply–side relationship? How much are the electricity demands of urban areas (megacities) and is the roof–top scheme a viable option to support their growing electricity demands? How the future technology shifts and efficiency developments will change the IWW under SSP and RCP scenarios? Which areas would be under high to severe freshwater stress and how much could be the freshwater savings for solar PV enhanced (PV_{enh}) scenarios. It includes several kinds of data sets from satellites, ground stations, and Integrated Assessment Model (IAM) to respond to these questions. The purpose of the current study is to estimate the global solar PV resource while considering meteorological and geomorphologic factors and linking them to the CWW through EW–nexus to see the reduction in the global freshwater scarcity under various uncertainties (scenarios) to lead to sustainability.

The light energy coming from the sun is converted into electrical energy using the solar PV modules arranged in the shape of an array. Downward shortwave radiation (SWR) is the main component needed for the generation of electricity. Bias corrected data for SWR near the earth surface is obtained from the Global Soil Wetness Project (GSWP3). We applied three kinds of efficiency corrections to the solar cell namely temperature, dust, and snow that do affect the solar PV yield. For temperature corrections, surface temperature (2m), wind speed (10m), and SWR obtained from GSWP3 is used to calculate the PV module as well as PV cell temperature. Aerosol Optical Thickness (AOT) from NASA Terra MODIS and loss factor for dust for optimum tilt–angles are processed as a proxy of dust deposition and natural cleansing through precipitation are also seen using the precipitation data from GSWP3. Then, snow water equivalent (SWE) from National Snow and Ice Data Centre (nsidc) and snow cover fraction

(SCF) from NASA Terra MODIS are used to calculate the snow depths which block the incoming radiation and reduces the transmissibility. Geomorphologic components like optimum tilt angles are also incorporated to see the final power output from solar PV at a global scale.

A global power plants database provided by the World Resources Institute (WRI, 2019) consisting of country scale data is used to calculate the electricity generation. Country scale electricity data is converted to 17 regions globally with the help of the AIM regional raster map. Cooling technology shares available with the past studies are incorporated to know the cooling technology distribution for each region for a variety of power plants. Using the WUI for different cooling types, and subtracting seawater from the total water withdrawn, the total freshwater withdrawal for cooling TEPPs are estimated for each region. Then, using the regional electricity demands and solar PV resources, the area needed by solar PV for each region is estimated for all three PV_{enh} scenarios for current. Current and future freshwater scarcity is assessed based upon a prominent water scarcity index; Withdrawal to availability (WTA) to know the population under various stresses situations. This analysis is extended for 2050 and up to the end of 21st century for various SSP and RCP scenario using the data sets from The Inter–Sectoral Impact Model Intercomparison Project–2b (ISIMIP–2b). Freshwater savings for every region for all PV enhanced scenarios are later worked out for 2050 and 2100 as well. From a demand point of view, dense urban clusters (megacities) requiring more electricity due to bigger populations and economic developments were also assessed. Using the gridded GDP, megacities electricity demands are calculated by downscaling the AIM regional electricity values. Lastly, the area available from the roof–top of megacities for 2010 is estimated using the dataset from Atlas of Urban Expansion.

The novelty of this study is in multiple ways: the development of global solar PV resource under different environment using multiple remote sensing and in–situ data sets; analysis is done at a global scale considering the meteorological and geomorphologic parameters; calculation of current and future CWW while generating the required electricity; present and anticipated freshwater scarcity mapping for various stress conditions; water available for each region while replacing TEPPs with solar PV scheme for various RCP & SSP scenarios and cost estimates of centralized and decentralized solar PV schemes. Based on our validations, we suppose that our methodology to calculate the solar PV resource is precise and could be helpful for policymakers

and planners for large–scale (Solar Parks) as well as small–scale (households) level globally. Such estimates are also equally important for several global models like integrated assessment models (IAM) and energy economy models etc. In addition, this study has a worthwhile implication for the IWW side to help alleviating water scarcity, especially in water–scarce regions.

Globally, the actual mean seasonal and annual solar PV resources were estimated using the local environment conditions and approximated solar cell efficiency of 15%. We used four seasons March–May (MAM), June–August (JJA), September–November (SON), and December–February (DJF) in our analysis. Results revealed that maximum seasonal losses (~90%) are from snow covers during DJF for the upper Northern Hemisphere, while, annual snow losses are recorded as 20.1% maximum. Likewise, severe dust effects causing a reduction of up to 11.5% of power output are seen for Sub–Saharan Africa for DJF. While the annual maximum dusts loss is recorded as 5.90% for the same region. It was also observed that precipitation was not enough to clean the accumulated dust for most regions. Therefore, we suggested the physical cleaning of the solar PV modules in severely dust–affected regions. Temperature reductions are recorded lowest among all limiting factors. The seasonal and annual losses are recorded as 8.75% and 5.23% respectively for Sub–Saharan Africa. Lastly, tilt angles are also shown to limit (1~8%) the solar PV yield depending upon the variation in the fixation angles. Our snow model shows some limitation in terms of over–corrections in some regions like Europe, Japan, and Northern America, where most of the power plants are affected by snow covers. The validations of our results are done with the actual observations available with the solar–wiki. The data set contains approximately 1374 sites globally. The high value for the coefficient of determination (R^2= 0.787) shows better performance of our models. In addition, we also performed the regional validation where most of the regions show very high values (R^2 >0.80).

The CWW by the TEPPs is calculated based upon the electricity generation of each power plant type in each region. Regional WTA then defines the water scarcity situations in each region of the world. It is seen that some parts of regions like China, India, The Middle East, and the Rest of Latin America is currently facing Severe Stress due to less available water resources for the mighty population. The number of peoples affected in these areas is 235.5mill, 140.2mill,

78.59mill, and 77.59mill respectively. Similar regions have 120.7mill, 70.8mill, 18.2mill, and 25.59mill number of people under High Stress situation as well. Whereas, some parts of USA, Europe, South Asia, Southern Africa and Southeast Asia are under medium and low stresses. For 2050, areas in the Rest of Latin America, China, India, and The Middle East are supposed to have a maximum population under absolute scarcity for SSP3–RCP6.0 scenario. Whereas, the impact is a bit lower for the other two scenarios. Likewise, for 2100, Sub–Saharan Africa, a part of South Africa, The Middle East, South Asia and a portion of China have witnessed a larger population under Severe Stress condition for SSP3–RCP6.0 scenario. It is also witnessed that in the areas under Severe Stress, TEPPs are drawing reasonable freshwater, which is adding to the water scarcity and unsustainability situation.

With the massive potential to offset conventional energy system, solar PV is thought to replace a number of existing TEPPs in the future. To see the potential benefits in terms of freshwater scarcity and the number of people saved from water scarcity, PV_{enh} scenarios are applied and PV sitting area required to generate needed electricity for 2050 and 2100 is also calculated. Later, freshwater savings for 2050 and 2100 are worked out after subtracting the withdrawals for PV_{enh} scenarios and business as a usual case (BAU). Results have shown maximum savings for the SSP2–RCP4.5 MEDIUM scenario for regions like the China, USA, Europe, former USSR, and Rest of Southeast Asia which could lead to improve anticipated water scarcity and will help to lower the numbers of affected population in such regions. Maximum freshwater saving of 198.18km^3, 129.38 km^3, 107.89 km^3, 79.59 km^3, and 59.53 km^3, for 2050 and 289.13km^3, 171.89 km^3, 256.06 km^3, 270.68km^3, and 166.87km^3 are witnessed for these regions respectively. In addition to that, Solar electric footprints of megacities are calculated where cities like Shanghai, Guangzhou, Moscow, and New York needs bigger areas for solar PV sitting to fulfil their massive electricity demands. These are calculated as 1383 km^2, 878 km^2, 787 km^2 and 759 km^2 for Shanghai, Guangzhou, Moscow, and New York respectively. Then, the suitable roof–top area of each megacity is estimated to know the area available for solar PV fixing. 11 out of 24 megacities are capable of producing all electricity demand through solar PV for 2010, while the rest can generate ~40% of the needed electricity. Finally, cost analysis have shown that regions like the Western US, Sub–Saharan Africa, the Middle East, Western China

and Australia has lower PV cost (<0.08USD/KWh) for centralized scheme, while such costs are ~5–12% higher for a decentralized systems.

This study has shown that the solar PV scheme has a great potential to offset a considerable amount of renewable electricity to the system and can help to minimize freshwater scarcity. Currently, even with a mere input in the total system, solar PV is proven to be a promising resource due to improving technology, decreasing costs, and being neat and clean. This eco–friendly resource if utilized in a proper way could lead to sustainable development in the region in terms of energy and water. In addition, it will help in achieving the United Nations Sustainable Development Goal No. 6–Water and Sanitation, Goal No. 7–Clean and Affordable Energy, Goal No. 11–Sustainable Cities and Communities and Goal No. 13–Climate Action.

Acknowledgment

Grateful to Allah almighty for his countless blessings and for providing me this great opportunity to do my Ph.D. from the University of Tokyo, Japan. I want to express my sincere gratitude to my supervisor Project Assoc. Prof. Hyungjun Kim for his continuous support and guidance through my doctoral degree course at The University of Tokyo. His patience, inspiration, and immense knowledge from the very beginning have fostered my research attitude and approach.

I am also grateful to all of my Ph.D. committee members, Prof. Taikan Oki, Prof. Wataru Takeuchi, Project Prof. Yoshihide Sekimoto, Project Prof. Akiyuki Kawasaki, and Assoc. Prof. Shinichiro Fujimori for polishing my research with their valuable comments and nice suggestions. It was excellent to work with all of them.

I may not be here at The University of Tokyo, Japan if I am not provided with financial support from my employer, Mirpur University of Science and Technology, (MUST) Mirpur under the faculty development program led by The Higher Commission of Pakistan (HEC). It was an honourable opportunity for me to empower myself through one of the top global research groups in the water sector. I am also grateful to all the members of the Oki lab for all their support and guidance. Their motivation and encouragement provided my days a bright colour of joy and happiness. Their hard-working and gifted talents motivated me to work harder.

I would not be able to continue my doctoral course if I had not always been supported by my family, especially my mother, my wife, my brother and sisters, and my beloved daughters, Safa and Marva. Their love and kindness were a kind of inspiration to my higher studies abroad. There were several moments that they helped and guided me to make the right decision. I am also thankful to my grandparents, in-laws, and relatives for their support throughout the study. I shall always remain indebted to my Pakistani fellows and friends at The University of Tokyo as well as those in Japan and in my home country. They enabled me to make my dreams come true. This thesis has been made possible by collective day-to-day support from my family and all of my friends, and colleagues. I sincerely thank each one of them from the bottom of my heart.

Table of Contents

Chapter 1: INTRODUCTION…..... 23
1. Energy and sustainable development...…..... 23
1.1 Renewables…..... 26
1.2 Solar energy and Photovoltaic……..……..... 27
1.2.1 Technical potential …….……..... 29
1.2.2 Meteorological factors affecting solar PV cell efficiency……..…… 29
1.2.2.1 Impact of temperature increase on solar PV cell efficiency……. 30
1.2.2.2 Impact of dust deposition on solar PV cell efficiency...…...……31
1.2.2.3 Impact of snow covers on solar PV cell efficiency……. 33
1.2.3 Geomorphologic analysis on solar PV Performance……... 34
1.2.3.1 Effect of PV module tilt–angle on energy yields……..... 34
1.2.4 Economic analysis of solar PV.……..……..... 36
1.2.4.1 Solar PV schemes.……..……..... 36
1.3 Water…..... 38
1.3.1 Components of water withdrawals…….....…..... 39
1.3.1.1 Irrigation water……..39
1.3.1.2 Domestic water ……40
1.3.1.3 Industrial water…….……40
1.3.2 Types of cooling…….……..... 41
1.3.2.1 Once–through cooling…….…….....41
1.3.2.2 Wet tower cooling…….……..... 42
1.3.2.3 Dry cooling…….……..... 43
1.3.3. Water scarcity…..... 44
1.3.3.1. Water Stress Indicators…….……..... 45
1.3.3.2. Cooling water required by thermoelectric power plants for electricity production…….…… 46
1.3.3.3. Freshwater scarcity by thermoelectric power plants ……..…… 46
1.4 Energy–Water nexus…….……..... 47
1.4.1 Energy in water: …….……..... 48
1.4.2 Water in energy: …….……..... 48

1.4.3 Energy–water nexus for sustainable development……... 49
1.5 Electricity demand and supply–side relationship……..... 51
1.5.1 Megacities and sustainable development…..... 52
1.5.2 Shared Socio–economic and climate change scenarios……53
1.6 Motivation of this study..... 54
1.7 Objective of this study..... 55
1.8 Novelty of this study 55

Chapter 2: METHODOLOGY 56
2.1 Solar PV resources mapping ……..... 57
2.1.1 Data and methods……..... 57
2.1.2 Data description ……..... 58
2.2 Decrease in solar PV cell efficiency due to meteorological limiting factors..... 59
2.2.1 Decrease in solar PV cell efficiency due to temperature change.....,,,..... 59
2.2.1.1 Solar PV module temperature (T_{mod})..……..... 59
2.2.1.2 Solar PV cell temperature (T_{cell})……..... 60
2.2.2 Decrease in solar PV cell efficiency due to dust deposition…….... 62
2.2.3 Decrease in solar PV cell efficiency due to snow covers …….....63
2.2.3.1 Snow depth calculations..... 63
2.2.3.2 Snow melts from solar PV panels.....65
2.2.3.3 Decrease in solar PV cell efficiency..... 66
2.2.4 Final solar PV cell efficiency..... 67
2.3 Effect of geomorphologic parameter on solar PV resource..... 68
2.3.1 Variations in solar PV module tilt–angle 68
2.4 Performance ratios 68
2.5 Final solar PV resources..... 69
2.6 Solar PV economic analysis..... 69
2.6.1 Suitable area for solar PV.....70
2.6.1.1 Suitability factor for centralized schemes..... 70
2.6.1.2 Suitability factor for decentralized schemes.....72
2.6.2 Cost estimation of solar PV electricity..... 74

2.7 Water scarcity assessments..... 76
2.7.1 Withdrawal–to–availability..... 76
2.8 Electricity generation..... 77
2.8.1 Cooling technology shares..... 79
2.8.2 Water use intensity..... 80
2.8.3 Final Fresh water withdrawals..... 81
2.9 Energy–Water nexus (EW–nexus)..... 83
2.9.1 New input scenarios for solar PV energy 83
2.9.1.1 Future solar PV resources for various SSP and RCP scenarios……84
2.9.2 Revised electricity generation by TEPPs and water withdrawals for PV_{enh} scenarios.....84
2.9.3 Electricity demand……..... 86
2.9.3.1 Global gridded electricity demand maps……..…… 86
2.9.3.2 Electricity demand of world megacities ……..…....87
2.9.3.3 Electricity demand flow of megacities for 21st century ……...88
2.9.3.4 Solar electric footprints of megacities ……. 88
2.9.3.5 Roof top areas available with megacities…….……. 88

3. RESULTS AND DISCUSSIONS..... 90
3. ENERGY..... 90

3.1 Temperature effects on solar PV efficiency reductions..... 90
3.1.1Solar PV module temperature T_m……..... 90
3.1.2 Solar PV cell temperature T_c ……..... 90
3.1.3 Solar PV cell efficiency reductions due to the affect of temperature rise..... 92
3.2 Dust effects on solar PV efficiency reduction……..... 93
3.2.1 Loss factor for dust reduction ($K_{L)}$…….……..... 93
3.2.2 Solar PV cell efficiency reductions due to the affect of dust……..... 94
3.3 Snow effects on solar PV efficiency reductions..... 96
3.3.1 Seasonal snow depths..... 96
3.3.2 Solar PV cell efficiency reductions due to the affect of snow covers..... 97

3.4 Effects of geomorphologic parameter on Solar PV power output..... 98
3.4.1 Optimal Tilt angles 98
3.4.2 Effective power ratio..... 99
3.5 Effective power (P_{eff}) 100
3.5.1 Performance ratio.....100
3.6 Final solar PV resource.....101
3.6.1 Actual estimated seasonal solar PV resource..... 101
3.6.2 Actual estimated annual solar PV resource..... 102
3.7 Validation of final power output..... 103
3.7.1 Global solar power plants output comparison for regions..... 103
3.7.2 Global solar power plants output.....104
3.8 Uncertainty analysis.....107
3.8.1 Solar PV cell type.....107
3.8.2 Solar PV cell efficiency…….....107
3.8.3 Changes in Solar PV optimum tilt–angles..... 108
3.8.4 Data source.....108

3.9 The economic analysis of solar PV electricity.....111
3.9.1 The cost of PV electricity for centralized scheme 111
3.9.2 Cost supply curves of PV electricity for centralized scheme.....111
3.9.3 The cost of PV electricity for decentralized scheme 112
3.10. Summary and conclusions for solar PV cost analysis…….....113

4. RESULTS AND DISCUSSIONS..... 115
4. WATER.....115
4.1 Water Scarcity…….....115
4.1.1 WTA for H08 ……..... 115
4.1.2 WTA for WATERGAP2……..... 116
4.1.3 People under various stress limits ……..... 116
4.1.3.1 H08 ……..…116
4.1.3.2 Percentage population under stress levels for H08……..……117
4.1.3.3 WATERGAP2…… 118

4.1.3.4 Percentage population under stress levels for WATERGAP2……119
4.2 Electricity generation…….....121

4.2.1 Thermoelectric Power Plants …….……..…….....121
4.2.2 Electricity generation demands by TEPPs.....121
4.2.3 Comparison of electricity estimates with literature…….....122

4.2 Water withdrawals…….....123
4.2.1 Cooling water for TEPPs……..... 123
4.2.2 Comparison of water withdrawal estimates with literature……..... 123

5. RESULTS AND DISCUSSIONS..... 125

5. ENERGY–WATER–NEXUS (EW–nexus) FOR FUTURE SUSTAINABILITY…….....125
5.1 Future solar PV resource …….…….....125
5.2. Future water withdrawals for BAU scenarios ……..126
5.3 Solar PV area needed for PVenh scenarios. ……..….... 128

5.3.1 Water withdrawals for PV_{enh} scenarios ……..... 129
5.3.2 Freshwater savings for PV_{enh} scenarios. …..…….…….130

6. RESULTS AND DISCUSSIONS..... 133
6. ELECTRICITY DEMANDS: MEGACITIES CASE STUDY….....133

6.1 Global gridded electricity demands map …….…….....133
6.2 Megacities electricity demands …….…..... 134
6.2.1 Electricity flow for world megacities for 21st century……..... 134
6.2.2 Comparison of electricity estimates with existing …… 135
6.2.3 Solar PV resource for megacities …….…….…….....135
6.2.4 Solar electric footprints of megacities…….…….…….....136
6.3 Solar PV rooftop scheme…..…….…….....137
6.3.1 Solar PV area available Vs needed…….…….…….....137

6.3.2 Comparison of electricity estimates with existing studies..... 138

6.4 Conclusion of solar electric footprints of world megacities …….139

Chapter 7: CONCLUSION..... 141

RECCOMMENDATIONS..... 143

Bibliography 145

LIST OF FIGURES

Figure 1.1 Conversion scheme of energy services; Primary energy to end–user energy.....24

Figure 1.2 Combined anthropogenic forcings compared with natural forcings and internal variability of the climate system for the period 1951–2010 …… 25

Figure 1.3 Potential of different renewable energy sources as compare to total energy needs. ..27

Figure 1.4: The generation of 20 TW of power, equivalent to the world's mid–century predicted demand, would need covering ~0.16% of Earth's land (red boxes) with 10%–efficient solar PV modules. ……..……...…...28

Figure 1.5: The incoming solar irradiance on a tilted array depends on the position of the sun as far as the solar PV module (α_s) and module's tilt–angle (β). ……..…….35

Figure 1.6: The solar photovoltaic schemes……..37

Figure 1.7: Schematic diagram for Once–through cooling system. ……... 42

Figure 1.8: Schematic diagram for cooling systems a) Wet tower cooling and b) Dry cooling...43

Figure 1.9: Energy–water associations; positive & negative inferences …….…….....50

Figure 1.10: Conceptual illustration for EW–nexus for future sustainability…….....51

Figure 1.11: Shared socio–economic scenarios. ……. 54

Figure 2.1: The basic scheme used in our study. Various satellite and ground–based datasets were used to produce the theoretical and actual estimated solar resource. Cooling water withdrawals for TEPPs are estimated using the AIM model outputs and water–use intensities. Lastly, the nexus between energy and water is explored through various linkages……..56

Figure 2.2: Methodology used for solar PV resources mapping in our study. Various satellite and ground–based datasets were processed to produce such maps. …… 57

Figure 2.3: Long terms daily mean (2001–2014) seasonal temperature at 2m height……..60

Figure 2.4: Long terms daily mean (2001–2014) seasonal shortwave radiations near the earth surface. …… 61
Figure 2.5: Long terms daily mean (2001–2014) seasonal Aerosol Optical Thickness……...62
Figure 2.6: Transmittance Loss Factor ($K_{L)}$ at optimum tilt angles is calculated by applying the curve fitting technique to the experimental data available with Elminir et al, (2006) ……..... 63
Figure 2.7: Long terms daily means (2001–2014) snow water equivalent (mm)…….64
Figure 2.8: Long terms daily means (2001–2014) snow cover fraction (%)……65
Figure 2.9: Snow melting from solar PV surface considering the mass balance is used to calculate the snow melts from solar PV surface for optimum tilt–angles and module temperature (P_T). ……..…. 66
Figure 2.10: Curve–fitting technique for transmittance and snow depth applied to the experimental data available with Perovich (2007)…….67
Figure 2.11: Methodology devised to calculate the costs and cost supply curves for centralized and decentralized PV schemes…….. 69
Figure 2.12: Global land–use/land cover types containing 19 land–use classes for 2015 (ESA)71
Figure 2.13: Roof–top area/ capita available for decentralized PV schemes as provided in Alsema and Brummelen, (1993) and IEA, (2001a) is plotted alongside the GDP per capita for 1995 by Hoogwijk (2004)…….....73
Figure 2.14: Global gridded population (numbers) for 2015. Higher population is seen for Western China and South Asia……..73
Figure 2.15: Global gridded GDP (USD) for 2015. Higher GDP is seen for Western USA, Europe, The Middle East, Western China, South Asia, and Japan……74
Figure 2.16: Global gridded area per person for 2015. Higher areas are seen for higher GDP/cap regions like for Western USA, Europe, The Middle East, Western China, South Asia, Australian, and Japan……..…..74
Figure 2.17: Raster regional map for AIM classifications (source: author)……78
Figure 2.18: Data processing to convert point based power plants electricity generation data into regional data, using AIM raster regional map. Then, cooling technologies are used to calculate regional shares, which are then multiplied with WUI. Lastly, sea water is subtracted to have final fresh water withdrawals (km3/yr) for each region…….……82

Figure 2.19: Flow chart to calculate revised electricity generation and new water withdrawals by TEPPs for solar PV_{enh} scenarios……85

Fig 2.20: Scheme for megacities roof–top area calculation for 2010……89

Fig 3.1: Long term mean of daily seasonal solar PV module temperature (T_m)……...91

Fig 3.2: Long term mean of daily seasonal solar PV cell temperature (T_c)..……92

Fig 3.3: Long term mean of daily seasonal solar PV efficiency reductions due to the effect of temperature changes ($\Delta\eta_T$)……93

Figure 3.4: Transmittance Loss Factor ($K_{L)}$ at optimum tilt angles (Jacobson and Jadhav, 2018) is calculated globally by applying the curve fitting technique shown in Fig. (2.5). …… 94

Fig 3.5: Long term mean of daily seasonal solar PV efficiency reductions due to the effect of dust ($\Delta\eta_D$)…..……..95

Fig 3.6: Long term mean of daily seasonal snow depth accumulated on top of solar PV modules……..96

Fig 3.7: Long term mean of daily seasonal solar PV efficiency reductions due to the effect of snow covers ($\Delta\eta_S$)……..98

Fig 3.8: Global optimum tilt–angles (β_{opt}) taken from Jacobson and Jadhav (2017). Higher tilts are observed for regions away from latitude…….….99

Fig 3.9: Global effective power ratio calculated for β_{opt}……...99

Fig 3.10: Final performance ratios (PR) calculated from all individual corrections and optimum tilt-angles……. 100

Fig 3.11: Global seasonal solar power resource in W/m^2. A solar cell efficiency of 15% is considered for final power output…….... 101

Fig 3.12: a) Global annual solar power resource W/m^2 obtained by annual seasonal mean power resource. **b**) Variation of seasonal and annual mean power resource along the latitude…….103

Fig 3.13: Scatter plot between observed power and the actual estimated power for all solar power plants globally. The coefficient of determination (R^2) is 0.787 while RMSE obtained is 17.12104

Fig 3.14a): Locations of existing solar power plants used in our validation, and taken from Wiki–Solar dataset. **b**) Scatter plot between observed power and the actual estimated power for global nine regions based upon their contribution to the total generation from solar PV……...106

Fig 3.15: Heat map for R^2 values for varying cell efficiencies and available four cell types. In addition, we introduced four virtual cells (VC1–VC4) between the normal cells based upon temperature resistance coefficients……..108
Fig 3.16a) Heat map for R^2 for changing tilt–angles in comparison to optimum ones for four cell types. **b**) Scatter plot for final power output for GSWP3 dataset and WFDEI dataset. A rational R^2 value of 0.99 is obtained between both of them…….109
Fig 3.17 Regional heatmap for R^2 values for changing tilt–angles in comparison to the optimum ones for four cell types…….110
Figure 3.18: Grid-scale spatial distribution of the centralized solar PV electricity generation costs at a global scale for 2015……111
Figure 3.19: Global and regional cost–supply curves for centralized PV scheme for 2015. The curve for 'Global' in the black square indicates the current electricity consumption along with the range of electricity generation costs (Goldemberg, 2000) .....……112
Figure 3.20: The global grid-scale spatial distribution of decentralized solar PV electricity generation costs……..…….…113
Fig 4.1: Water scarcity maps obtained while using WTA for H08 model along with two GCMs, HadGEM2–ES and MIROC5. The ensemble mean is also calculated for both GCMs..…….115
Fig 4.2: Water scarcity maps obtained while using WTA for WATERGAP2 model along with two GCMs, HadGEM2–ES and MIROC5. The ensemble mean is also calculated for both GCMs……..116
Fig 4.3: Population (numbers) under various stress limits for the ensemble mean of H08 for AIM regions globally……117
Fig 4.4: Percentage of population (%) with respect to the total population under various stress limits for the ensemble mean of H08 for AIM regions globally……..118
Fig 4.5: Population (numbers) under various stress limits for the ensemble mean of WATERGAP2 for AIM regions globally……119
Fig 4.6: Percentage of population (%) with respect to the total population under various stress limits for ensemble mean of WATERGAP2 for AIM regions globally……..120
Fig 4.7: Geographic location of all TEPPs (Coal, Oil, Gas and Nucl) as obtained from World Resources Institute (WRI. 2018)…….….121
Fig 4.8: Electricity demands for AIM regions by TEPPs (Coal, Oil, Gas and Nuclear)…….122

Fig 4.9: Scatter plot between electricity generations by our method with the AIM model outputs. A rational R^2 value= 0.931 shows higher coverage of our database globally…….122
Fig 4.10: Water withdrawals (Km^3/yr) while generating electricity by TEPPs for AIM regions using the TEPPs database……123
Fig 4.11: Scatter plot between electricity water withdrawals (Km^3/yr) by our method with Huang et al, (2017). A rational R^2 value= 0.942 is obtained between both studies……124
Fig 5.1: Future **s**olar PV resource (W/m^2) and difference (%) of current and future PV resources for various SSP and RCP scenario combinations.....……126
Fig 5.2: Future water withdrawals (Km3/yr) for BAU case for various SSP and RCP scenario127
Fig 5.3: Solar PV area (km^2) needed for PV_{enh} scenarios for AIM regions globally……..128
Fig 5.4: New water withdrawals (km^3) for PV_{enh} scenarios for AIM regions globally……..130
Fig 5.5: Fresh water savings (Km^3/yr) for each region for PV_{enh} scenarios in comparison to the BAU scenario……...…131
Fig 6.1: Global gridded (0.5°) electricity demand map for 2010. Using grid–based GDP, AIM regional electricity demands are downscaled to draw the above map…….133
Fig 6.2: Electricity demand and GDP/cap flows for 27 megacities for 21st century……...134
Fig 6.3: Comparison of electricity estimates for megacities for our study and Kennedy et al, (2015) …….….135
Fig 6.4: Seasonal solar PV resource available for all megacities. Most of them have good PV resource during all seasons, but, during SON and DJF, cities like Paris, Moscow, London and Istanbul have less resource due to snow covers……...136
Fig 6.5: Solar electric footprints of world megacities derived from electricity demands and solar PV resource for each city for 2010……..137
Fig 6.6: Solar electric footprints vs. roof–top area available for 2010. For 11 out of 24 cities (top), entire electricity demand can be met if all available roof tops are covered with PV, while remaining 13 cities (bottom) can produce around 40–50% of their required electricity…….138
Fig 6.7: Comparison of roof area availability estimates and existing literature for some of megacities……139

LIST OF TABLES

Table 1.1 Withdrawals and consumption for various fossil fuel power plants (EPRI, 2000)…...44

Table 2.1: Data set description …… 58

Table 2.2: The supposed suitability factors obtained from values suggested by Sørensen (1999), the area of different land–use types as a fraction of total area with similar land–use types. …. 71

Table 2.3: Regional classifications used in AIM model. …… 79

Table 2.4: The cooling system shares (%) for various regions for thermoelectric power production technologies in 2005 80

Table 2.5: Correlation between electricity consumption per capita and other variables for AIM regions……... 87

Table 5.1: Summary of AIM regional water savings (km^3) for PV_{enh} scenarios globally……..132

Chapter 1: INTRODUCTION

1. Energy and sustainable development

Energy has a key role in the overall development of the economy and mankind. The energy scheme accounts for the whole of the sector which supplies energy, it converts the primary energy to different energy drivers, and the final technologies required to convert these energy drivers to provide the requisite energy services (Fig. 1.1). Energy has undergone significant changes with time. Out of those, two notable evolutions can be distinguished in the past times of the energy system (Grübler, 1998). The first transition was during the late 18th century, when industrialized countries used coal to run their steam engines, as coal could more easily be transported and stocked at that time. This technology developed significantly with time and offered great power potential and relevant services in almost all main sectors including industry and transport. By the start of the 20th century, almost all primary energy in industrialized countries was accomplished by coal. The second move was associated to the generation of electricity, followed by a diversification of both sources of energy supply and end–use technologies. Electricity was the first major form of energy that could simply be transformed to heat, light or work, etc. for different end–users. Also, with the development of the internal combustion engines, mobility with cars, buses and airplanes increased, and it stimulated the oil used for transportation. Such innovations caused a move in the mix of energy sources available on a commercial scale from wood to coal, oil, and then natural gas. An increase of about 40 times is seen for primary energy source usage from 1850 to 1990 (Grübler, 1998).

Though, the development of the energy system has changed over the globe. Currently, we are living in a place where almost four billion people use these fossil fuels as their main energy sources and rely on 16% of electricity for energy services. While 2.4 billion populations depend upon traditional fuels and energy resources like biomass etc. to fulfill their energy needs (IEA/OECD, 2002a). Since the later energy consumption related to only 11% of the total primary energy utilization, therefore, is not dominant and sometimes neglected in statistics relating to energy consumption (Goldemberg, 2000). Likewise, such disparities in the accessibility of energy services show the inequality for the development of the economy.

Energy plays a vital direct and indirect role in a way to achieve the United Nations (UN) targets for sustainable development. The UN Rio+20 summit (UN. 2012) held in 2012 in Brazil during the UN General Assembly, it was promised to set up sustainable development goals (SDGs) which must supplement the Millennium Development Goals (MDGs) after their finish by 2015. The energy was one of the key issues at the session. In addition, saving the Earth's life–support system and reduction of poverty must be among the topmost desires for SDGs due to the growing human population. Thriving lives and livelihoods, sustainable water & food security, clean energy for the universe, healthy and dynamic ecosystems, and governance for sustainable civilizations are the essentials in the era of Anthropocene. As humans are transforming the planet, Griggs et al, 2013 argued that it is not enough to just extend MDGs, but, indeed, the stability of the planet must be combined with UN targets to fight against poverty and accomplish human well–being. Energy has the key role in overall efforts to achieve sustainable development, its need of the hour that all plans and reforms for energy development must be in line with these goals (Vera et al, 2007).

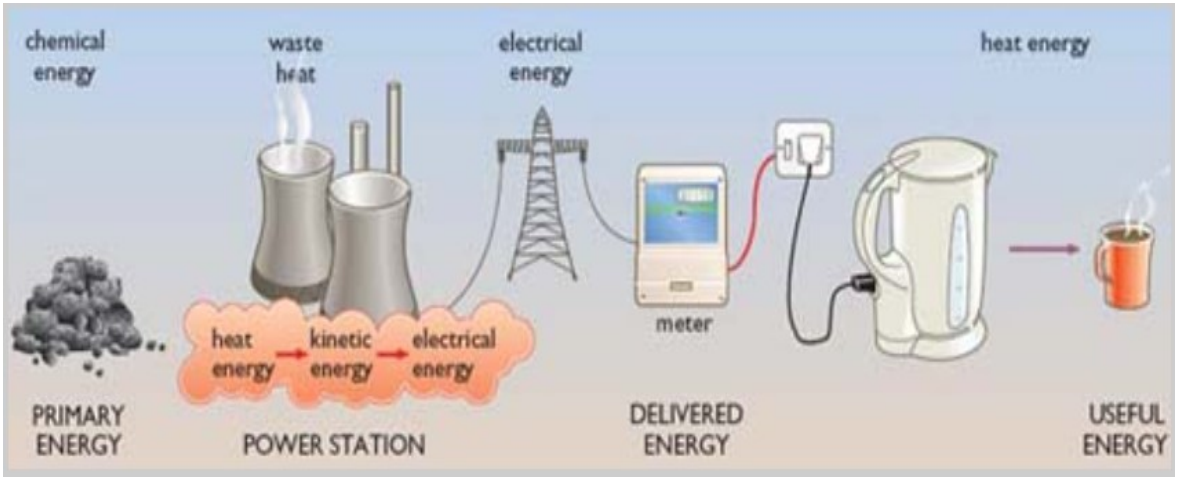

Figure 1.1: Conversion scheme of energy services; Primary energy to end–user energy (www.open.edu)

With the growing population, world energy crises are an important concern of the 21st century. In 2002, Johannesburg's World Summit on Sustainable Development, the international community agreed to half the poverty rate by providing appropriate energy to the poor people by 2015 as stated by the UN statement of the world summit on sustainable development, New York (UN. 2002). During the past century, amazing opportunities were provided to mankind in various

sectors of life by means of fossil fuels invention. Besides, human has to face critical challenges due to over–exploitation of this energy resource. Until 2006, the world usage for oil has grown–up to 1000 barrels a second (Tertzakian et al, 2006) equivalent to 2 liters per person per day (Kerr et al, 2006). Increased uses of fossil fuels are putting pressure on available reserves, emitting harmful pollutants to threaten human lives along with greenhouse gases (GHG) associated with global warming (Simmons et al, 2005).

Major disasters like floods etc. for the past century were associated with anthropogenically induced climate change (Hirabayashi et al, 2009) causing global warming. An increase of 0.15°C a decade in earth surface and mid–troposphere temperature, averaged over the sphere, is seen for the past 25 years (Kerr et al, 2006). This rise in temperature is assumed to further increase the probability of flooding (Dankers et al, 2014). Though abrupt climate changes can happen for many reasons, it is plausible that human forcing of climate change is intensifying the likelihood of large and abrupt events (Alley et al, 2004). Radiative effects of these forcings are causing an increase in the global water cycle along with a subsequent increase in the risk of a flood (Milly et al, 2002). Fig. (1.2) shows that Human drivers are likely to be the extreme dominant source of the observed global warming for the 20th century. The severity of destructive human–induced climate change does not depend only on the degree of the change, but also on the likelihood of irreversibility. The changes taking place due to an increase in CO^2 concentration are mostly irreversible for about 1,000 years even after emissions cease (Solomon et al, 2009). Consequently, the world needs acting faster: notable shortenings are required to minimize the risk of globalmean temperature growing 2 °C above pre–industrial levels (IPCC, 2014).

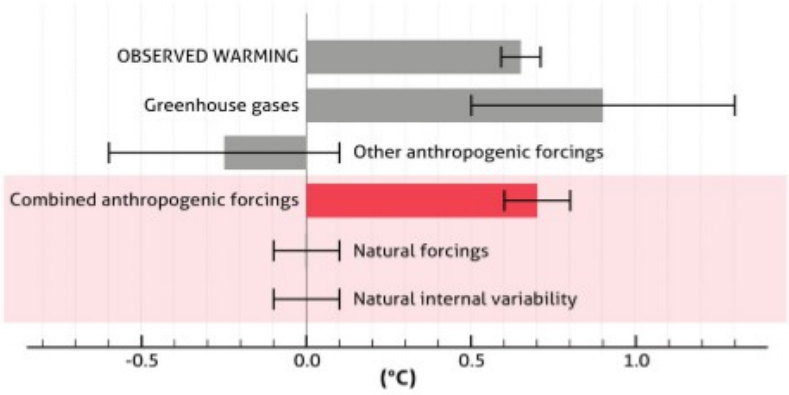

Fig 1.2: Collective anthropogenic forcings compared with natural forcings and internal variability of the climate system for the period 1951–2010 (IPCC. 2014).

Globally, electricity is considered a major form of energy. Its availability is vital for infrastructural development and economic growth, as an assurance of the sufficient supply of electricity guarantees a higher level of economic development and leads to prosperity (Chen et al, 2007). It is seen that economic activities are mostly concentrated in highly populous areas. For 2011, the top 27 megacities of the world added 14.6% to the world's Gross Domestic Product (GDP) and consumed almost 9% of total global electricity (Kennedy et al, 2015). Both GDP and electricity consumption are extremely dependent. For urban areas with GDP/capita less than 10,000 USD, an increase in electricity usage is witnessed for increasing economic activities; on the other hand, this rate is not significant for higher GDP values (Creutzig et al, 2015). Additionally, a strong correlation between GDP and electricity consumption is confirmed for industries in Taiwan, where, 1.72% lift in the GDP is seen for 1% additional usage in the electricity (Lu et al, 2017). It is therefore obvious that if the rapidly increasing global electricity demands are to be met, an alternate energy system should be adopted with zero or minimum harm to the environment.

1.1 Renewables:

Renewable Energy (RE) resources like solar energy, biomass energy, wind energy, and geothermal energy have the potential to offer energy services with no or minimum air pollutants and GHG emissions. These resources are available in a huge amount almost all over. They have the capacity to meet the current and future electricity demands globally as presented in Fig. (1.3) provided by Asif et al, (2007). With technological development, an increase in the usage of RE has been seen for the past few years. For five years from 2000, the rate of growth recorded for RE was: 60% in grid–connected solar Photovoltaic (PV) cells, 17% for off–grid PV, 28% for wind power, 25% for biodiesel, 13% for geothermal heat capacity & 11% for ethanol as reported in Renewables 2005–Global Status Report by Worldwatch Institute, Washington, DC (2005). Accordingly, Mathiesen et al, (2011) presented a model based on a 100% RE system to replace fossil fuels for Denmark to be applicable by 2050. Moreover, for Sub–Sahara African countries, RE's potential was utilized to develop a low–cost electricity solution to fulfill the future demand of 2030 (Barasa et al, 2018). It has been assessed that total electricity demand of 866.4TWh in

addition to the power required for desalination of 319 million m^3 of water could thoroughly be met by renewable.

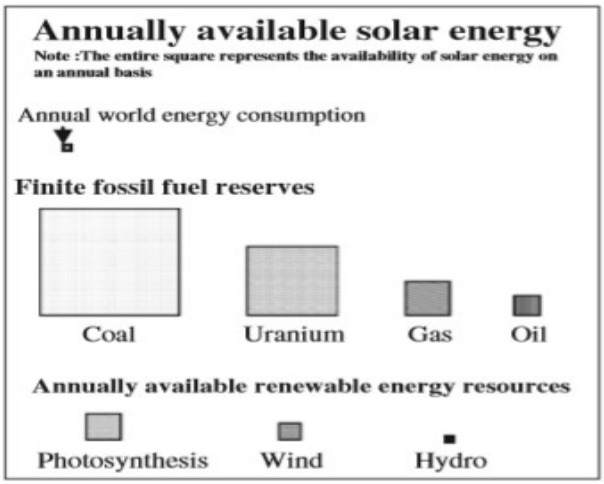

Figure 1.3: Potential of different renewable energy sources as compared to total energy needs (Asif et al, 2007).

1.2 Solar energy and Photovoltaic:

Presence in abundance and infinite makes solar energy unique from others. Being clean & simple, it can easily be transformed into different forms of energy. The quantity of daylight radiations received from the sun is equaled to 86,000 Terawatts (TW, 1TW= 1012 Js^{-1}), however due to the land–use, meteorological & topographic barriers, the useable energy is about 400 to 8,800TW (GEA. 2012), which is still far enough to accomplish the human needs of 18TW in 2014 (IEA. 2017). About 20TW of power could be obtained by just covering 0.16% of land surface with 10% efficient solar panels (Service et al, 2005).

Solar PV technology offers the method of converting the light energy from sun into the electrical energy. Various semi–conductors are used in this process and the most prominent one is silicon. This zero–carbon resource (solar PV) has the potential to meet the rapidly growing worldwide electricity demands (Chander et al, 2015). Additionally, the impact of PV over existing land is very small. For the United States, it is seen that approximately 140 million acres of land is covered by cities and infrastructure. The entire electricity needs could be met by just covering 7% of this built–up area. Moreover, it does not need even one–acre extra land, like parking lots, roof–tops, walls along the highways and sides of tall buildings offer sufficient area

for PV fixations (US Department of Energy, 2004). In the same way, rooftops of highly populous areas, megacities offer large space for fixing solar PV modules, which will result a decrease in solar PV installation cost by avoiding lengthy transmission lines. For Mumbai, 31–60% of the morning peak electricity loads and 12.8–20% of the daily average demand for several months can be accomplished by covering roof–tops with solar PV (Singh et al, 2015). In the same way, Dhaka offered 10.5 km^2 roof–top areas in 2006, capable to produce 1000 MW electricity from solar PV (Kabir et al, 2010). It is therefore obvious that solar PV does not require any additional or large space for its fixing (Fig. 1.4).

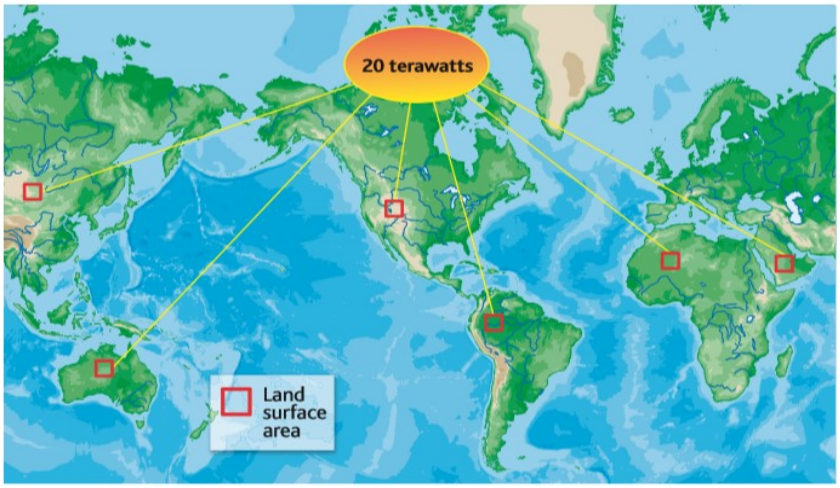

Figure 1.4: The generation of 20 TW of power, equivalent to the world's mid–century predicted demand, would need covering ~0.16% of Earth's land (red boxes) with 10%–efficient solar PV modules (courtesy of Professor Nathan Lewis, Caltech, Pasadena).

One drawback for solar PV is that it is quite expensive now i.e., the cost for 1KWh delivered in the USA for the year 2005–2010 was $0.20, but, due to the technological improvement, it is projected to decrease up to $0.10/KWh in the near future (2020) (Fthenakis et al, 2009) which is much similar to the conventional power generation cost for fossil fuels, $0.08 (EIA. 2009a). Another plus is that the current and future (2030) external environmental cost of solar power generation is zero as compared to fossil fuels as seen for the USA in a report published by National Research Council (NRC. 2010). These characteristics make solar PV an environmentally friendly & low–priced source of energy, being in line with United Nations SDG 07; Affordable and Clean Energy. With further technological enhancements like load

transference with demand, system flexibility & energy storage, it is becoming easier to couple solar PV with the traditional electric power system.

1.2.1 Technical potential

The total installed solar PV capacity for 2018 was 500 GW worldwide (REN21. 2019). This is quite small compared to other major RE resources like hydropower and wind etc. On the other hand, solar PV's technical potential per unit area is much larger, so the yields of solar PV would be comparatively high compared to remaining RE resources. Solar PV technical potential mainly depends on two factors, the solar irradiation and land area suitable for its fixation. Globally, two studies exist that evaluated such potential of PV for both centralized and decentralized schemes in the longer–term including cost analysis. It includes the work done by Hoogwijk (Hoogwijk. 2004) as well as by Hofman et al, (2002). Also, some global statistics are provided by Johansson et al, (2004), and in the report by World Energy Assessment (UNDP. 2000).

Both studies conducted by Hofman et al, (2004) and Hoogwijk. (2004) considered the technical potential of a solar PV at a grid–scale level based on available solar irradiation, land–use suitability factors, and some assumptions on future cell efficiencies. The former study focused on the year 2020, but, it did not cover all countries. While latter focused on the late future, i.e. 2050, and is more realistic on the future capacity of solar PV, as it assumed higher efficiencies, a practical suitability factor for land–use and did not exclude any area due to narrow solar radiation, and assumed that the whole area can be used for the installation of solar PV. But, none of them considered the limiting meteorological factors affecting the solar PV resource; hence one can say that they did not estimate the actual potential of solar PV. This study deals with the calculation of the actual technical potential of solar PV considering all limiting factors.

1.2.2 Meteorological factors affecting solar PV cell efficiency

Solar PV technology is best known for producing electricity with the help of semiconductors, which convert incoming light energy from the sun into the electrical energy.

The power output of the solar PV system mostly depends on the intensity of incoming solar irradiance, the area provided for solar PV fixation, and solar cell efficiency. The theoretical power is usually not obtained because of different limiting factors such as snow, dust, and temperature, etc. (Principe and Takeuchi, 2019). Both the increase in solar cell temperature above a certain value (Meneses–Rodríguez. 2005) and dust covers (Goossens. 1993) causes a decrease in solar PV cell efficiency. Similarly, snow blocks the solar radiation, reduces transmissibility and promotes PV module surface wear and tear (Andenaes. 2018). Finally, varying tilt angles for solar PV fixing are also proven to change the module power output (Asl–Soleimani et al, 2001). The following sections explain the relevant research performed to describe the effects of above–mentioned meteorological limiting factors individually as well as in a whole on various scales to limit the solar PV power output.

1.2.2.1 Impact of temperature changes on solar PV cell efficiency

The PV cell temperature is an important environmental factor affecting the performance of a solar cell which is described by means of an open–circuit voltage (VO_{oc}), short–circuit current (I_{sc}), and maximum power output (P_{max}), cell efficiency (η_c), and fill factor (F_f,) (Chander et al, 2015):

$$F_f = \left(\frac{I_{max} \times V_{max}}{I_{sc} \times VO_{oc}}\right) \quad (1.1)$$

Where, I_{max} is the intensity of light, and V_{max} is the maximum voltage.

The F_f is basically a measure of solar cell quality as it corresponds to the actual maximum theoretical power which can be produced, and it is directly proportional to the solar cell efficiency. With a temperature increase, VO_{oc} decreases and it reduces the η_c as well (Meneses–Rodríguez, 2005). The decrease in terms of solar cell efficiency with increasing temperature beyond the Nominal Operating Cell Temperature (T_{NOC}) the limit is almost linear and can be explained by a single value of temperature coefficient (Kaldellis et al, 2014). For example, the findings of Chander et al, (2015) reported the efficiency values for temperature efficiency coefficient ($d\eta/dT$) for a single, series and mono–Silicon (c–Si) solar cells connected in parallel as −0.005 − 0.095/°C, −0.013 − 0.029/°C and −0.012 −0.020/°C, respectively. Several

investigations (Skoplaki et al, 2008; Alsayed et al, 2013) involved wind data in their computations and concluded that wind offers a cooling effect on the solar cells and helps improving power output. Solar PV module temperature (T_{mod}) is calculated using Eq. 1.2 provided by the National Renewable Energy Laboratory (NREL. 2013) as the empirical equations by them has the best results among all (Zouine et al, 2018)

$$T_{mod} = G_{POA} \times \{e^{(a+b*WS)}\} + T_a \quad (1.2)$$

G_{POA} is the solar irradiance at the plane of an array; e is Euler's constant, WS is the speed of wind at 10m height, while a and b are empirical constants taken from King and Boyson (2004), T_a is the near–earth surface temperature at 2m height.

In solar PV installations, T_a is measured using sensors installed at the meteorological station or in the vicinity of a solar power plant (Schwingshackl et al, 2013). As there is no definite product of T_a from weather/ solar power plant stations and remote sensing satellites. So, the rational alternative is the land surface temperature (LST). LST could be calculated from the observations of the thermal radiance coming back from the land surface and retrieved by satellite. Therefore, T_a is measured at 2 m above the ground level on meteorological weather stations using sensors protected from radiation and properly aerated (Mildrexler et al, 2011). Hence, to compute the variations in T_{mod}, conversion techniques can be applied first to derive the T_a using the LST (Jin et al, 2010), and then computing the T_{mod} from the above equation.

1.2.2.2 Impact of dust deposition on solar PV cell efficiency

Dust or soil is defined as a particulate substance with a diameter of less than 500 μm (Darwish et al, 2015). In the case of solar PV arrays, dust that covers the surface is mostly less than 10μm depending on local environment (Maghami et al, 2016). Mani & Pillai, (2010) confirmed that dust present in the atmosphere is from a variety of sources, such as dust moved by the wind, pedestrian and transport movement, volcanic activities, and pollution. It promotes light scattering which results in the reduction of incoming solar beam radiation (Duffie and Beckman, 1974.). Elminir et al, (2006) presented that dust settlement decreases as the tilt–angle increases because dust particles often tend to roll and fall from the surface due to the gravity. In terms of particle size, finer dust particles accumulated on solar module surface has a higher negative

effect on its performance as compared to courser particles since finer particles are distributed in a more uniformly manner which minimizes the voids (spaces) between particles from which light can transfer (El–Shobokshy and Hussein, 1993). There is a broad range of local and regional studies that reported the effect of dust buildup on solar PV performances. They include dust effects on transmittance in the United States (USA), Kuwait, and Egypt (Ward. 1955; Hasan. 1992 and Elminir et al, 2006); power output in Kuwait, Saudi Arabia by (Said. 1990 and Wakim. 1981); and lastly solar cell efficiency in Saudi Arabia and Malaysia, (Said, 1979 and Mekhilef 2012). Most of the above–mentioned studies were performed on a laboratory scale or in a very small localized area (e.g., rooftops of buildings, a small solar park on the ground) and as such, the implication of their study was also of limited scope. In addition, the study period also varied from some days (Elminir et al, 2006) to a month (Kimber et al, 2006) or maximum up to a year (Said. 1990) which may also be a cause why different researchers reported different values to a particular PV output even for the same region or country. For example, a percentage reduction to solar cell efficiency in Saudi Arabia was reported as 30% and 40% by (Sayigh. 1978) and (Said. 1979) respectively. Like the above–mentioned studies formed the starting point of the design and rating of solar PV arrangement such as the conventional flat–plate modules (Ward. 1955; Maghami et al, 2016), they all mostly share similar limitations on the spatial area under consideration.

The spatial limitations were mainly because of the nature of the experimental setup where a few solar PV panels or solar cells efficiencies and reductions were tested under dust and no–dust conditions. With the advancement in technology and the beginning of satellites which offer a contiguous and very high spatial regional and global coverage, such limitations can be solved. Numerous studies have dealt with the retrieval of aerosol properties using satellite data sets for dust reduction analysis. They include Hsu et al, (2004) and Jalal et al, (2015) for Moderate Resolution Imaging Spectroradiometer (MODIS), and Kikuchi et al, (2018) for Himawari–8 satellite. The obtained aerosol properties, e.g., Aerosol Optical Thickness (AOT) along with the angstrom coefficient can be used as input parameters for dust effects modeling on solar PV systems. For example, provided with a threshold value for AOT and particle size characterization (Salinas et al, 2009; El–Shobokshy and Hussein, 1993), the corresponding dust effect on light transmission, and finally output power can be calculated. Most of the researchers (Sayigh. 1978; Principe & Takeuchi, 2019) used a fixed value of 0.3 for dust loss factor (K_L); however, such

values vary with tilt–angle changes (Sayyah et al, 2014). Therefore, we improved the method by applying a curve fitting technique to the experimental data from Elminir et al, (2006). Lastly, the effect of precipitation as a natural cleanser to the dust deposition on solar PV panels should also be incorporated (Kimber et al, 2006) to have a true representation of the whole phenomenon.

1.2.2.3 Impact of snow covers on solar PV cell efficiency

Snow covers are supposed to be the most prominent solar cell efficiency reduction factor among others, especially in snowy areas during the cold weather. They adversely affect the output of the solar PV systems by blocking the incoming solar radiation because of high albedo. In addition, snow also promotes surface wear and tear by introducing mechanical loads, which may cause bending or even breakage of entire solar panels (Andenaes et al, 2018). The property mainly affecting the performance of solar cells includes the snow depth. Relative to the standard test conditions (STC), more or less 10 cm of snow blocks 95% of solar radiation, leading to an output of 1–5% of a PV system. The amount of solar light that can penetrate the accumulated snow and reach the solar PV module has a direct (exponential) relationship as seen from Perovich. (2007). As a result, a snow cover of 10 cm and 2 cm might reduce incoming solar light transmission by 95% and 90%, respectively (Andrews et al, 2013). Another important factor affecting the power output under snow covers is the fixation angles of solar PV modules as snow is expected to slide for higher tilt–angles due to the gravitational forces as compared to flat angles. For example, a study by Powers et al, (2010) suggested that power output losses for snow covers are directly proportional to the square of the cosine of PV module tilt angles. They found that the annual output power losses due to snow covers are 18% for horizontal PV surface in comparison to the modules fixed at 39° whose losses were about 12% in total. Finally, new snow can have a thermal conductivity equals to that of fiberglass insulation (Ross. 1995) and thus can behave as an insulating cover which prevents convective heat loss of the PV module surface and also promotes snow melting and sliding (Andrews et al, 2013). However, the melting rates may vary depending on the solar PV cell types. Bogenrieder et al, (2018) demonstrated that the maximum melts and sliding is for amorphous silicon (a–Si) and microcrystalline tandem solar PV modules without any framing (Riggs and Hall, 2015).

Similar to other solar cell efficiency factors, the effects of snow in solar PV systems were only studied at a localized scale. Hence, snow properties obtained from satellites are believed to be a better alternative in analyzing the snow's effects on the performance of solar PV. Snow depth can be calculated from the Snow Water Equivalent (SWE) product from The National Snow & Ice Data Centre (nsidc) which comes in 0.5° resolution with global coverage (Chang and Rango, 2000) along with snow cover fraction (SCF) product from NASA Terra MODIS (MOD10). Moreover, our model is improved by incorporating the findings from previous experimental studies dealing with snow depth effects on solar PV module's performance. Besides, it also includes the effect of optimum tilt–angle on efficiency losses along latitude and addition of snowmelt scheme from PV surface.

1.2.3 Geomorphologic analysis on solar PV Performance:

In addition to various meteorological parameters, fixation angle (tilt–angle) at which solar PV module is placed is proven to increase the power output due to an increase in the incident solar irradiance. These angles are supposed to vary across the globe due to the change in sun position and elevation angle which varies during the daytime as well as in the seasons.

1.2.3.1 Effect of PV module tilt–angle on energy yields:

The tilt angle at which the solar PV module is fixed is considered as a major factor contributing to the power output. They are optimum if the yield reaches its maximum. They affect the power output of the PV system by varying solar irradiance (Palmer et al, 2018). It also affects the intensity of snow covers (Powers et al, 2010) and helps in the reduction of dust deposition (Elminir et al, 2006). Recently, we have one–axis as well as two–axis tracking PV systems in addition to the fixed ones. The primary objective is to take the maximum benefit of incoming solar radiations which changes during the daytime. Though, for fixed systems, particularly those which are mounted directly on the inclined roof surface, such a tracking mechanism may not be available. For such cases, existing roof features and natural ground slopes where solar panels are to be installed may be studied. Digital elevation models (DEM) are mostly

used in geomorphologic studies including solar radiation estimates (Ruiz–Arias et al, 2009), design of coastal flooding (Eakins and Grothe, 2014), and another flood–prone area (Hawker et al, 2018). High accuracy DEM provides the information of terrain characteristics (Yamazaki et al, 2017) and is often used to define both Digital Terrain Models (DTM) and the Digital Surface Models (DSM). DTM represents the ground surface without any features and it is useful in flood modeling. Whereas, DSM represents the ground surface with existing features (Hirt. 2016). In solar PV studies, the latter is important as it is mostly assumed that solar panels are to be fixed on the existing features like rooftops or sometimes on the ground.

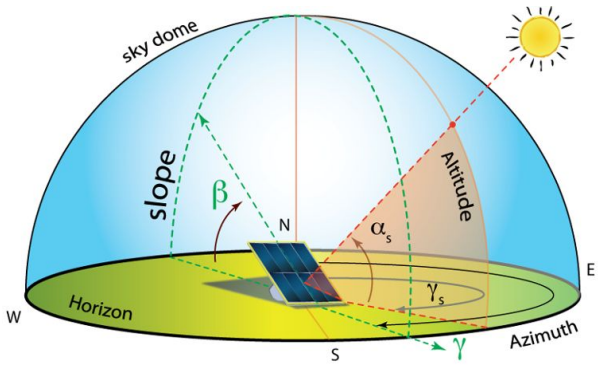

Figure 1.5: The incoming solar irradiance on a tilted array depends on the position of the sun as far as the solar PV module (α_s) and module's tilt–angle (β) (www.pinterest.co.uk)

The incoming solar irradiance on a tilted array depends on the position of the sun with respect to solar PV module (α_s) and its tilt–angle (β) as shown in Fig. (1.5). Calculated module optimum tilt angles (β_{opt}) and α_s can be used to calculate the incoming solar irradiance on an inclined surface using the methodology in Eq. (1.3) by Honsberg and Bowden (2018):

$$R_{opt} = R'\sin\{90° - \text{ø} + 23.45°\left[\frac{360}{365} \times (284 + d)\right] + \beta \qquad (1.3)$$

Where: R′ is the incident solar irradiance, ϕ is the latitude, d is a day of the year, and β is the module optimum tilt angle. Assuming fixed solar irradiance for a given period at a particular location, Eq. (3) implies that the incident radiation on a solar PV module surface varies with the tilt angle. For solar PV systems, the fixation angle is considered optimal (β_{opt}) once it produces maximum energy output (Palmer et al, 2018).

1.2.4 Economic analysis of solar PV

Recently solar PV has undergone rapid cost reduction among other renewables and energy technologies (Trancik and Cross–Call, 2013). Due to such cost reductions in addition to cell efficiency performance improvements, PV deployment at a global scale has grown–up rapidly (Trancik. 2014). Its massive deployment could facilitate reduce GHG emissions and other harmful pollutants from energy systems (Hertwich et al, 2015), and contributes toward climate change mitigation efforts (Trancik and Cross–Call, 2013). For solar PV deployment at household and large scale levels, mainly when considering the extra expenses involved in addressing solar intermittency (Braff et al, 2016), additional cost reductions are preferably required (U.S. Department of Energy. 2012).

Some studies dealing with the potential of solar PV have been performed in the past, largely focusing on particular applications, e.g. attached to the buildings (IEA/OECD, 2001a) or in large centralized schemes (Kurokawa, 2003). They also had geographical limitations at a national or regional level. However, some studies like (Ascencio–Vásquez et al, 2019; Hofman et al, 2002) have calculated the potential of solar PV electricity at a global scale. But, Ascencio–Vásquez et al, (2019) do not include an economic analysis of PV based upon his estimates. A study performed by Hofman et al, (2002) included cost estimates, but it is only for one year and relied on concentrated solar power technologies (CSP) in addition to the electricity generation for solar thermal systems. Also, the study was performed on a regional scale. Hoogwijk. (2004) performed such analysis at a global scale but it did not consider meteorological limiting factors that affect the solar resource. Therefore, there was a need to perform such economic analysis at a global scale considering the actual solar PV potential, and with the most recent parameters involved with its installation. Such global estimates of PV economic analysis will provide a better insight into the anticipated participation of solar PV in the whole energy system. It includes current PV deployment costs at both household and large scale levels and also provides an insight into keeping the pace of further improvement in the near future.

1.2.4.1 Solar PV schemes

This study deals with two main types of onshore PV applications, shown in Fig. (1.6): centralized (on–grid) and decentralized (off–grid) grid–connected schemes. In our analysis, both

are described and estimated separately, which indicates that there is no connection or overlap among their potentials.

i) Centralized (grid–connected) solar PV scheme: It includes semi–to large–scale solar PV schemes (>10 kWp), provided on open ground in the shape of big solar parks. As they need larger areas, hence this scheme has small competition among land use types.

ii) Decentralized (off–grid) solar PV scheme: It includes small– to medium–scale systems (<10 kWp) for household electricity supply, fixed on roof tops or near to houses, structures or industries. Mostly installed on rooftops, so do not require any special land for its fixation.

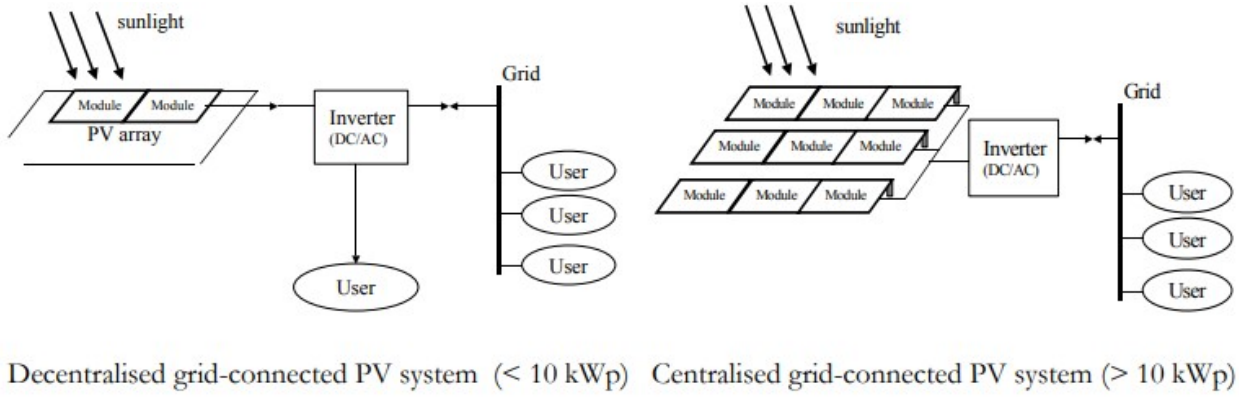

Figure 1.6: The solar photovoltaic schemes (Hoogwijk. 2004)

1.3 Water

Water is among the basic need of every human being. Freshwater is considered a renewable source, but on the same time it is finite, as there are many signs that human being's use is exceeding sustainable limits. By 2025, greater than 60% of the global population will live in regions/countries with considerable disproportions between water needs and supplies, mostly in Latin America, Africa, and Asia. Currently, more than a billion people do not have an access to safe drinking water, and about 2.4 billion people do not have the access to improved sanitation (The Atlantic Council, 2005). Also, water governance has an important role in controlling water resource allocation, which is further associated with access to safe drinking water and sanitation among developing and non–developing countries (Tidar et al, 2019).

Rivers are considered as a major source of freshwater globally. About 3800 km3 /year of blue water, freshwater available in rivers and streams, is currently taken by human beings (Oki & Kanae, 2006), and it accounts for not more than 10% of the available freshwater globally. Why should we be worried about freshwater availability when currently only 10% of freshwater is consumed? The rationale is the large variability of existing water resource distribution in time and space (Postel et al, 1996). For example, river discharges have more variations in smaller river basins, and more in daily river discharge than the monthly ones. Due to these temporal variations, it is hard to use all (100%) of the available freshwater for human needs. Similarly, flow during the floods and high flow seasons cannot be used during the dry (low flow) seasons except storage systems exist.

The Intergovernmental Panel on Climate Change (IPCC) in its inclusive assessments of climate change (Arnell & Liu, 2001) has provided the summaries of the expected broad–ranging consequences of climate change on available water resources especially rivers. The reports include impacts on the variability and volume of river discharge, seasonal changes in the water supply availability, and change rates of river sedimentations. Studies related to river basins have shown that variations not only on climate side but also in economic development, population, and remaining socio–economic issues may cause considerable changes in water use and continue to affect future water resources as well (OECD. 1998). Due to higher significance, access to Clean Water and Sanitation along with Climate actions is set as UN SDGs in 2015.

1.3.1 Components of water withdrawals

Global freshwater withdrawals are increased from about 2500 km^3 a year in 1970 to about 4000 km^3 a year in 2010 (Shiklomanov. 2000; Wada and Bierkens, 2014) with the speedy growth in population, industrialization, and energy and food demands, such as massive human water use have imparted significant impacts on the ecosystem, hydrologic cycles, and the human society. For instance, irrigation has reallocated both surface water and groundwater resources, and disturbed terrestrial hydrology by means of changes in evapotranspiration and streamflow (Taylor et al, 2013), which has resulted in changed surface air temperature and precipitation patterns at both regional and global scale (Lobell et al, 2009; DeAngelis et al, 2010). Also, Rost et al, (2008) demonstrated that irrigation intensified global evapotranspiration by about 2% and reduced river discharge by ~0.5% for the period of 1971–2000, whereas Müller Schmied et al, (2014) calculated an increase of worldwide evapotranspiration of ~1.3% and a decline of river discharge of ~1.8 % due to human water use. Likewise, industrial and domestic water withdrawals make 19% and 11% of global water withdrawals respectively (FAO. 2016). Such withdrawals are expected to increase with growing food and energy demands, which are believed to limit the economic development, mainly in arid and semi–arid regions, e.g., Northern China, India, and the Middle East (Wada et al, 2011; Taylor et al, 2013). The details of the main components involved in human water withdrawals are provided in the below section.

1.3.1.1 Irrigation water

This sector accounts for the largest quantity of water withdrawals among all sectors and makes up to 70% of the total water withdrawals (FAO. 2016a). It sustains approximately 40% of worldwide food production (Abdullah. 2006). For various countries, like Pakistan, India, Iran, and Mexico, where irrigation supports food production and the income of millions of people to a large extent, irrigation water withdrawals (IrWW) even go beyond 90% of the entire water demand (Fischer et al, 2007). Globally, from 1900 to 2005, the area used for irrigation has grown to six–fold from ~0.5 million km^2 to approximately 3.0 million km^2, which nearly equals the size of India (Freydank and Siebert, 2008). This growth occurred quickly at a rate of almost 5% a year from 1950s–1980s, except it has come down (<1%) since the late 1990s. For the future, the global irrigated land is not likely to expand radically because of limited land and water

availability (Turral et al, 2011; Faurès et al, 2002), but still, it will grow slowly and stimulate the IrWW (Fischer et al, 2007).

1.3.1.2 Domestic water

Domestic water withdrawals (DWW) include water used for drinking, cooking, bathing, and washing, etc. It accounts for 12 % of the total water withdrawals (Hanasaki et al, 2008a). From 1980 to 2010, DWW has increased 2.3 times from 201km³ to 469km³, with a yearly growth rate of 4.4%. The highest growth rates are seen in Asia and South America (Afraz. 2020). Although, IWW is the largest whereas DWW is the smallest water use sector, but researchers like Hejazi et al, (2013) estimated a large change of share for future global water withdrawals. Likewise, WaterGAP2 (Alcamo et al, 2007) estimated 41%, 28%, and 31% of global water withdrawal for the agricultural, industrial and domestic sector by 2075 respectively, whereas Shen et al, (2008) projected them as 52%, 37%, and 11%. Although domestic water is vital for humans, however, unlike agricultural and industrial demand, it cannot be met by virtual water trade (Neverre & Dumas, 2015). Like agriculture, an increase in domestic water usage is expected for the coming years. Wada et al, (2016) calculated that future domestic water withdrawals will be 700–1500 km3 per yr until 2050, showing an increase of about 50−250% related to the current water use intensity (400–450 km^3/yr in 2010)

1.3.1.3 Industrial water

Industrial water covers the water use in cooling, transportation, manufacturing various products, or as a final product (Shiklomanov. 2000). In addition, it is vital for the extraction of primary energy and biofuel (Wada et al, 2016). After IrWW, Industrial water withdrawal (IWW) is the major sector contributing towards the total withdrawals and accounts for 19% (FAO. 2016a) The major water consumers in this sector are thermoelectric power plants (TEPPs), which require a huge amount of water for cooling purposes while generating the electricity. Depending upon the technology used in the manufacturing processes, IWW may vary for various industries. It also depends on the climatic conditions as IWW appears to be quite lower in the

northern areas than in the southern regions due to lower air temperatures (Shiklomanov. 2000). Mainly IWW has two components; manufacturing and water use in electricity production. This study mainly deals with the fresh water scarcity due to the water used by TEPPs, and, will only be described here.

1.3.2 Types of cooling

Almost all kinds of TEPPs plants boil water to generate steam, which next runs the turbines to generate electricity. The fuels used to boil water can be of many types like coal, oil, gas, a nuclear reaction, or directly from the sun or geothermal source. Once steam goes through a turbine, it should be cooled down into water before it can be reused to generate more electricity as colder water cools the steam efficiently.

For TEPPs, it is first to know the difference between water withdrawal and consumption. Withdrawal means the water withdrawn from a water body or aquifer and is later returned to the watershed. However, consumption relates to water withdrawn that is usually not returned back to the water body. The amounts of water withdrawals are much higher than the consumption. The water comes out of a thermal plant, usually has a very high temperature, causes thermal pollution along with chemical pollutants (Heugens et al, 2002), so it is mostly not available for downstream users without any treatment. TEPPs water withdrawals are also represented by water use intensity or sometimes referred to as efficiency, which means water use per mega–watt hour (MWh) of electricity generation. A higher efficiency power plant has a lower water usage. The principal cooling system types and associated tradeoffs are presented in brief in the below sections.

1.3.2.1 Once–through cooling

Once–through cooling (OTC) is also known as open–loop cooling system, and it involves taking out water from the surface water body mainly the river or sea. This water runs past a heat exchanger, gets the waste heat, and discharges it to the same waterbody, at higher temperatures. The schematic diagram is shown in Fig. (1.7). The water consumption of this method is higher due to higher evaporation losses as compared to other cooling systems. But, this cooling

technique has the benefit of being simple and low cost; where cold water is available in excess. Though, it can have some adverse environmental impacts in addition to the environmental ones (Holmstrup et al, 2010) as the amount of water withdrawn is very high. Also, the increased temperature of the discharge back to the water body may have harmful effects on the local ecosystem. For such reasons, OTC has not been used in many of the newly built power plants in countries like the US for some years.

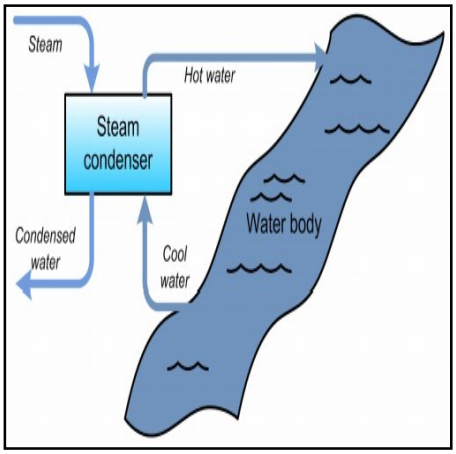

Figure 1.7: Schematic diagram for Once–through cooling system (source: Rutberg. 2003)

1.3.2.2 Wet tower cooling

Wet tower cooling (WTC) technology uses a recirculating circle of fresh water for cooling. Once running through the waste heat exchanger, the warm water is sprayed down from a cooling tower onto the chunk of lattice–like material which increases the flow surface area. Simultaneously, a fan like arrangement or natural draft withdraws air from the base of the cooling tower up throughout the fill, and then out to the atmosphere. During the process, the flow of air and water behaves as a heat exchanger, heat transport from the water to the air. What is more, a small portion of the water evaporates as it passes the tower, and the latent heat of this evaporated water cools the leftover water. The cooled water collected at the bed of the tower is sent back to the waste heat section and evaporated water volumes are added from the outside freshwater source. The schematic diagram is shown in Fig. (1.8a). The wet towers technique withdraws far less water than OTC systems. However, due to the evaporation, the water

consumption of wet towers is rather more than OTC system (Feeley et al, 2008), and the cost, and complications are more. Also, cooling towers may bring out aesthetic objections; they generate vapor plumes in certain circumstances, and normal draft–type cooling towers are a hundred feet high structure.

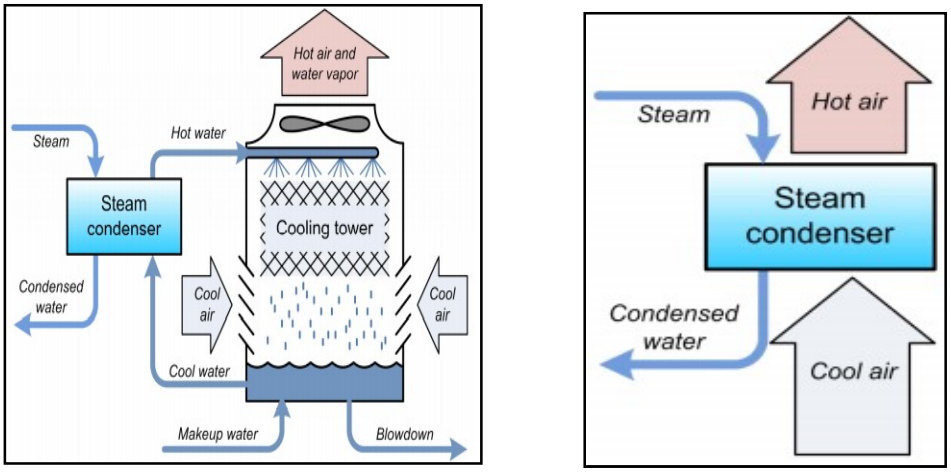

Figure 1.8: Schematic diagram for cooling systems a) Wet tower cooling and b) Dry cooling (source: Rutberg, 2003)

1.3.2.3 Dry cooling

Air cooling or dry cooling rejects residual heat to the atmosphere without using water. However, other processes in the same power plant may use a small amount of water, for system maintenance and cleaning, which is not significant. Dry cooling systems use an enormous size radiator which offers a bigger surface area to refuse the power plant waste heat. The schematic diagram of a dry cooling phenomenon is shown in Fig. (1.8b). It is usually three to four times expensive than a similar wet tower cooling system. In addition, the overall performance of a thermal plant depends on efficient cooling; during hot days, the usefulness of a dry cooling system goes down, and as a result, the power plant's total efficiency reduces. Moreover, hot days generally coincide with large electricity demands as well

This study mainly deals with freshwater scarcity owing to higher water withdrawals, mainly by TEPPs. Therefore, we will only include OTC and WTC types of cooling techniques which are usually responsible for freshwater scarcity in many parts of the world. Table 1

provides summary of the withdrawals and consumption for the above two cooling techniques for various kinds of Thermal plants. For future analysis, the Carbon Capture and Storage (CCS) technique is also included is believed to be used in the near future.

Table 1.1 Withdrawals and consumption for various fossil fuel power plants (EPRI. 2000)

Plant and Cooling System Type Water	Withdrawal (liters/MWh)	Consumption (liters/MWh)
Fossil fuel/biomass/waste | once-through cooling	76 000 – 190 000	1 000
Fossil fuel/biomass/waste | closed-loop cooling	2 000 – 2 300	2 000
Nuclear steam | once-through cooling	95 000 – 230 000	1 500
Nuclear steam | closed-loop cooling	3 000 – 4 000	3 000

1.3.3 Water scarcity

Uneven distribution of water both in space and time makes the water availability finite to the users. Such limited quantities quantity may give rise to water shortage type of situations known as water scarcity. Moreover, climate change and global warming are affecting the limited water recourses around the world making this essential resource highly vulnerable (IPCC WGII AR5. 2012). Currently, water scarcity is a growing global concern. Humans and other living beings on the planet Earth need water for their survival; consequently ensuring adequate water supplies are very important.

Freshwater scarcity is one of the critical dilemmas for sustainable development. It was ranked as one of the top global risks faced by human beings by the World Economic Forum (World Economic Forum, 2015, 2019). During water scarcity, available water cannot meet the needs of all sectors, which mainly includes agriculture, industry, domestic, and environment, etc. (UNDP. 2006). It has two types; one is physical, and another one is economical. In the first, there is not sufficient water for human demands, however, in the latter one, there is enough water; but, due to lack of adequate infrastructure, people can't use it for their needs (UNDP. 2006). Available freshwater is although enough for human beings, still, due to its uneven distribution across the globe, some regions are facing a water scarcity situation. For example, the Mediterranean region is home to about 7.3% population but it only includes 3% of world water resources (Margat & Treyer, 2004). Also, limited access to freshwater hinders economic

development globally (Feeley et al, 2008). It is therefore evident that water scarcity is one of the main issues faced by human society in the 21st century.

Spatially water availability varies region by region; also, it has temporal limitations for seasons to interannual. Predicting such variations is quite hard, and one of the most challenging part of water resources managers and planners. These are very much helpful for policymakers in addition. In the most advanced countries, by developing a high–cost infrastructure on the supply–side, they are trying to overcome such uncertainties to meet adequate supply and to reduce risks. However, it poses certain negative impacts on the environment and human beings. Likewise, many countries are realizing that those supply–side solutions only are not sufficient to meet ever–increasing demands; thus, other solutions like demand management should be addressed to overcome water insufficiency (UN–Water. 2008). Hence, investigating available water and their demands is very important for proper resource allocations and policy makings.

1.3.3.1. Water stress indicators

The inevitable rise in demand for water to produce food, supply to industries, and sustain rural and urban lives has led to an increase in freshwater scarcity in numerous parts of the world. Many rivers now run dry before entering the sea for considerable periods of time. In many parts, groundwater abstraction rates exceed replenishment, underneath aquifers and the river base flows are depleted (Postel. 2000). Progressively more, governments, corporations, and societies are worried about the sustainable supplies of water and future availability (UN. 2009).

During the past few decades, researchers have developed a lot of metrics to assist map, characterize and predict the water scarcity globally and regionally. These include, for example, the proportion of renewable water supply to the population size (Falkenmark. 1989), the fraction of water withdrawals to the water availability (Oki & Kanae, 2006; Alcamo and Henrichs, 2002; Raskin et al, 1997), and the fraction of water consumption to the monthly discharges which occur under dry conditions (Alcamo. 2007). These water scarcity indices have shown the difference between freshwater availability and demands, and have supported document the changes of water scarcity over time. Nowadays, water scarcity estimates underpin worldwide assessments of poverty and human development (UNDP. 2006), food (IWMI. 2007), business and economic prospects (World Economic Forum, 2015), and environmental assessment (World

Resources Institute. 2005). We will use the novel water stress indicator, withdrawal to availability (WTA, Raskin et al, 1997) to provide a current and future water scarcity picture with various stress levels causing water shortages and harm to the ecosystem within the river basin across the globe.

1.3.3.2. Cooling water required by thermoelectric power plants for electricity production

Electricity is considered as the main form of energy, whose availability ensures economic growth and leads to sustainable development (Chen et al, 2007). According to International Energy Agency (IEA. 2017), TEPPs supply 80% of the world's electricity. In 2010, they consumed 540 km^3 of water for cooling, about 70% of IWW or 14% of the global all water withdrawals (IEA. 2012). For the USA, it is estimated that in 2005 about 41% of freshwater withdrawal was used for electricity production, largely for cooling (Kenny et al, 2009). Similarly, in 2010, the European Commission (Eurostat. 2010) wrote that the cooling water withdrawals for TEPPs in France and Germany were 22 km^3 and 20 km^3 respectively. So, there is growing concern that water use for electricity production might enhance competition among major water sectors, like agriculture, industrial (manufacturing), and domestic ones, and may also become a key reason that promotes freshwater scarcity. Besides, water shortages could harm energy security as electricity shortages have just been reported due to the water shortages in the southeastern USA, the Pacific Northwest, and parts of Europe as well (Bartos et al, 2015). Our study estimates the current and future global cooling water withdrawals (CWW) for TEPPs using the novel approach and recently published datasets. Such analysis provides an insight into the technology shifts, water–use efficiency improvements among various regions for the future.

1.3.3.3. Freshwater scarcity by thermoelectric power plants

The thermal power generation industry mainly consists of TEPPs. It is a water–intensive sector, and therefore promotes regional as well as global freshwater shortages. Water footprints are the quantity of water required for the production of various goods and services etc. belong to various water–use types for a country (Hoekstra and Chapagain, 2007). The blue water corresponds to the freshwater available in rivers and streams while green water is the water available in the soil etc (Mekonnen and Hoekstra, 2010). The blue water footprints of TEPPs for

electricity generation are very high and globally, about 19 billion cubic meters of fresh water, which is equivalent to the basic needs of more than a billion people, is used every year (Greenpeace International. 2016). According to Spang et al, (2014), this value is as high as 52 billion m^3 for 150 countries. For China, about three–fourth of available freshwater is consumed by TEPPs which belong to water–stressed regions (Zhang et al, 2017). If current policies continue, these withdrawals are estimated to increase more than 4.3 times from 2014 to 2050 (Liao et al, 2016). Likewise, TEPPs in Europe are consuming 43% of their total withdrawals (Rübbelke and Vögele, 2011), and in Egypt, 25% of fresh water is used to cools the electricity generation system (Siddiqi et al, 2011). Water withdrawn by TEPPs are mostly returned back to the system, however, as they draw a massive amount of water and it has to be there every time, so putting a lot of pressure on available freshwater resources and making sectoral water allocation challenging. As mentioned earlier, water sent back to the waterbody has a very high temperature along with pollutants (Heugens et al, 2002) and, therefore, it is not available to the downstream users unless treated. So, it is essential to identify the main contributors to global freshwater stress.

The cooling water needed by TEPPs is one of the main drivers of freshwater stresses, and strategies to overcome such freshwater resource exhaustion needed to be implemented. An efficient water resource management technique for the power generation sector is proven to end the possible water crisis (Lv et al, 2018). Also, sustainability for both energy and water could be ensured by linking research on the water requirement of TEPPs with some mitigation policies for energy–based water–use in terms of energy–water nexus. Moreover, when discussing different ways to mitigate or lessen the water demand of TEPPs, it is critical to think about the development of RE like solar PV as a solution to freshwater scarcity (Lohrmann et al, 2019).

1.4 Energy–water nexus

Energy and water demands are increasing with the growing population. Climate change is already influencing the hydrological cycle, so, knowing the trade–offs for energy–water nexus (EW–nexus) is becoming key for managing resources and proper planning. A better understanding of these links is also essential to develop policies for more adaptable and resilient communities (Newell et al, 2011). Before use, water is extracted from aquifer (or river/stream), purified, conveyed, and distributed. Similarly, after use, it is treated and reused; all of these

require energy (Blanco et al, 2009). In a similar fashion, energy–related processes like manufacturing synthetic fuels and refining various crude oil products also consume significant amount of water (Berkhout et al, 1997).

With an increase in energy and food demands, industrialization & growing competition among communities, it is seen that global water use (withdrawals) has increased by nearly 8 times from 500 km^3/yr to 4000 km^3/yr from 1900–2010 (Falkenmark et al, 1997 & Wada et al, 2013a) and this trend is expected to be followed in the future (Wada et al, 2011) with slight changes. Therefore, EW–nexus is the key to success during the planning and resource allocation phases in almost all projects.

1.4.1 Energy in water:

Energy is used to manage the fresh waters and it is seen, around 7 % of commercial energy is being used globally to manage the freshwater supply (Biswas et al, 2001). In many islands & water–scarce areas, energy is used for the desalination of saline water. For a region like the Middle East & North Africa (MENA), which is renowned for two–third of world oil reserves, but, with 1.4 % of freshwater supplies (Khater. 2001), Siddiqi et al, (2011) found that water required for desalination is projected to reach 15mill m^3 by 2030, which would require additional power (33 to 67%) for some of the countries to run the desalination plants. Also, groundwater pumping and desalination is consuming 9% and 5–12% of total electricity for Saudi Arabia and Arabian Gulf respectively. For Texas, the largest electricity generator and consumer in the USA, Stillwell et al, (2011) examined the energy used by wastewater treatment plants and water supply systems, and the CWW for cooling TEPPs during power generation. He concluded that 1.8~2.8 TW–hours of electricity is consumed for water supply and wastewater treatment respectively, this electricity is sufficient for 100,000 people for one year. Similarly, for cooling TEPPs to generate 400 TW–hours of electricity, approximately 595,000 mega–liters of water are used annually which is enough to fulfill yearly demand of more than three million people.

1.4.2 Water in energy:

Water is indispensable for every energy generation process. Though, not only hydroelectric plants are using water to work. TEPPs, driven by coal, fuel–oil, uranium, gas, and

biomass also need water (freshwater). For 2010, 583 billion m^3 of water, equivalent to 15% of the world's total water withdrawals were used in the energy sector only (Hightower et al, 2008). While in the USA, the energy sector is the alone leading consumer of water in its economy, as 80% of electricity is generated by thermoelectric facilities, utilizing 44% of national water withdrawn and about 6% of consumed one for 2005. This consumption of water by the energy sector is projected to increase 50% from 2005 to 2030 (Carter. 2010). Similarly, for Europe, this number has risen to 43% (Rübbelke and Vögele, 2011) and in Egypt; freshwater cools about 25% of country's electric generation system (Siddiqi et al, 2011).

Electrical energy production is one of the processes, consuming maximum water globally. Unlike the hydropower plants, TEPPs boil water to produce a stream to move the turbines for electricity generation. Whereas, conventional TEPPs burn fossil fuels to obtain heat, while, nuclear plants do this by nuclear reactions. For facilities to work properly, this heat must be dissolved in the cooling system. Every type of TEPPs needs a different amount of cooling water because of a difference of temperatures depending on fuel types. The cooling activity involves the largest amount of water during the course and, nuclear power plants require maximum water per megawatt–hour generated as compared to others (IEA. 2012). In turn, each cooling system, either wet or dry, involves different amounts of water, but, the water required by a dry system is the least. Hence, water is a limiting factor for power plants globally (Rodriguez et al, 2013) as electricity demands are projected to increase in the future. Also, International Energy Agency in his report (World Energy Outlook. 2018) provides critical thinking & analysis on energy demand & supply-side trends along with their consequences for environmental safety, economic developments, and energy security.

1.4.3 Energy–water nexus for sustainable development:

Electricity is considered as a major source of energy across the globe. The input from electrical energy is a stimulator for both infrastructural and socio–economic development. It is the electricity, whose use actually fuels up the economy, both in short–run and long–run (Mohanty et al, 2015). The assurance of adequate supply of electricity can promise a higher level of economic growth (Chen et al, 2007). Almost all types of electricity generation include water as an essential component; hence, its presence in abundance is vital for the production of

necessary electricity to support the economy. The TEPPs are the main source of electricity production in the world and require an adequate amount of water for cooling, and the insufficiency in CWW may result in economic losses. For the Middle East & Africa, Zhou et al, (2018) assessed that global economic losses due to insufficiency of cooling water availability for the future climate change scenarios (RCP8.5 & RCP2.6) are 0.57% and 0.27% respectively. However, for Europe, Asia, America & Soviet Union, this number is less, i.e., 0.05% to 0.18%. Also, the projection of global IWW is estimated to range 196–1463 km^3/year until 2100 under climate change & socio–economic scenarios (Fujimori et al, 2017). The cooling water for TEPPs, being a major component of IWW, needs to be managed properly. Also, a synchronized systematic approach is necessary to solve the issues for EW–nexus as the security of both energy and water is interlinked and essential for sustainable development (Fig. 1.9) (Hussey et al, 2010).

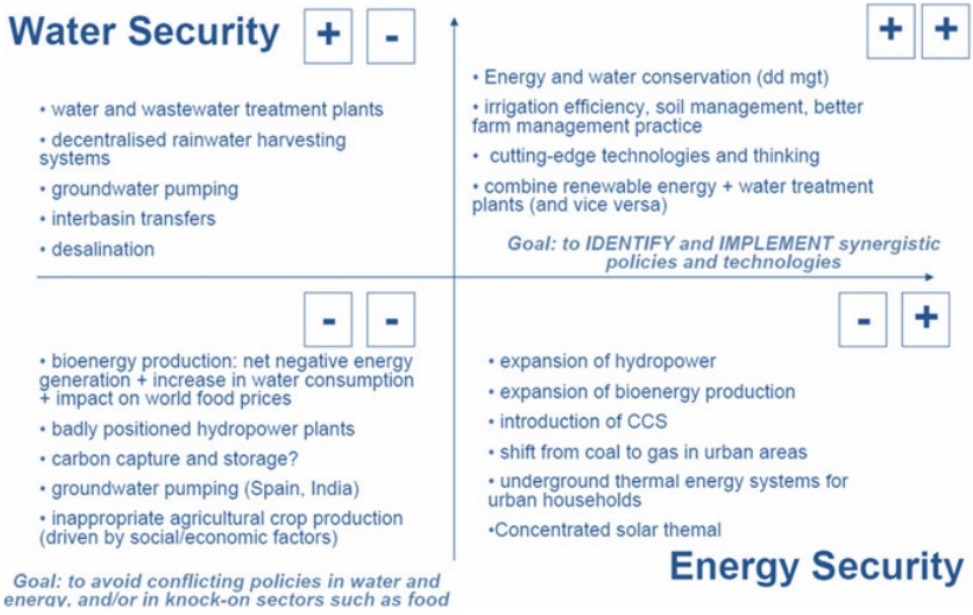

Figure 1.9: Energy–water associations; positive & negative inferences (Hussey et al, 2010)

The EW–nexus is vital in the overall efforts to achieve sustainability in terms of both the energy and water sectors. Below is the conceptual diagram of a conceptual illustration for both scenarios. For business–as–usual (BAU), more electricity will be generated through TEPPs and it will require a huge amount of fresh water for cooling the plant body for proper functioning. More or less this amount of water (grey color) goes back to the system. However, due to the excess amount of chemical pollutants and very high temperature, this water is not available

downstream unless treated. Such a phenomenon is making unsustainable conditions in the region in terms of freshwater availability. In addition, the excess electricity production by TEPPs is harmful to the environment due to GHG emissions. In the 2nd case (PV_{enh}), more electricity would be generated through solar PV and it will cut down a lot of freshwater needed by the TEPPs in the earlier case. Hence more freshwaters would be available to the system. Furthermore, electricity produced by solar PV is sustainable both for the environment and available freshwater.

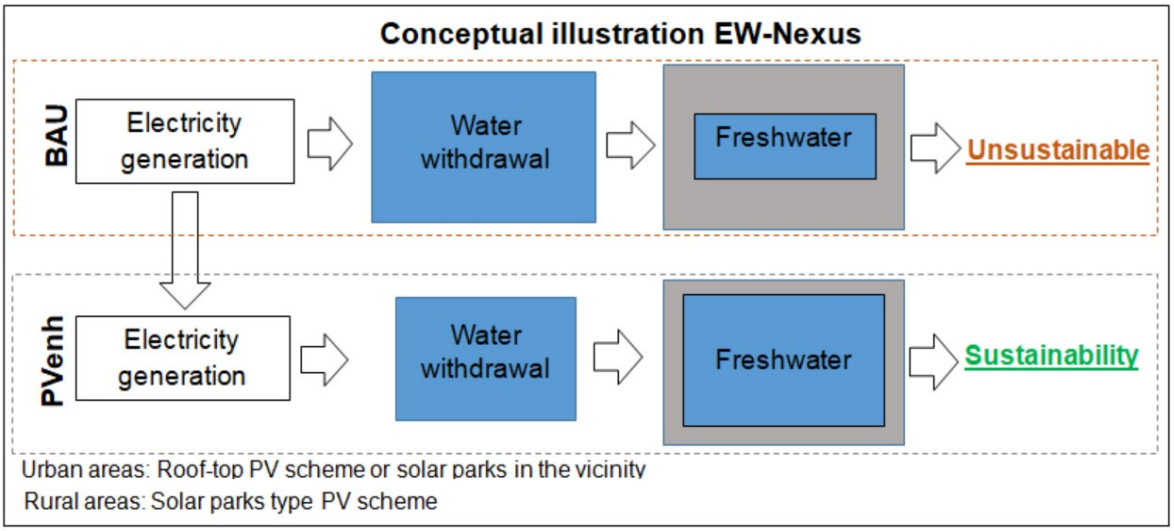

Figure 1.10: Conceptual illustration for EW–nexus for future sustainability.

1.5 Electricity demand and supply–side relationship

The electricity demand–side data is the most important input required to identify the needed or potential areas to be supplied with the electricity. In addition, this will help in proper resource allocation and investment strategies. For example, knowing electricity demand–side data, planners and the investors may be able to know where to install a PV power plant and in what capacity the installation should be done? Failing to provide such information that identifies potential regions may waste such investments and all efforts. In addition, line losses and high electricity costs involved due to longer transmission lines could be minimized while selecting a proper place for the resource to be installed. Therefore electricity demand and supply-sides are

believed to be strongly correlated with each other and equally important for resource planning and management strategies.

The regional electricity demand data is obtained from the AIM model outputs. Using the parameters which strongly affect the electricity consumption, such regional electricity demand values are downscaled to 0.5° resolution globally. These global electricity demand maps are helpful to know the potential areas for electricity provision for current and for coming years. In addition, these can also be overlaid to the available solar PV resource maps to see the PV potential available with them.

1.5.1 Megacities and sustainable development

Nearly 54% of the world's total population is living in urban areas which are consuming 70% of total energy use (IPCC. 2014, UN Department of Economic and Social Affairs Population Division. 2015). In 2007, 1.5 billion people made up the top 600 cities and were home to 22% of the total population. The phenomenon of rapid urbanization has irritated the development of thickly populous urban areas known as megacities, the cities with populations greater than 10 million (UN. 2018). Owing to their sheer size and complexity, these areas are frequently at high global risk, threatened by environmental and economic issues with an acute level of vulnerability and poverty (World Economic Forum. 2019). Whether megacities can develop as sustainable cities depend on how they obtain, distribute, and handle their resources like materials and energy, etc. Improper management and mishandling of such resources may cause environmental degradation (Mulder et al, 2008). Kennedy et al, (2015) reported that the top 27 megacities are making 6.7% of the worldwide population, consuming 9% of global electricity, and contributing 14.6% to the global GDP. In these cities, growth in GDP is highly correlated with growth in oil usage by transportation and energy (electricity) sector.

To fulfill the electricity demand of these megacities, solar PV could be a promising source as it is seen that megacities offer rational rooftops for its setting. For Mumbai, 31–60% of the morning peak electricity demand and 12.8–20% of the mean daily demand for various months could be met by covering city rooftops with solar PV (Singh et al, 2015). Likewise, Dhaka offered 10.5 km^2 rooftop areas in 2006, which was able enough to produce 1000 MW

electricity from solar PV (Kabir et al, 2010). As per the 5th assessment report of IPCC (IPCC. 2014), the majority of carbon releases from absolute energy use are produced by urban areas. Therefore, this zero–carbon resource could be applied to meet the rapidly growing global electricity demands (Chander et al, 2015). In addition, this will help saving water needed for electricity production and is believed to potentially contribute towards Sustainable cities and communities (SDG No. 11) in addition to SDG No. 13–climate action in a quantitative manner.

1.5.2 Shared Socio–economic and climate change scenarios

The future evolution in energy and system adaptation will be shaped by available energy resources along with socioeconomic conditions and drivers (Baeur et al, 2017). In this modern era, in addition to climate change, it was necessary for researchers to develop new energy scenarios in the light of these social and economic development indicators i.e., shared socioeconomic Pathways (SSPs) (O'Neill et al, 2014a). They actually guide and assist researchers to categorize the prevailing situations under their wide framework along with possible challenges and mitigations which could further help in sharing and comparing the results with similar studies to have the uncertainties involved (Trutnevyte et al, 2016). Additionally, in our study, these SSPs are joined with Representative Concentration Pathways (RCPs) to have a better exposure of climate change to socioeconomic conditions for future energy usage, demands, production and the possible challenges along with mitigations needed, as a combination of SSPs and RCPs has evidenced better representation of climate change and socio–economic development investigations for the future (Eyring et al, 2015). As such, many global environmental & climate models are incorporating SSPs & RCPs as an input. For example, earth system models (ESMs), an integrated assessment models (IAMs) and air pollutant release and land–use statistics; impact, adaptation, and vulnerability (IAV) models are using climate data (RCPs) and socioeconomic circumstances (SSPs) to assess the possible future projections. Recently, Fujimori et al, (2012) developed Asian–Pacific Integrated Model (AIM) to calculate land–use and gridded emissions data (0.5 degrees) for land use type, pollution, and carbon dioxide. SSPs and RCPs scenarios have been incorporated in the model to compile narratives mostly defining the societal development and climate influence considering population, GDP, energy, land use, and emissions.

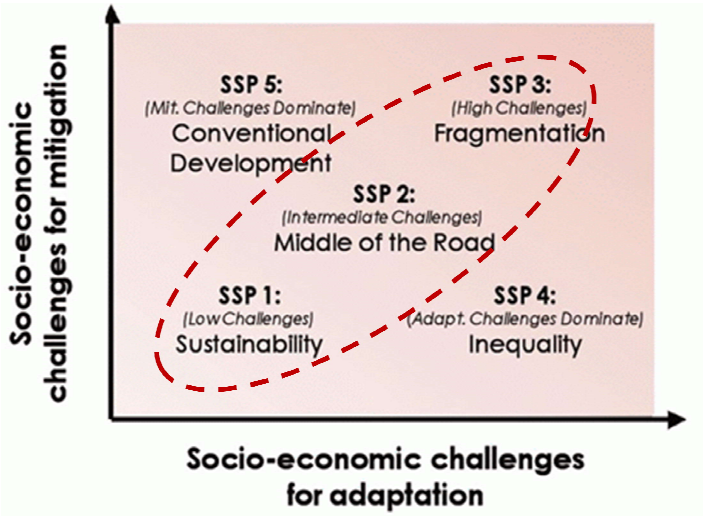

Figure 1.11: Shared socio–economic scenarios (O'Neill et al, 2014a).

1.6 Motivation of this study

Freshwater scarcity is a major concern worldwide and cooling water withdrawals for electricity generation are believed to be a major cause of such scarcity. To overcome this issue, the world needs to transform the current conventional energy generation system into renewables. A massive amount of energy is received by the earth from the sun and can meet the global electricity demands. This required an estimation of actual solar PV resources available on earth in addition to electricity demands and global freshwater scarcity mapping. Existing solar PV studies mostly concern about a single or two limiting factors, and were limited to small areas (laboratory scale) or a region. Hence, there was a dire need for a study that does consider all reduction factors affecting the solar PV resources simultaneously and provides such global information about actual PV resources to the public and policymakers. In addition, EW–nexus, using solar PV as an energy resource and water (CWW) by TEPPs is not yet explored globally which has many important implications; especially on changes in future energy demands, associated cooling water withdrawal demands, and technology shifts. These energy–water trade–offs are key to develop policies for more adaptable and resilient communities in the future.

1.7 Objective of this study

The aim of this study is to provide a reliable assessment of current and future solar PV resources for all seasons and on annual basis for all kinds of local environments at a global scale. It does include a global economic analysis of various solar PV schemes as well. To seek the potential of megacities rooftop PV scheme to fulfill their electricity demands. Current and future scenarios of freshwater scarcity levels, and to see how beneficial is the solar PV resource in controlling those stresses for various RCPs and SSPs. Moreover, the aim is to help transform current energy dominant resources (fossil fuels) with renewables (solar PV) and to assist in achieving UN SDGs, Affordable and Clean Energy (Goal 07), Sustainable Cities and Communities (Goal 11), and Climate Action (Goal 13) by adopting off–grid and on–grid solar PV schemes.

1.8 Novelty of this Study

The novelty of this study is in multiple ways: the estimation of current and future seasons as well as annual actual solar PV resources using multiple remote sensing and observation–based data sets; analysis is done on a global scale considering the meteorological and geomorphologic parameters; and the solar electric footprints of world megacities. The analysis does consider multi–models and various RCP and SSP scenarios to have wide coverage of uncertainties involved. Based upon our estimation, we suppose that our methodology to calculate the solar PV resource is reliable as it does consider many uncertainties in the shape of cell efficiency, material type, and changes in optimum tilt–angle, and data sets used in the investigation. This study could be helpful for policymakers and planners for large–scale (Solar Parks) as well as small–scale (households) level PV schemes worldwide. In addition, this study has a worthwhile implication on the IWW side to help to alleviate freshwater scarcity, especially in water–scarce regions.

Chapter 2: METHODOLOGY

This chapter provides the research framework of the thesis which includes three main sections, energy, water, and the nexus between them. The overview of methodology is provided in Fig. (2.1). The flow chart just shows the main components involved in the overall analysis of all sections. For individual sections, detailed methodology along with datasets used will be discussed in the relevant sections of the thesis.

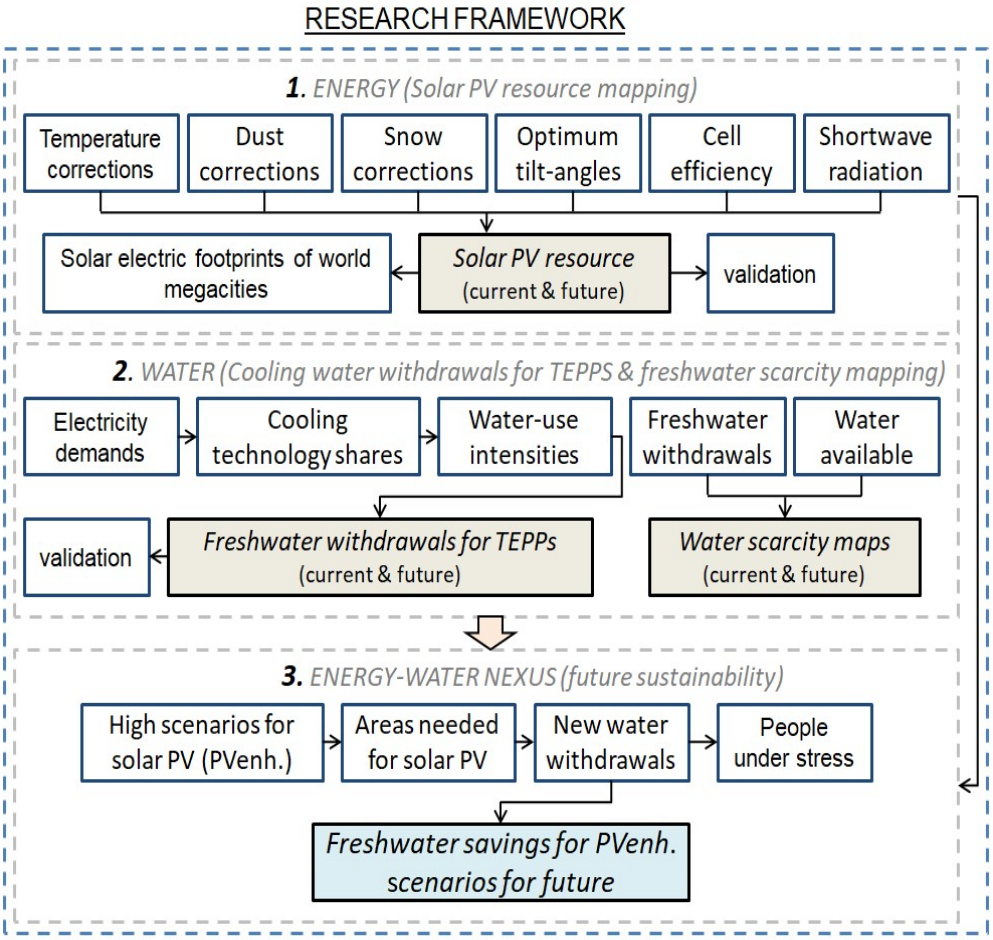

Figure 2.1: The basic scheme used in our study. Various satellite and ground–based datasets were used to produce the theoretical and actual estimated solar resource. Cooling water withdrawals for TEPPs are estimated using the AIM model outputs and water–use intensities. Lastly, the nexus between energy and water is explored through various linkages.

2.1 Solar PV resources mapping

2.1.1 Data and methods:

The basic concept used in the energy section is given in Fig. (2.2). Two main factors influencing the available solar PV resource namely, meteorological, and geomorphologic are analyzed separately on daily basis on a global scale. The investigation on meteorological and geomorphologic factors will provide the actual solar resource available on the solar PV module level, which will be used to multiply with solar cell efficiency to have the solar PV performance ratios globally. Flowcharts involved for each section are provided and particulars are discussed in detail in the proceeding sections of this part.

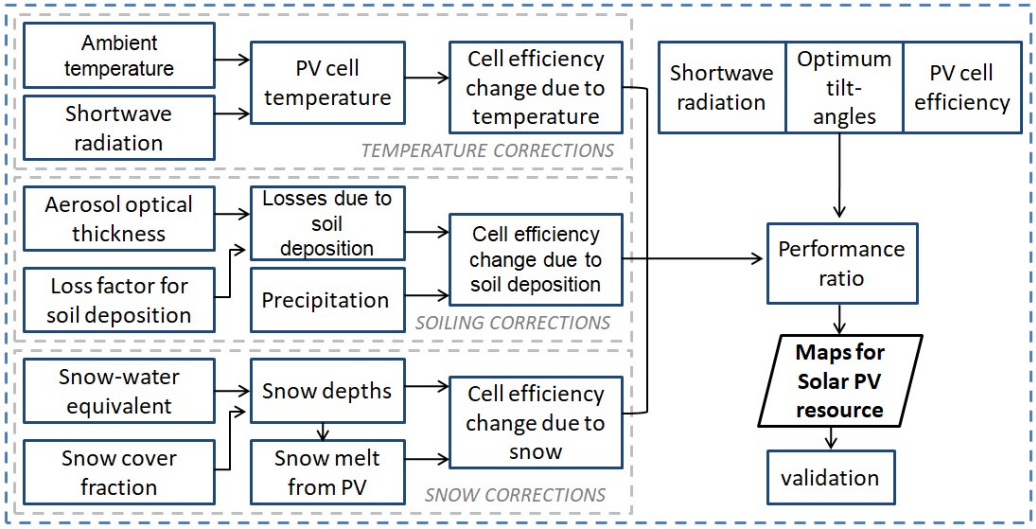

Figure 2.2: Methodology used for solar PV resources mapping in our study. Various satellite and ground–based datasets were processed to produce such maps.

The theoretical solar PV Power potential (P_T) was calculated using the bias–corrected shortwave radiations (SWR). First, the effect of temperature change ($\Delta\eta_T$) using SWR, wind speed, air, and PV cell temperature (2m). Then, the effect of dust deposition ($\Delta\eta_D$) was analyzed using AOT from NASA MODIS and dust loss factors for optimum tilt–angles. Cleaning through precipitation was also observed for all seasons using optimal dust removal thresholds. Also, the reduction in the output due to the snow covers ($\Delta\eta_S$), calculated from snow water equivalent (SWE) of National Snow & Ice Data Centre (nsidc) and snow cover fraction (SCF) data of NASA MODIS. The snowmelt from the solar PV surface is also seen using mass balance

equations to know the actual snow depths. The actual power (P_{act}) calculated after all losses are then compared to P_T to calculate the solar PV performance ratio (PR) globally for all seasons. These ratios along with solar PV cell efficiency are used to develop the global maps of solar PV resource. Lastly, the computed solar PV resource was validated against the outputs from actual solar PV power plants regionally and globally.

2.1.2 Data description:

The first step to work out the P_{act} needs the solar resource data near the earth's surface. The bias–corrected SWR data was obtained from the Global Soil Wetness Project Phase 3 (GSWP3) developed by Kim. (2017), which has a global coverage of 0.5–degree and 3–hourly daily solar climatological values near the earth surface from 1901–2014. More information is available at http://hydro.iis.u–tokyo.ac.jp/GSWP3/index.html. For SR, we used shortwave radiation (SWR) incident on a solar PV surface, which is the total solar irradiance on a horizontal or inclined plane at the surface of the earth. The mean of each day is estimated as the numerical average of 3–hourly readings for each day. The details of data sets along with their spatial–temporal resolutions are provided in Table 2.1.

Table 2.1: Data set description

Sr. No	Variable	Data Source	Temporal resolution	Spatial resolution
01	Shortwave radiation	Global Soil Wetness Project Phase 3 (GSWP3)	2001–2014 (daily)	0.5–degrees
02	Temperature	Global Soil Wetness Project Phase 3 (GSWP3)	2001–2014 (daily)	0.5–degrees
03	Rainfall	Global Soil Wetness Project Phase 3 (GSWP3)	2001–2014 (daily)	0.5–degrees
04	Aerosol Optical Depth	NASA Terra MODIS	2001–2014 (daily)	0.5–degrees

05	Snow cover fraction	NASA Terra MODIS	2001–2014 (daily)	0.5–degrees
06	Snow water equivalent	The National Snow & Ice Data Centre (nsidc)	2001–2014 (daily)	0.5–degrees

2.2 Decrease in solar PV cell efficiency due to meteorological limiting factors

2.2.1 Decrease in solar PV cell efficiency due to temperature change

After obtaining the biased corrected data, the next step was to compute ($\Delta\eta_T$). We used Eq. (2.1) to see the reduction in solar PV cell efficiency due to temperature changes. The daily reductions are calculated which are later averaged to the seasonal ones. We used four seasons, namely March–May (MAM), June–July (JJA), September–October (SON), and December–February (DJF) in our analysis as most variations for meteorological parameters like temperature, and snowfall, etc are more or less similar for those seasons. Temperature coefficient of power ($d\eta/dT$=0.45%/°C), cell operating temperature (T_{cell}), and temperature for the standard tests conditions (STC=25°C) at every ith day for every season with (n) number of days is calculated as:

$$\Delta\eta_T = (\frac{d\eta}{dT})(\sum_{i=1}^{n} T_{cell} - T_{STC})/n \quad (2.1)$$

The details of other parameters involved in the above equation are discussed in the following sections.

2.2.1.1 Solar PV module temperature (T_{mod})

Solar PV cell temperature (T_{cell}) is calculated through the Module operating temperature (T_{mod}), which was computed using the Eq. (2.2) provided by the National Renewable Energy Laboratory (King e al, 2004)

$$T_{mod} = G_{POA} \times \{e^{(a+b*WS)}\} + T_a \quad (2.2)$$

G_{POA} is the solar irradiance at the plane of an array; e is Euler's constant (e=2.71), WS is the speed of wind (m/sec) at 10m height, while a and b are empirical constants, which depends on the type of solar PV arrangements (ground/roof–mounted), and were obtained from King et al, (2002). Lastly, the near–earth surface temperature (2m) was taken as T_a, which was obtained from GSWP3 and shown in Fig. (2.3).

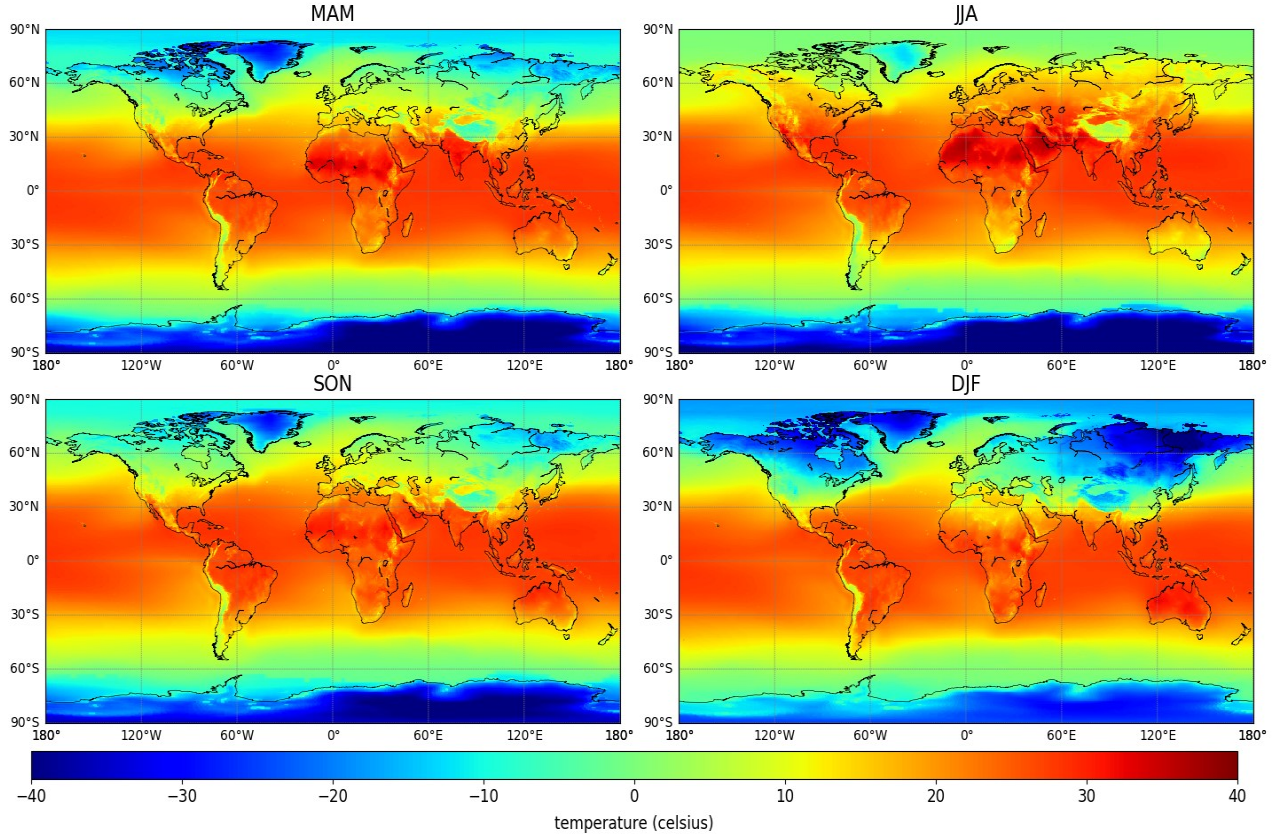

Figure 2.3: Long terms daily mean (2001–2014) seasonal temperature at 2m height.

2.2.1.2 Solar PV cell temperature (T_{cell})

Then, the T_{cell} is computed by multiplying ΔTcnd to the ratio of G_{POA} and G_{STS}, which is then added to the T_{mod} as presented in Eq. (2.3)

$$T_{cell} = (\frac{G_{POA}}{G_{STC}}) \times \Delta Tcnd + T_{mod} \quad (2.3)$$

G_{STC} is the reference irradiance for the correlation and it is usually constant at 1,000 W/$m^{2.}$

Whereas ΔTcnd is the conduction temperature drops available with King et al, (2004). Solar PV modules are additional described by a power–temperature coefficient (dη/dT). We used Monocrystalline silicon (c–Si) modules in our study, since this technology has the maximum share in the market as mentioned by Płaczek–Popko. (2017). For c–Si, dη/dT= −0.45%/°C and projected output power of the solar PV module at STC (SWR=1000W/m^2, T_{STC} =25°C) (Ascencio–Vásquez et al, 2019). Then, $\Delta\eta_T$ for every season with n number of days in a season is calculated by taking the seasonal mean of daily temperature correction at every ith day as:

$$\Delta\eta_T = 0.45(\sum_{i=1}^{n} T_{cell} - T_{STC})/n \quad (2.4)$$

Out of available 114 years of data with GSWP3, we used fourteen years (2001–2014) in our analysis to harmonize it with other datasets.

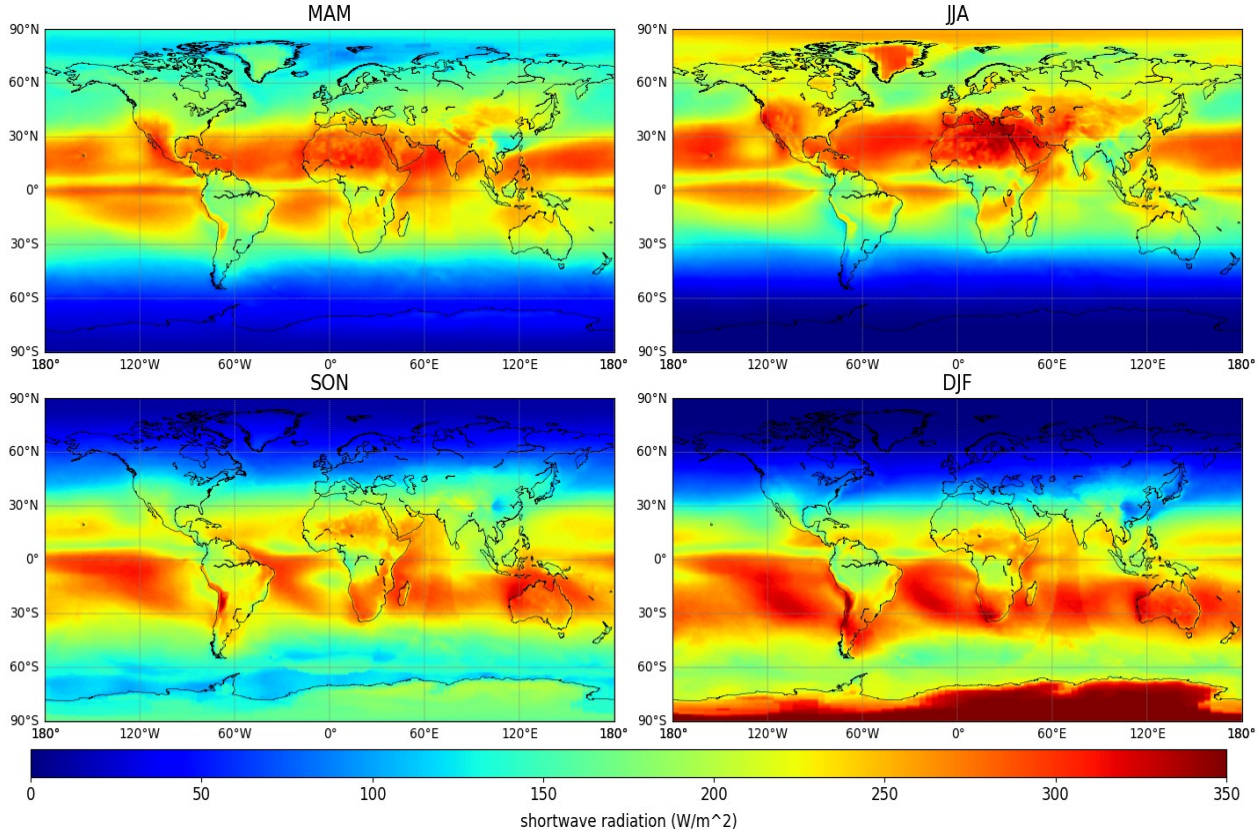

Figure 2.4: Long terms daily mean (2001–2014) seasonal shortwave radiations near the earth surface.

2.2.2 Decrease in solar PV cell efficiency due to dust deposition

The reduction in solar PV cell efficiency due to the accumulation of dust particles ($\Delta\eta_D$) is calculated using Eq. (2.5) proposed by Principe and Takeuchi, (2018), where they used AOT (Fig. 2.5) along with a constant value of 0.3 as a transmittance loss (K_L) from dust as reported by Sayigh. (1978). However, transmittance losses due to the dust covers vary with the changing solar PV module tilt–angles (Sayyah et al, 2014). Therefore, K_L for varying tilt angles is calculated by applying the curve fitting technique to the experimental data available with Elminir et al, (2006) and presented in Fig. (2.6).

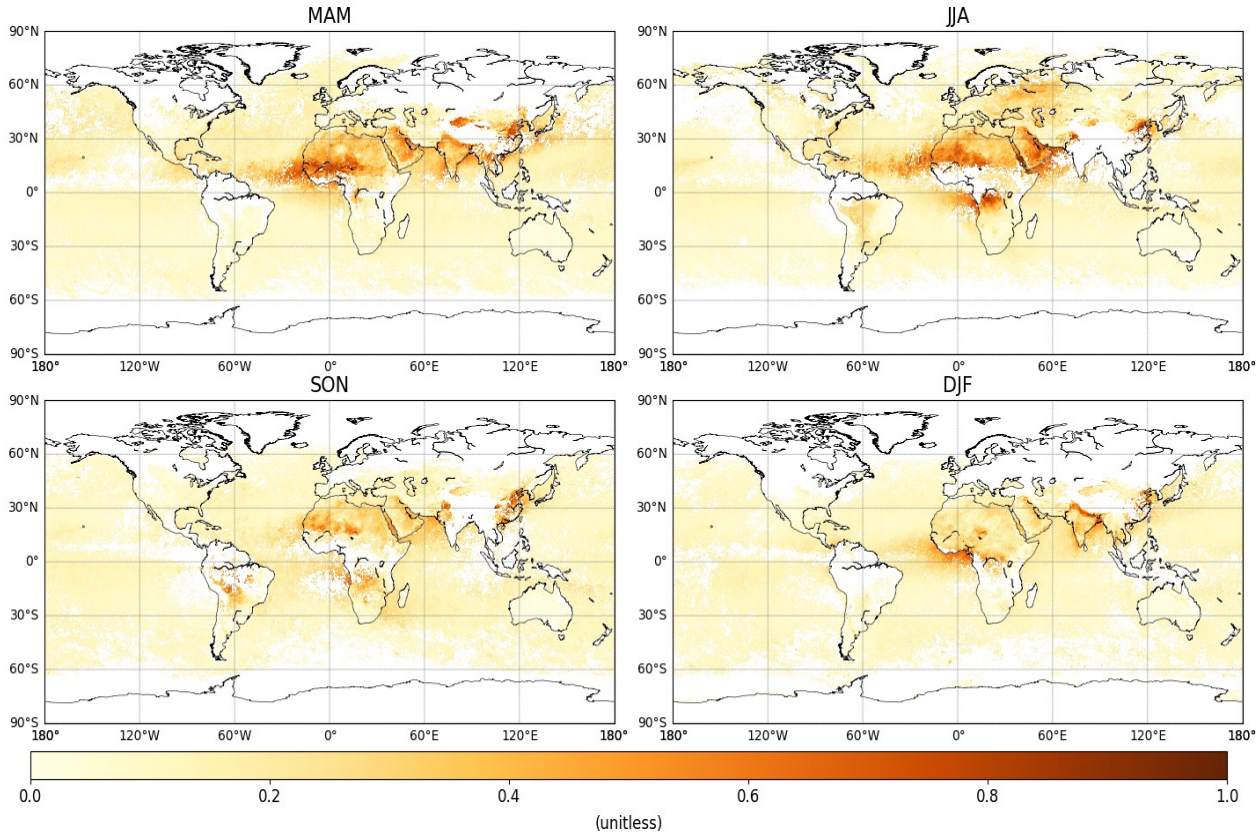

Figure 2.5: Long terms daily mean (2001–2014) seasonal Aerosol Optical Thickness.

The daily Aerosol Optical Thickness (AOT) from the Moderate Resolution Imaging Spectroradiometer (MODIS) at a resolution of 0.5° from 2001–2014 is used as a proxy of dust deposition (Levy et al, 2013). In Eq. (2.5), m_d is the dust mask, either 0(AOT ≤0) or 1(AOT >0) for the non–dust days and those days with dust, respectively. Similarly, m_r is the rainfall mask, which is either 1 or 0 for the days with no rain and with rain, respectively. This technique, therefore, considers the natural cleansing effect on PV modules through rainfall. The threshold

for cleaning is obtained from Kimber et al, (2006). Then, for each season with n number of days, $\Delta\eta_D$ is calculated by taking the seasonal mean of daily dust correction at every ith day as:

$$\Delta\eta_D = K_L(\sum_{i=1}^{n} m_{di} \times m_{ri})/n \quad (2.5)$$

Where

$m_{di} = 0,\ if\ AOT < 0.2$ Otherwise AOT

$m_{ri} = 0,\ if\ rainfall > 5mm/day$ Otherwise 1

$m_{di} = soiling\ mask\ \ \&\ m_{ri} = rainfall\ mask$

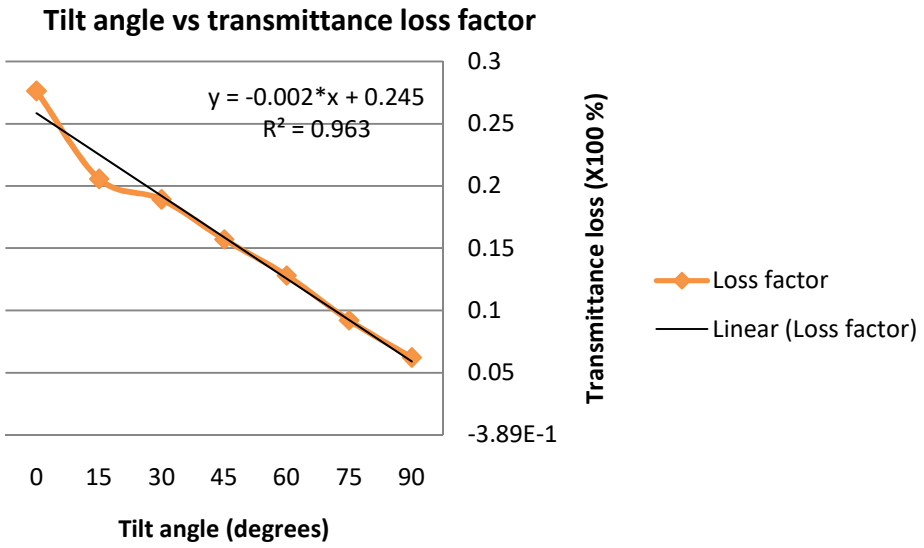

Figure 2.6: Transmittance Loss Factor ($K_{L)}$ at optimum tilt angles is calculated by applying the curve fitting technique to the experimental data available with Elminir et al, (2006).

Later, using optimum tilt angles from Jacobson and Jadhav (2018), K_L is calculated globally.

2.2.3 Decrease in solar PV cell efficiency due to snow covers

2.2.3.1 Snow depth calculations

Snow Effects the Solar PV cell efficiency by blocking the incoming radiations. $\Delta\eta_S$ After that, $\Delta\eta_S$ is derived from the snow parameter, snow depth (Sdp). Observation–based daily Snow

water equivalent (SWE), from the National Snow and Ice Data Center (NSIDC) along with daily snow cover fractions (SCF) from MODIS are used to compute the values of Sdp using Eq. (2.6). The MODIS products showed good agreement with the station data, ranging from approximately more than 80% (Simic et al, 2004). SWE and SCF are shown in Figures 2.6 and 2.7 respectively

$$Sdp = \frac{SWE \times SCF}{\rho} \tag{2.6}$$

Where: Sdp = snow depth (cm); SWE = Snow Water Equivalent (cm), SCF = Snow Cover Fraction (0–100), and ρ is snow density (g/cm3)

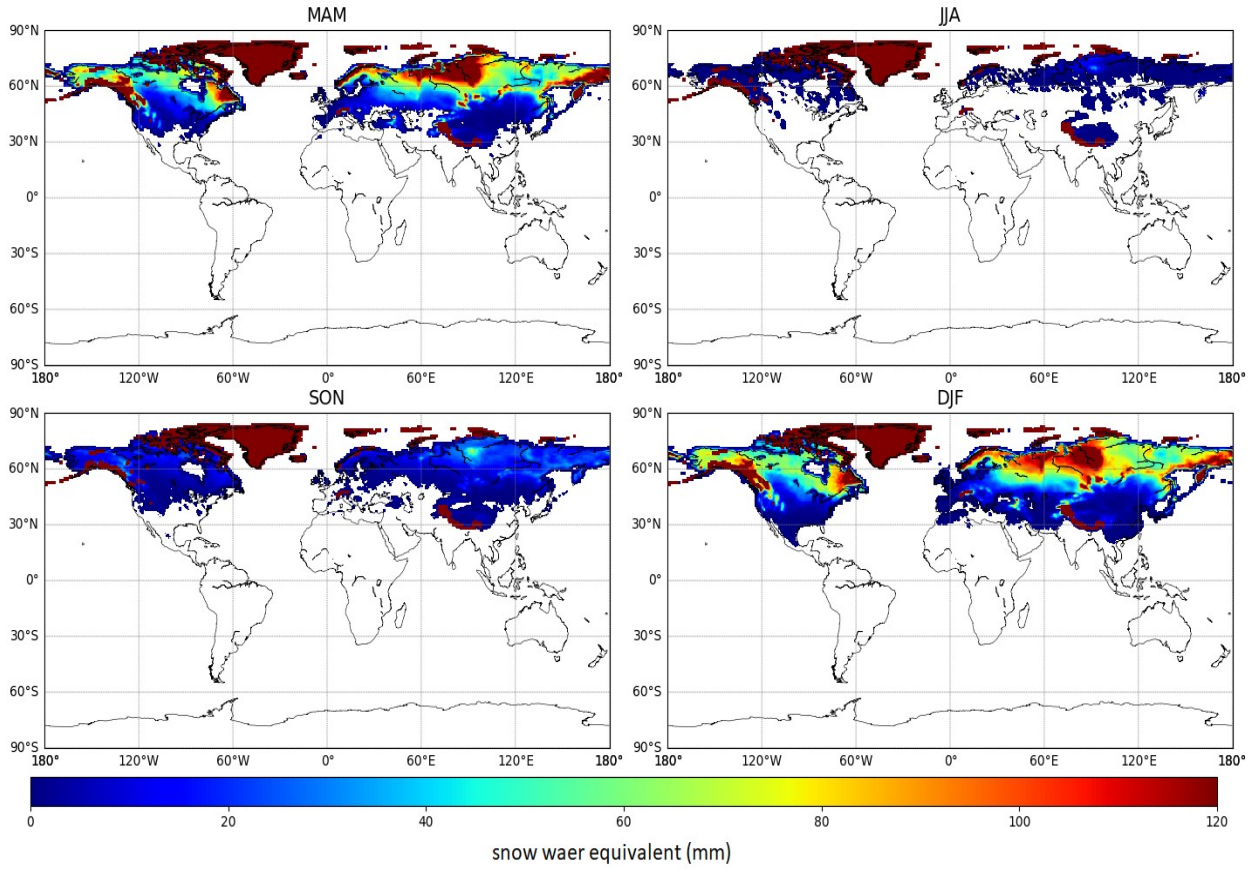

Figure 2.7: Long terms daily mean (2001–2014) Snow Water Equivalent (mm).

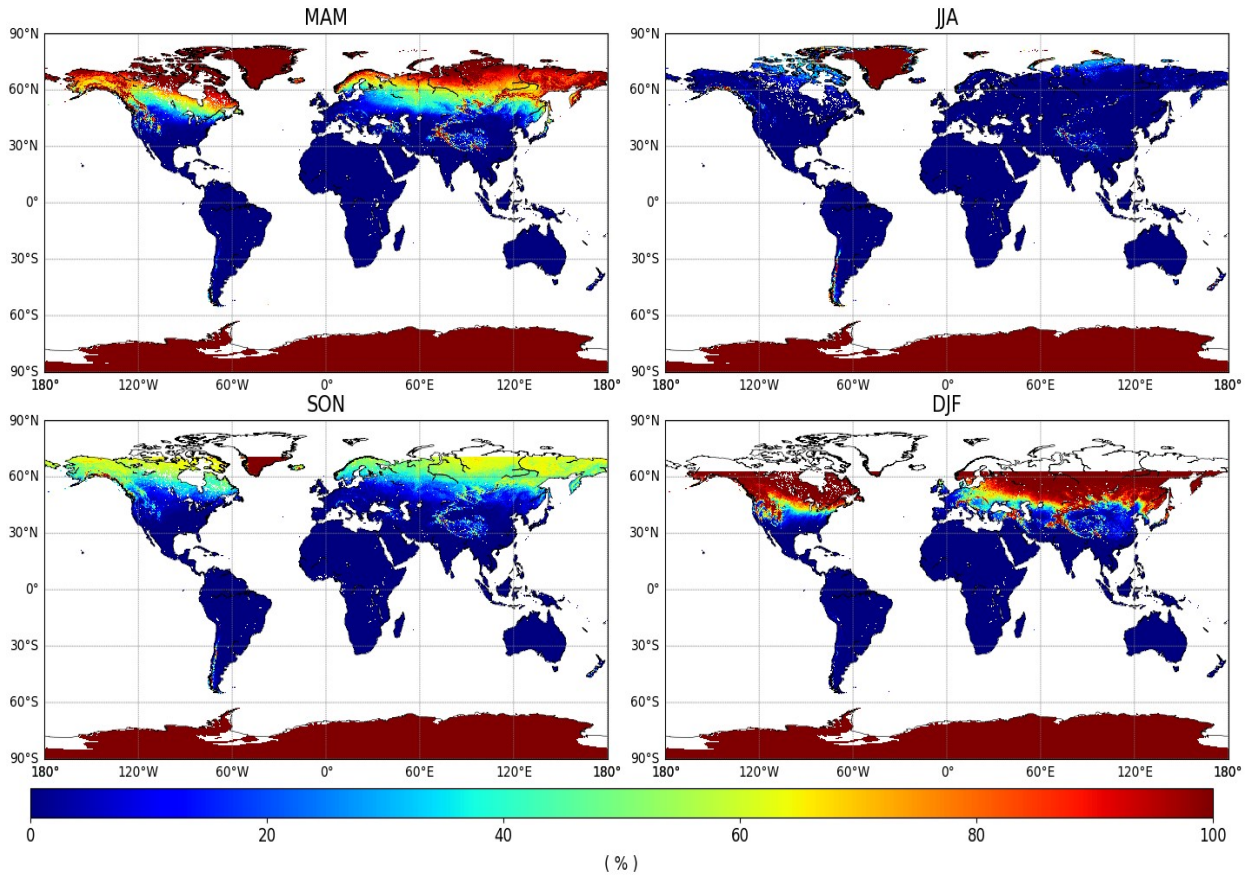

Figure 2.8: Long terms daily mean (2001–2014) Snow Cover Fraction (%).

2.2.3.2 Snow melts from solar PV panels

The snow accumulation on solar PV module is a function of its fixation as snow is believed to slide from the surface at higher fixation angles as Powers et al, (2010) reported that the depth of snow is less for higher angles which helps in snow sliding. Likewise, snow melting from solar PV surface is a function of solar PV module temperature and incoming SWR (Rahmatmand et al, 2019). A simple methodology that considers mass balance is used to calculate the snow melting from solar PV surface for optimum tilt–angles and presented in Fig. (2.9).

Snow melts only start when $T_m > 0°C$. T_m is calculated using the Eq. (2.2) provided above, which utilizes ambient temperature (T_a) and incoming SWR etc. The ds and dm correspond to the depth of snow and melt layer respectively, calculated by Wanielista. (1997). Whereas, Darcy's Law is used to calculate the runoff for melting snow and corresponding snow-

mass through the melt density. A snow density value of 0.3 g/cm^3 is used for fresh snow; though, 0.45 g/cm^3 are used for an older snow (UBC. 2018).

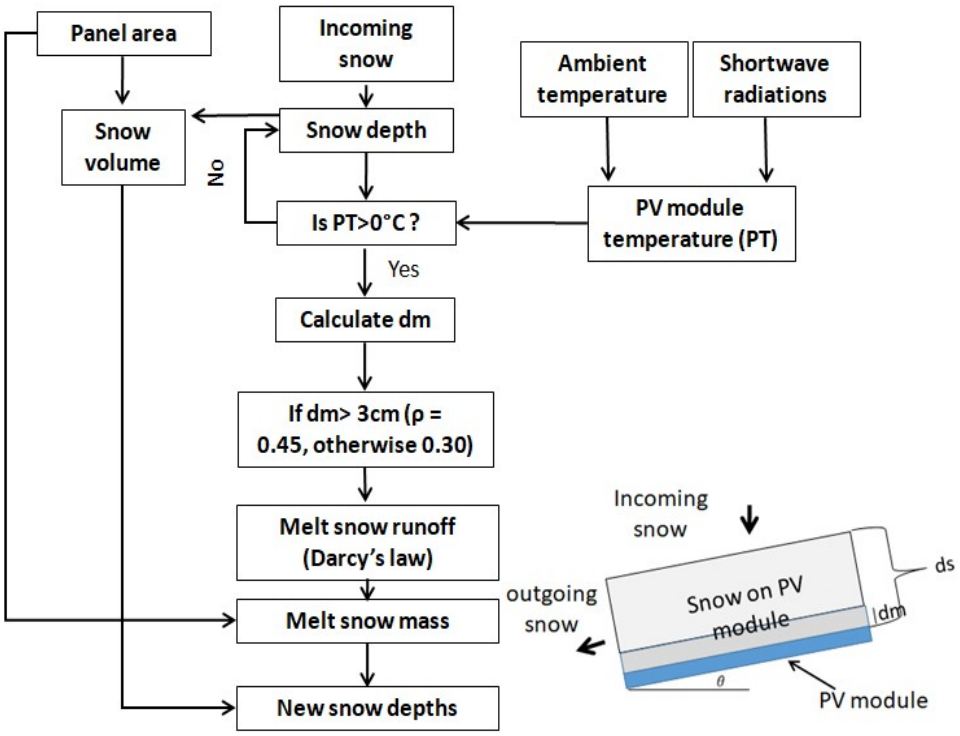

Figure 2.9: Snow melting from solar PV surface considering the mass balance is used to calculate the snow melts from solar PV surface for optimum tilt–angles and module temperature (P_T)

2.2.3.3 Decrease in solar PV cell efficiency

The melt snow calculated above is subtracted from Sdp to have the actual snow values for solar PV panels. Next, $\Delta\eta_S$ for every season with n number of days is calculated by taking the seasonal mean of daily snow corrections at every ith day as:

$$\Delta\eta_S = \sum_{i=1}^{n} \Delta\eta_{s,i}/n \qquad (2.7)$$

As the decrease in cell efficiency is directly proportional to the decrease in sunlight transmittance (Perovich. 2007). Using a similar technique, Eq. (2.8) is derived from an exponential curve fitting for snow depth and transmittance (Fig. 2.10).

$$\Delta\eta_{S,i} = 1 - 0.8173 \times e\,(-0.21 \times Sdp) \quad (2.8)$$

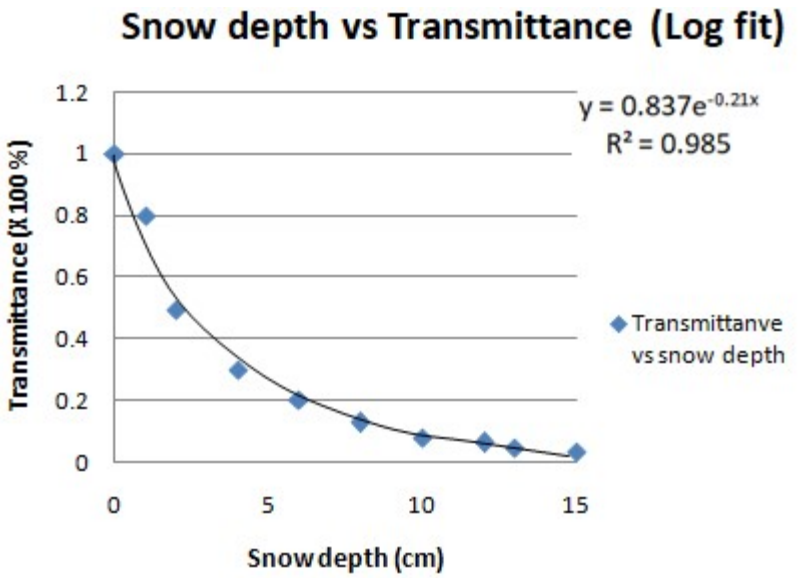

Figure 2.10: Curve–fitting technique for transmittance and snow depth applied to the experimental data available with Perovich. (2007).

It is seen that the transmission approaches zero approximately when Sdp is more than or equals to 12 cm.

2.2.4 Final solar PV cell efficiency

The final solar PV cell efficiency (η_f, %) available is estimated using Eq. (2.9) after incorporating all efficiency reductions calculated above for $\Delta\eta_T$, $\Delta\eta_D$ and $\Delta\eta_S$ respectively. For c–Si PV modules, we used the value of 15% for cell efficiency (η_c) as reported by Tyagi et al, (2013).

$$\eta_f = \eta_c\,(1 - \Delta\eta_T - \Delta\eta_D - \Delta\eta_S) \quad (2.9)$$

Researcher like Green at el, (2003) and Oliver and Jackson (2000) reported different values for η_c (12−20%), for that, we performed sensitivity analysis which will be discussed in a separate section.

2.3 Effect of geomorphologic parameter on solar PV resource

2.3.1 Variations in solar PV module tilt–angle

Solar PV output varies with changing tilt–angles which actually affects the incoming SWR. We used the fixed type (non–tracking) solar PV modules in our study; either fixed to the rooftop or in a solar park (ground–mounted), inclined in a way to face South for maximum power output, as the output of a solar PV system is the function of Sun position (Azimuth and Zenith angles) and the fixation angle of the solar PV module. The fixation angle is taken optimal once the PV system generates maximum energy yield (Palmer et al, 2018). To know the SWR for a tilted array, optimal position and tilt angles are taken from Jacobson and Jadhav, (2018). Then P_{act} is calculated using SWR' (W/m^2), cell area (A_{cell}, m^2) and η_f by Eq. (2.10).

$$P_{act} = SWR' \times A_{cell} \times \eta_f \tag{2.10}$$

Initially we take unit area, 1m^2 in the calculation of P_{act}.

2.4 Performance ratios

A performance ratio (PR) corresponds to the ratio of effective power (P_{eff}) to the theoretical power (P_T). P_{act} is calculated above while P_T is calculated using the fixed cell efficiency ($\eta_c = 15\%$) in Eq. (2.11).

$$P_T = SWR \times A_{cell} \times \eta_c \tag{2.11}$$

Here using SWR' (W/m^2), cell area (A_{cell} = 1m^2) and η_c for cell efficiency described above. P_T is always more than P_{eff} as it does not consider any losses due to the meteorological parameters. However, it is usually not achieved due to the losses mentioned in section 2.2.1, 2.2.2 and 2.2.3 respectively. Then, PR is calculated by just dividing P_{eff} by P_T for all seasons globally.

$$PR = P_{act}/P_T \quad (2.12)$$

2.5 Final solar PV resource

After calculating all parameters like efficiency reductions, P_{act} and PR, final solar PV resource is calculated globally for all four seasons as well as annually using the Eq. (2.13).

$$P' = SR' \times PR \times A_{cell} \times \eta_f \quad (2.13)$$

This final solar PV resource is a function of SWR on a surface inclined at optimum angles, PR, A_{cell} and η_f which does consider for all kind of efficiency reductions related to the meteorological parameters for local environment.

2.6 Solar PV economic analysis

The technical potential of solar PV has been elaborated on before. Such potentials can be discussed individually, as they are not influenced by various other energy choices. However, this is different for the economic potential calculated here; as such potentials cannot be investigated by discarding other contesting energy options, which is outside the scope of this research. As a result, our economic analysis is restricted to the calculation of global gridded cost estimates of various PV schemes and eventually generation of global as well as regional cost supply curves of PV electricity. These curves can later be compared with current cost estimates of conventional electricity generation technologies. The flow chart is presented in Fig. (2.11):

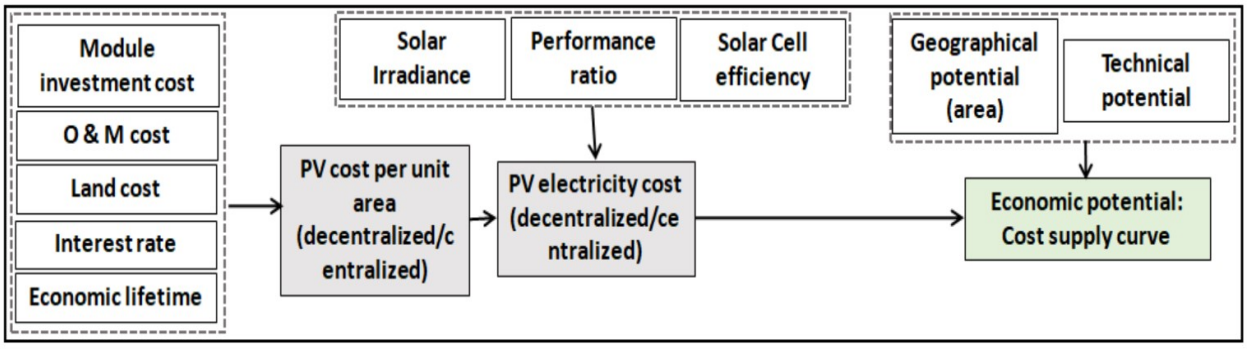

Figure 2.11: Methodology devised to calculate the costs and cost supply curves for centralized and decentralized PV schemes.

2.6.1 Suitable area for solar PV

As solar PV cannot be installed at every place, like on very steep slopes or water bodies, etc. Therefore, one should think about the suitable area as a function of each location. Our technical potential does not consider such geographical limitations and those may be explored. To quantify such geographical limitations, we include a suitability factor (f_i). It shows the portion of the cell i (A_i) available for the fixation of solar PV modules and is expressed as:

$$A_{a,i} = f_i \times A_i \tag{2.14}$$

F_i is calculated independently for both centralized and decentralized schemes as the available area is exposed to different constraints for both systems. So, we used two different approaches to calculate such areas.

2.6.1.1 Suitability factor for centralized schemes

Centralized systems are mostly installed on the land surfaces in the shape of medium–to big solar parks. Therefore, the available area highly depends on various competing land–use choices, like urban area, agricultural land, grassland, etc. A dynamic system type approach is not included in this research, as data for the largest part of contesting land use options do not exist at such a detailed level compulsory for an extensive assessment. Instead, based upon literature, we introduced suitability factors for various land–use types, and are shown in Table 2.2. These factors/ fractions do consider the competition among land–use types. For land–use types, we used the dataset provided by the European Space Agency (ESA) at a spatial resolution of 300m and considering 19 land–use types. Various land–use types for 2015 are shown in Fig. (2.12).

For each land–use type, the fraction (unitless) for a suitable area for solar PV centralized scheme as well as total area (km^2) is calculated using the information provided in Table 2.2 below. Important areas like agricultural ones have fewer fractions (1% of total area) for solar PV; whereas, open and redundant areas like the desert and extensive grasslands etc. have more fractions (5% of total area) towards solar PV fixation.

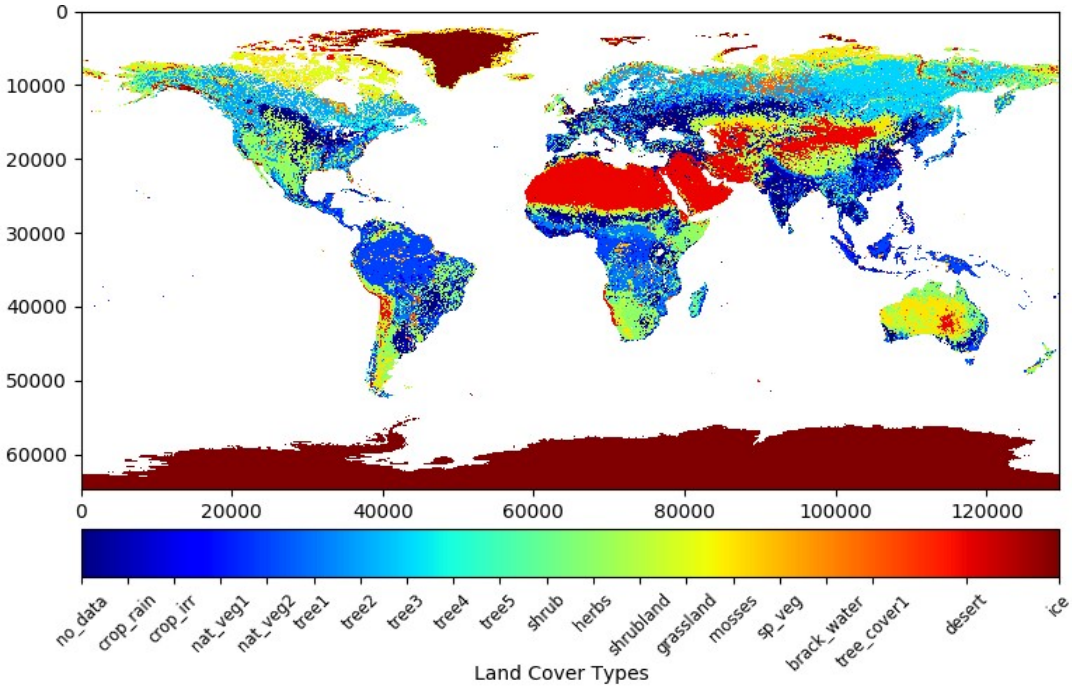

Figure 2.12: Global land–use/land cover types containing 19 land–use classes for 2015 (ESA).

Table 2.2: The supposed suitability factors obtained from values suggested by Sørensen. (1999), the area of different land–use types as a fraction of total area with similar land–use types.

Sr. No	Land use type	Land–use suitability factor f_i (%) for centralized scheme	Suitability factor f_i (%) for decentralized scheme
01	Urban area	0	As per calculations
02	Bioreserve	0	0
03	Forest	1	0
04	Agriculture	1	0
05	Shrubland	1	0
06	Extensive grassland	1	0
07	Desert	5	0

2.6.1.2 Suitability factors for decentralized schemes

Decentralized systems are installed on roof–tops, parking lots and utilities nearby. So, the total on hand area for off–grid system is mostly related to the roof–top areas and neighboring settlements. For such an area in a grid cell, we needed a global database of roof–tops for residential and other main buildings types. To date, just two studies have analyzed the roof–top area per person for PV installation, and they include, IEA/OECD. (2001a) and Alsema and Brummelen, (1993). They gave estimates of the suitable building (structure) roof–top areas (km^2), based upon roof–top surfaces at buildings like residences, offices and industries at country scale for all European countries (OECD), and also the study conducted by IEA for Australia, Canada and Japan etc. The whole area fit for PV installation is limited by architectural constraints (shading/ historical features etc.) as well as by sun orientation reasons (roof orientation etc.). By combining the above–mentioned suitability factors in comparison to the floor area provides the utilization factor; approximately, 0.15 for parking lots and 0.40 for roof–tops are used. From such utilization factors and the floor area per person obtained from several sources, the appropriate roof–top area was estimated. The IEA study estimated the available roof area for solar PV from the floor area/capita of buildings, while Alsema and Brummelen, (1993) directly used statistics for average roof–top areas. Both studies were limited in terms of the number of countries etc. However, in our analysis, we have to imitate the results to the entire world. We followed the technique by Hoogwijk. (2004) that relates the available area to income (GDP/capita), as the increase in GDP (economy) results in an increase in size and number of settlements, as well as associated utilities. In Fig. (2.11), the results of both studies for the existing area per capita against the GDP per capita are shown. It can be realized that there is not a significant relationship between the calculated existing PV rooftop area and the GDP/capita. However, due to non–existence of such global datasets, we adopted the technique as used by Hoogwijk. (2004) which fitted the data from the IEA, and also from Alsema and Brummelen, (1993) using a logarithm function. This results in a weak correlation with the GDP and the presented data points that has a form of power law (Fig. 2.13). Per capita rooftop for solar PV ($RT_{c,i}$) (m^2/cap) in a grid cell (i) as a function of the GDP per capita is shown as below:

$$RT_{c,i} = 0.06 \times GDP_{cap}^{0.6} \tag{2.15}$$

Using this approach we admit that we may overestimate solar PV available areas for regions with high GDP like parts of China, Japan, and the USA, etc. Consequently, this will

result in an overestimation of solar PV technical potential for the decentralized schemes by two to three times as of old studies. However, for most areas, PV technical potential is still in line with the IEA study.

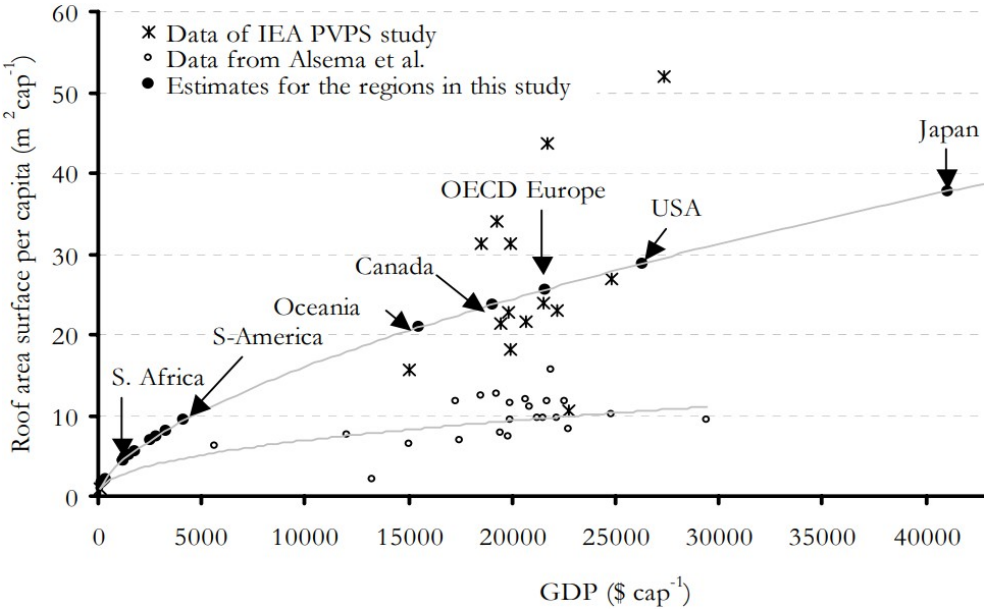

Figure 2.13: Rooftop area per capita available for decentralized PV schemes as provided in Alsema and Brummelen, (1993) and IEA. (2001a) is plotted alongside the GDP per capita for 1995 (Hoogwijk. 2004).

Hoogwijk. (2004) used statistics for 1995. However, we devised results based upon the latest population and GDP statistics from CGER, NIES, datasets (Murakami and Yamagata, 2016. Spatial plots for population, GDP, and area per person are provided in Fig. (2.14), Fig. (2.15), and Fig. (2.16) respectively.

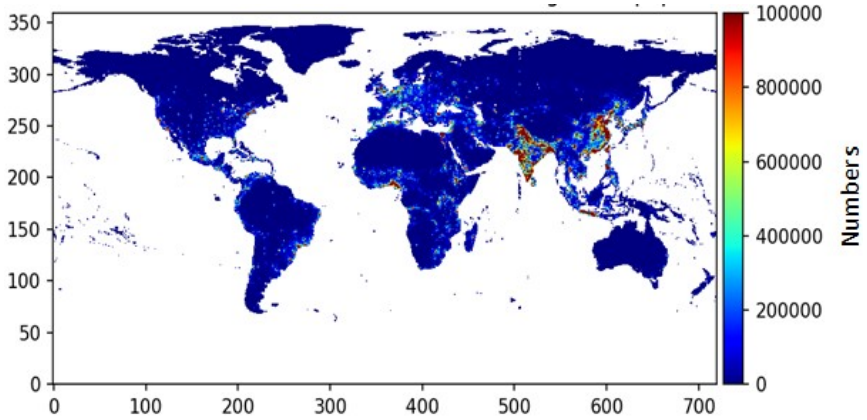

Figure 2.14: Global gridded population (numbers) for 2015. Higher population is seen for Western China and South Asia.

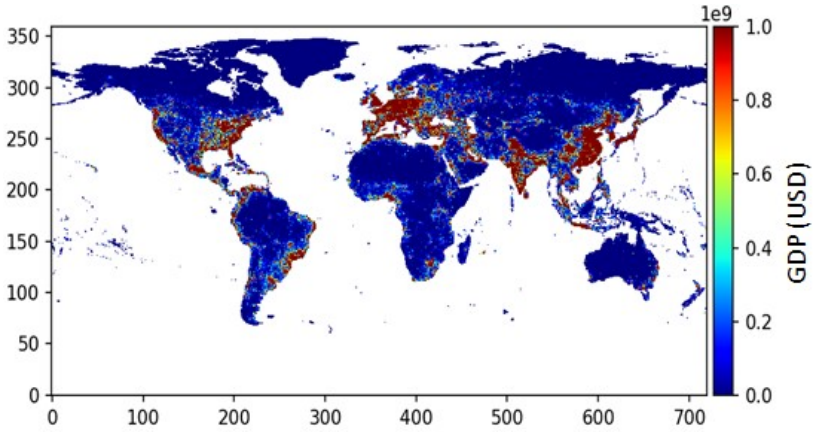

Figure 2.15: Global gridded GDP (USD) for 2015. Higher GDP is seen for Western USA, Europe, The Middle East, Western China, South Asia, and Japan.

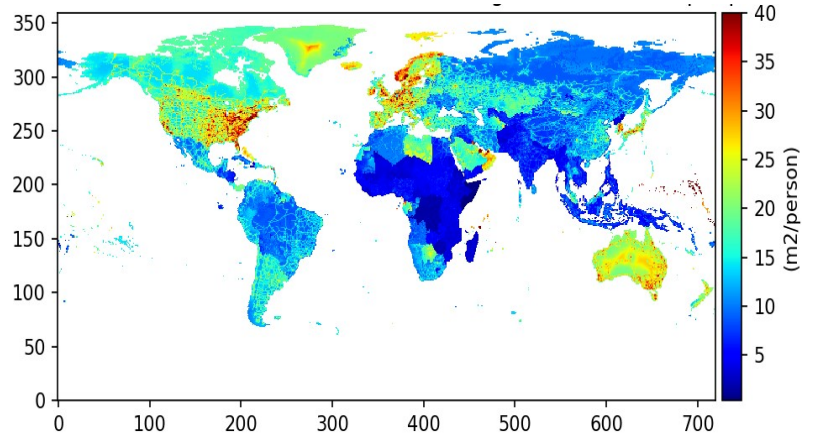

Figure 2.16: Global gridded area per person for 2015. Higher areas are seen for higher GDP/cap regions like for Western USA, Europe, The Middle East, Western China, South Asia, Australia, and Japan.

2.6.2 Cost estimation of solar PV electricity

The Levelized Cost of electricity generation of solar PV scheme is based on various parameters involved in it. It mainly includes costs involved in Operation and Maintenance (O&M) as well as turnkey investments. A terminology Balance of System (BOS) costs is introduced which is later added to a PV module costs to make up the total investment costs. The investment cost of an off–grid system is relatively low as it can often be fixed on rooftops, major support structures, fences, and on top of parking lots by avoiding costs involved in land acquisition (Oliver and Jackson, 2001). For on–grid (centralized) schemes, in contrast, land acquisition costs and cost involved for support structure have to be integrated. This mainly

depends upon the purpose or demands of other land use options like agricultural use, lawns, etc. We did not consider such competition among land–use types as this would need to run a dynamic economic land–use model. As a substitute, we considered the land rental costs available in the literature. For croplands, the non–irrigated land rental price paid by farmers vary from 25–570 $/ha/yr (FAO. 1997), while some other studies (Faundez. 2003; van den Broek et al, 2000) mentioned such costs vary from 0–840 $/ha/yr. As most of them did not provide any linkage between cost and quality of the land, hence, we are not able to figure out a correlation between land rental price and soil types and its quality. In addition, no relationship was seen for population density, GDP and land rental costs. Therefore, a universal figure of 200 $/ha/yr is used as a global average land rental price in our analyses. The PV electricity generation cost ($ kWh^{-1}) in a grid cell (i) can be estimated as below:

$$Cost_i = \frac{(a\times (M+BOS))+(C_{O\&M}\times(M+B\quad))+L}{p_i} \tag{2.16}$$

Where a (y^{-1}) is known as annuity factor, M is the investment cost ($/ m^2), BOS is the balance of system cost ($/ m^2), $C_{O\&M}$ is the annual operation and maintenance costs ($/ m^2 /y) and L is the annual land rental cost ($/ m^2 /y). Lastly, p_i is the explicit yearly electricity yield ($kWh/m^2/y$) of a cell (i) and it is defined as the technical potential of a cell in a unit area (m^2).

The PV module costs (M) have declined with time, i.e., 6 $\$Wp^{-1}$ in 2002 (solarbuzz. 2002) to 0.70 $/KWp in 2020 (Fthenakis. 2009). However, here we assume inferior module prices for a centralized scheme than for decentralized modules. In conclusion, for 2015, we assume a 1.25 $/KWp price for the centralized scheme and a slightly higher price (1.4 $/KWp) for decentralized systems. As per Hoogwijk. (2004), the BOS costs (BOS) are assumed to be ~70% of module price, while, $C_{O\&M}$ is taken as 3% and 5% of total investment costs for centralized and decentralized systems respectively. It should be kept in mind that BOS costs do not consist of grid connection, but do contain fixing costs.

2.7 Water scarcity assessments

In the past, many water stress indices (WSI) have been developed to assess various kinds of water scarcity regionally and globally. We dealt with physical water scarcity which is mainly due to the excessive withdrawals as compared to the available water. The approaching section describes the WSI used in our analysis.

2.7.1 Withdrawal–to–availability

We used the novel water stress index, withdrawal–to–availability (WTA) by Raskin et al, (1997) to map the current and future water scarcity by indicating various stress levels causing water shortages and environmental harm to river basins across the globe. Withdrawal is the actual amount of freshwater drawn from surface water bodies like rivers, streams, reservoirs, and groundwater aquifers. While, demand is the potential freshwater need for any purpose, irrigation, industry, or domestic ones. This index is also named WWR by Hanasaki et al, (2008) and it is calculated as the ratio of annual withdrawal (W) to annual water availability (A) using Eq. (2.17)

$$WTA = \frac{\sum_{i=1}^{365} W_i}{\sum_{i=1}^{365} A_i} \tag{2.17}$$

Raskin et al, (1997) proposed that for WTA > 0.4 (withdrawals of more than 40% of the natural discharge), an area suffers high water stress and with WTA > 0.8 extreme water stress. Although WTA > 0.4 is far less than WTA > 0.8, still it can cause severe environmental damage and puts water users under stress (Alcamo et al, 2000). Similarly, 0.2> WTA < 0.4 shows medium scarcity level and WTA< 0.2 stands for less or no water scarcity. It is still a well–known indicator as mentioned by Oki et al, (2001) and also by Vörösmarty et al, (2000) applied either on river basin scale or national scale. However, there may be a limitation of the WTA–ratio that it uses yearly mean values, hence seasonal stresses or shortages are overseen. Normally it does not account for return; meaning that water is withdrawn, used, and returned into the water cycle mostly changed to rivers and groundwater, e.g. through outflow from thermal power plant cooling, drainage fields, and sewage treatment plants. Physical changes of return flow may include changes such as higher temperatures while performing cooling or chemical changes like pollution with heavy metals etc.

We considered river discharges as a main source of freshwater availability (A) and assumed that water used after cooling is not available to the downstream users because of being polluted and bearing very high temperatures. Similarly, withdrawal (W) accounted for a sum of irrigation sector, industrial sector, and domestic sector water abstracted from rivers. The river discharge along with other sectoral discharges (irrigation, industry, and domestic) data was obtained from The Inter–sectoral Impact Model Intercomparison Project 2b (ISIMIP2b) for 2001 to 2015 with 0.5° resolution. ISIMIP is a community–based climate–impact modeling project aimed at contributing to a quantitative and cross–sectoral combination of the differential impacts of climate change, and their related uncertainties. It proposes a unified framework for cross–sectoral and cross–scale modeling of climate change impacts. The main objective of ISIMIP is to add to the wide–ranging (cross–sectoral) perceptive of the impacts of politically as well as scientifically–relevant climate–change circumstances.

We used two Global Hydrological Models (GHMs) namely H08 (Hanasaki et al, 2008), and WATERGAP2 (Alcamo et al, 2003) along with two Global Climate Models (GCMs), the Hadley Centre climate model (HadGEM2–ES, Jones et al, 2011) and Model for Interdisciplinary Research On Climate (MIROC5, Watanabe et al, 2010) in our study and took the ensemble means of their outputs. The purpose of using ensemble means of more than one model and GCM is to remove any uncertainty or limitations available within a single model.

2.8 Electricity generation

Electricity production is one of the processes, consuming maximum water worldwide. It is the main part of IWW and roughly adds half to the total IWW withdrawals. As per IEA (IEA. 2017), TEPPs are the major component of electricity generation across the globe and supplies 80% of world's electricity. They withdraw massive amount of fresh water globally and are critical to be studied in context with water scarcity conditions.

We processed newly published Global Power Plant data from World Resources Institute (WRI. 2018). The Global Power Plant Database is a complete, open source power plants global database. It unifies power plant data to make it simpler to explore, compare and map insights for any kind of investigation. This covers around 30,000 power plants from many countries (164)

and carries thermal plants (e.g. coal, oil, gas , nuclear, biomass, and geothermal etc.), and also renewables (e.g. hydro, wind, and solar). Every power plant is geo–referenced and entries include information on power plant capacity, production, ownership, and type of fuel etc. As we are mainly dealing with TEPPs, so we discarded non–fossil fuel power plants.

TEPP available in the above dataset includes four types, Coal, Oil, Gas and Nuclear (Nucl). We processed them separately as their water use intensities (WUI) are linked with the generation technologies, i.e. coal, gas etc. due to scarce data available per grid (0.5°) as well as country scale, we first converted existing point based power plants data to the regional one. Globally, we used 17 sub–regions as mentioned in AIM, an integrated assessment model. Figure (2.17) shows the raster for regional distribution used in our analysis on global scale. The reason to use such coarse resolution is because of the availability of WUI on global scale for all those regions (Davies et al, 2013)

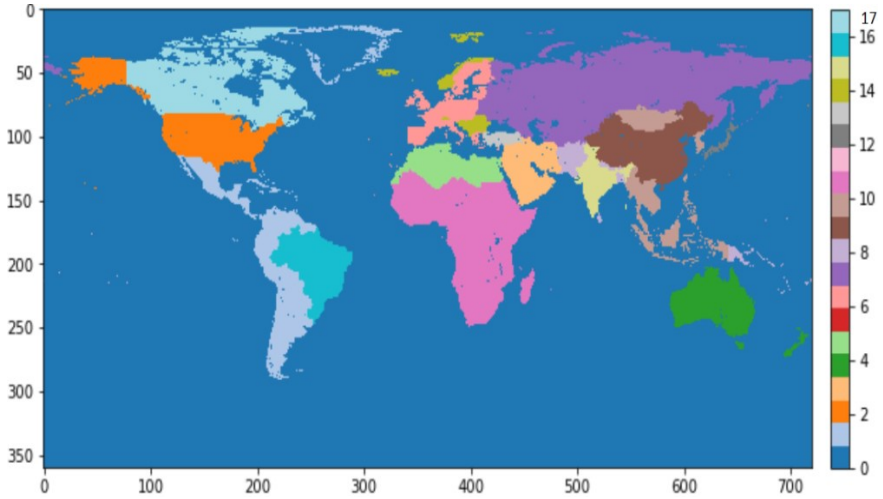

Figure 2.17: Raster regional map for AIM classifications (source: author).

The raster map shown above is used to convert point based power plants data to the 17 regions based upon generation types. The energy production is in Gigawatt hours (GWh), which remains the same after conversion. However individual power generations for similar plants, based upon generation technologies, are added up to have the final generation inside a region for each individual technology.

The simple methodology to add up similar kind of electricity used Eq. 2.18 and flow chart is shown in Fig. (2.17)

$$Elec_{coal,i} = \sum_{i=1}^{n} (Elec)_{coal,i} \quad (2.18)$$

$Elec_{coal}$ is electricity generation from coal power plants, n is total number of power plants for similar technology in a region, r.

Similarly, all four technologies are added to have regional electricity generation values in GWh.

Table 2.3: Regional classifications used in AIM model.

Region number	Name	code	Region number	Name	code
01	Rest of Latin America	XLM	10	Rest of East and South East Asia	XSE
02	Canada	CAN	11	Other Africa	XAF
03	The Middle East	XME	12	Japan	JPN
04	Oceania	XOC	13	Turkey	TUR
05	North Africa	XNF	14	Rest of Europe	XER
06	EU25	XE25	15	India	IND
07	Former Soviet Union	CIS	16	Brazil	TUR
08	Rest of Asia	XSA	17	The United States	USA
09	China	CHN			

2.8.1 Cooling technology shares

Cooling system shares were compulsory for all electricity technology types in each AIM region for the base year, 2015. But, the essential data was scarce; like the one by World Electric Power Plants Database (Platts. 2011) applied by Vassolo and Döll, (2005) to calculate global water use by the electricity sector contained cooling system information for just 11% of its provided TEPPs. Also, electricity production inventories by technology do not contain the details of cooling systems, like IEA, (2010). Cooling system share in the US, Australia, and also for China were existing in the literature; shares in all remaining regions were calculated by Davies et al, (2013) as demonstrated here. First, shares for dry cooling were set for each region. Second, regional shares of seawater–based OTC flow systems were allocated. Third, using literature, region wise electric–sector water withdrawal estimates were established. Lastly, region–specific

shares of OTS and WTC cooling systems were estimated so that the addition of every region's electricity sector water withdrawal is in line with the literature–based calculations. The region wise shares from Davies et al, (2013) are enlisted in Table (2.4). These estimates were developed for base year 2005 and we used similar proportions for our base year, 2015, due to lack of any other consistent and reliable information regarding TEPPs cooling shares globally. Also, regional names are after their study.

Table 2.4 Cooling system shares (%) for various regions for thermoelectric production technologies in 2005 (Davies et al, 2013)

Region	Sea[a]	Coal			Other fossil/bio			Combined cycle			Nuclear		
		1-thru	WT	Dry	1-thru	WT	Dry	1-thru	WT	Dry	1-thru	WT	Dry
USA[b]	30	39.1	48	0.2	59.2	23.8	0	11.6	76.7	10	38.1	43.6	0
Canada	10	71	29	0	71	29	0	71	29	0	71	29	0
Western Europe	20	27.7	69.6	3	27.7	69.6	2.7	27.7	69.6	2.7	27.7	72.3	0
Japan	97	90	6.5	3.5	90	6.5	3.5	90	6.5	3.5	100	0	0
Australia & NZ	66	36.8	56.3	6.9	100	0	0	49.9	50.1	0	0	100	0
Former Soviet Union	10	37.4	62.6	0	37.4	62.6	0	37.4	62.6	0	37.4	62.6	0
China[b]	13	20	64.9	8.1	20	64.9	8.1	20	64.9	8.1	20	73	0
Middle East	96	60	38.2	1.8	60	38.2	1.8	60	38.2	1.8	60	40	0
Africa	30	12	76	12	12	76	12	12	76	12	24	76	0
Latin America	30	18	77.9	4.1	18	77.9	4.1	18	77.9	4.1	18	82	0
Southeast Asia	87	75	21.5	3.5	50	46.5	3.5	50	46.5	3.5	95	5	0
Eastern Europe	10	34.5	65.5	0	34.5	65.5	0	34.5	65.5	0	34.5	65.5	0
Korea	97	20	76.5	3.5	20	76.5	3.5	20	76.5	3.5	100	0	0
India	30	47	49.5	3.5	47	49.5	3.5	47	49.5	3.5	47	53	0

2.8.2 Water use intensity

There are various studies about the WUI of each energy source. Macknick et al, (2011) provided the least, median, and highest WUI, while Kyle et al, (2013) utilized median WUI obtained from Macknick et al, (2011), including some adjustments to earlier estimates of water use by electricity sector. Kyle et al, (2013) found that the WUI of coal, combined cycle integrated coal gasification, and the natural gas power plants fitted with Carbon Capture and Storage (CCS) technology were around 20 to 100% higher than the plants without CCS technology. However, they did not consist of the WUI of oil, gas, and biomass power plants having CCS. But Davies et al, (2013) assumed that the intensities of oil, gas, and biomass power plants were ~30% more than the plants without CCS. The WUI of CCS has more uncertainty, as

CCS is a novel technology and it is not extensively used. Therefore in our current analysis we did not consider CCS technology

In TEPPs, water is mainly used for cooling. TEPPs with cooling systems have the maximum impact on water use for a provided category of thermal energy source (IEA. 2012), and the divisions of types of cooling system in use are equally important when calculating electricity generation water use. We will consider mainly two kinds of cooling technologies, OTC and WTC system; because most of the power plants across the glove use one of these two cooling systems (Clarke et al, 2007). Dry cooling systems don't use water and are mostly valuable in water–stressed areas. Due to the inconsistencies in WUI mentioned above, we used median of WUI values from Electric Power Research Institute (EPRI. 2002) and were listed in Table 1.1 (section 1.3.3)

2.8.3 Final Fresh water withdrawals

After calculating regional electricity for various technologies, cooling type shares and associated WUI, we calculated the water withdrawn by TEPPs for each region by multiplying total electricity generation with WUI for specific cooling type. As we are dealing with fresh water usage only hence we need to deduct the amount of seawater used in the cooling process. Seawater proportions are high for countries like Japan, Korea etc. who uses bigger proportions for nuclear electricity generation which requires higher water volumes for cooling. Davies et al, (2013) also provided such numbers which were subtracted from total water withdrawals to know the fresh water withdrawals. Flow chart of data processing is shown in Fig. (2.18). First, point based power plants electricity generation data is converted to regional data, using AIM raster regional map. Then, cooling technologies are used to calculate regional shares, which are then multiplied with WUI, and lastly, sea water proportion is subtracted to have final fresh water withdrawals (km^3/yr) for each region.

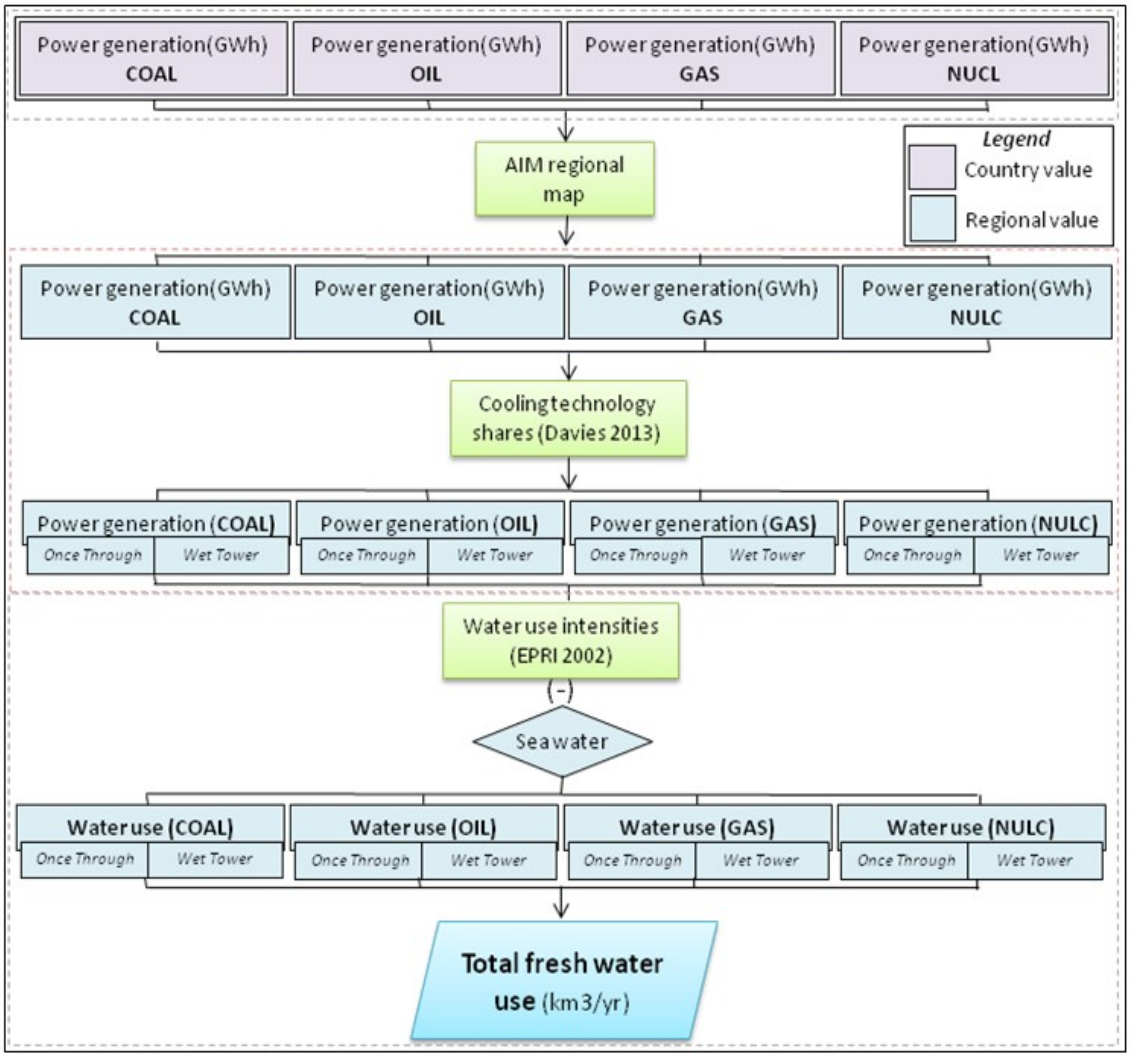

Figure 2.18: Data processing to convert point based power plants electricity generation data into regional data, using AIM raster regional map. Then, cooling technologies are used to calculate regional shares, which are then multiplied with WUI. Lastly, sea water is subtracted to have final fresh water withdrawals (km^3/yr) for each region.

2.9 Energy–water nexus (EW–nexus)

EW–nexus has gone much importance nowadays as both of them are highly inter–connected. Failure to consider their interdependence may introduce vulnerability and misleading towards proper planning and resource allocation. The sub–sections briefly explains about EW–nexus while considering solar PV as an energy input for TEPPs water withdrawals.

2.9.1 New input scenarios for solar PV energy

Recent improvements in the technology like solar PV cell efficiency (Tyagi et al, 2013), cost decrease (Delucchi and Jacobson, 2011) and being eco–friendly has made solar PV a vital resource. Also, a lot of regions like China, Europe, Japan, and the USA have witnessed improved input in the total electricity for this resource in comparison to the business–as–usual trends, which is mostly fossil–based scenario. Due to massive potential, many researchers are nowadays trying to design, implement and assess the impacts of solar PV to replace partially or fully ongoing energy generation system with solar PV resource. A few of them includes Asif et al, (2007), Barasa et al, (2018), Denholm et al, (2007), and Waldman et al, (2019). The encouraging thing of all the above studies is that they mentioned all those higher PV scenarios don't need new or much land for their implementation.

Due to its promising results both on policy side, and implementation sides, several countries are these days reforming their already set energy policies under the guideline of UN SDG, mainly Goal No. 7, Goal No. 11, and Goal No. 13 related to Affordable and Clean Energy, Sustainable Cities and Communities, and Climate Action. Outputs from several IAM models seem to be inconstant with the real world as they underestimate the future potential and penetration of solar PV in the system and therefore needed to be revised accordingly. In order to setup solar PV electricity input scenarios for the future, we used governmental public strategy targets for capacity deployment presented by various countries globally. The set figures available with Koberle et al, (2015) show the expected capacity targets for solar PV in the years 2020, 2030, and 2050. Also, some national targets were taken from REN21 (REN21. 2013) and DOE (DOE. 2012). It is obvious that almost all of the countries are trying to double to triple their

inputs from solar PV. However, there might be chances that those targets are not achieved or reached earlier.

To set the harmonized enhanced scenarios for solar PV (PV_{enh}) regionally, we set up three targets as 10% (LOW), 20% (MEDIUM) and 30% (HIGH); and 25% (LOW), 35% (MEDIUM) and 45 % (HIGH) for 2050 and 2100 respectively, as most of researchers (Barasa et al, 2018; Denholm et al, 2007) followed the same trends by defining "LOW", "MEDIUM" and "HIGH" input scenarios for renewables. This study considers three RCP along with three SSP scenarios. Based upon SSP narratives provided in Fig. (1.11), it is witnessed that SSP1 leads to sustainability; therefore HIGH PV scenario belongs to SSP1–RCP2.6, while, SSP2 has low mitigation and adaptation challenges, hence LOW PV scenario relates to SSP2–RCP4.5 scenario. Lastly, SSP3 has very high challenges to adaptation and mitigation and therefore may have low input from solar PV. So we assigned LOW PV scenario to SSP3–RCP6.0. The whole analysis is compiled on the basis of these scenarios building in the context of SSP and RCP narratives.

2.9.1.1 Future solar PV resources for various SSP and RCP scenarios

The solar PV resource is highly influenced by meteorological parameters like temperature, rainfall intensity, and aerosols distribution in the atmosphere as well as snowfall. All such parameters are believed to vary in the future due to the climate change impact. ISIMIP2b datasets for various models like Max–Planck Institute Earth System Model (MPI–ESM), Norwegian Earth System Model (NorESM), and Model for Interdisciplinary Research on Climate (MIROC5) were utilized in this study. The spatial–temporal resolution of these datasets are the same as of GSWP3 i.e., daily at 0.5° at a global scale. Daily long term mean corrections were applied to calculate the future solar PV resources available. In addition, the differences are also estimated to see which are has undergone an increase or decrease in the resource.

2.9.2 Revised electricity generation by TEPPs and water withdrawals for PV_{enh} scenarios

Using the solar PV resource maps, electricity generation from TEPPs, and PV_{enh} scenarios, we calculated revised water withdrawals by TEPPs. Flow chart in the Figure (2.19)

shows the step we followed in our methodology. First, based upon the water scarcity maps and TEPPs locations, we identified the potential areas for solar PV installations. Second, using solar PV resource map, we calculated the areas needed for solar PV_{enh} scenarios for each region. Third, based upon PV_{enh} scenarios, the electricity estimates from TEPPs are also revised for new scenarios. Then, based upon the similar methodology as shown in Figure (2.18), we calculated new fresh water withdrawals after subtracting from old scenario, BAU. Accordingly water scarcity maps were revised to see the number of people out of stress and water savings (Km^3/yr) for new scenarios.

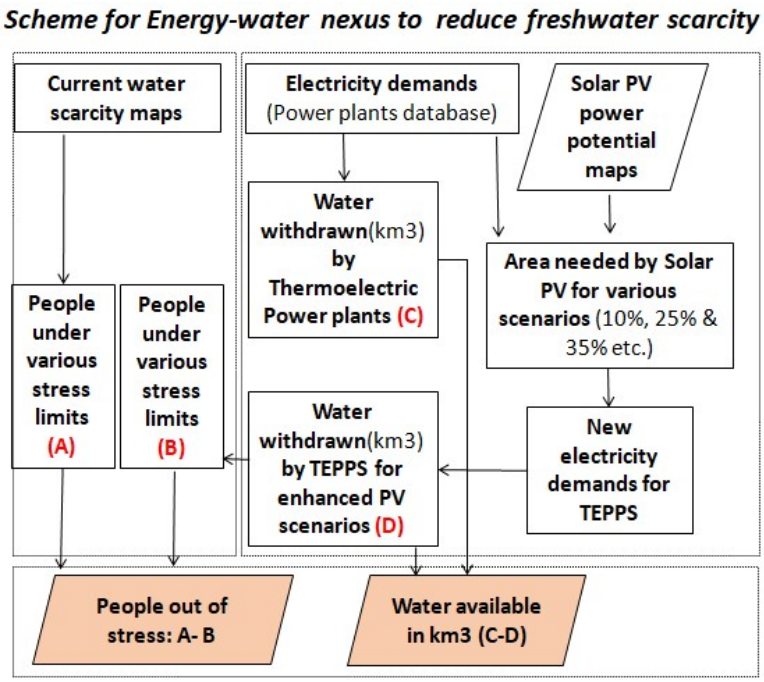

Figure 2.19: Flow chart to calculate revised electricity generation and new water withdrawals by TEPPs for solar PV_{enh} scenarios.

2.9.3 Electricity demand

2.9.3.1 Global gridded electricity demand maps

The electricity demand data is the fundamental input needed to identify the potential areas for the provision of electricity from the source. The regional electricity demand data is taken from AIM. The advantage of using AIM is that it evaluates climate impacts and adaptation measures through socio–economic scenarios (SSPs) in addition to the RCPs. A methodology to downscale AIM regional electricity data to a global gridded electricity demand map is devised to know the electricity demands at a finer scale.

For GDP, GDP growth, population, urbanized area per person, Heating Degree Days (HDD) as well as Cooling Degree Days (CDD), we used country wise statistics and aggregated them to the AIM regional values. For urbanized area per person, we identified urban regions based upon a threshold of ≥1500 inhabitants per km^2 (Moran et al, 2018). For CDD, HDD, we used threshold temperatures as 27.5°C, and 18.5°C respectively. We found a significant relationship between GDP and electricity consumption per capita (Table 2.5). However, a weak correlation is seen for other variables like GDP growth, population, and urbanized area per person, HDD, and CDD. Therefore, we used the GDP to downscale AIM regional electricity values to the grids (0.5 x 0.5 degree) using the relationship provided in Eq. (2.19). The GDP data is obtained from the Centre for Global Environmental Research, National Institute for Environmental Studies, Tsukuba, Japan. This dataset summarizes GDP in 0.5–degree grids globally from 1980–2100 with 10 years intervals under three SSP scenarios namely SSP1, SSP2 and SSP3. More details of datasets can be seen from Murakami and Yamagata, (2016). Electricity consumption in any grid (x, y) inside the same region (reg, i) can be calculated by Eq. 2.15. We assumed each megacity fits inside the half–degree grid.

$$(Elc)_{x,y} = (GDP)_{x,y}\, X\, \frac{\sum_{i=1}^{n} Elc_{reg,i}}{\sum_{i=1}^{n} GDP_{reg,i}} \tag{2.19}$$

Where *Elc* is the electricity consumption (EJ/yr), *GDP* is the Gross Domestic Product (PPP2005 USD) for the same region (i), and n is the total number of grids inside a region.

Table 2.5: Correlation between electricity consumption per capita and other variables for AIM regions

Region	GDP per cap (USD)	Area (Sq. m) per person	GDP growth (%)	CDD (degree days)	HDD (degree days)	GDP (PPP 2005 USD)	Population (mill)
XLM	0.99	–0.99	–0.89	0.96	–0.82	0.96	0.99
CAN	0.98	0.55	–0.94	NA	–0.76	0.91	–0.52
XME	0.98	–0.97	–0.85	–0.37	–0.83	0.92	0.92
XOC	0.96	–0.15	–0.84	0.88	–0.81	0.85	0.11
XNF	0.93	–0.79	–0.69	0.67	–0.59	0.95	0.89
XE25	0.97	0.99	–0.87	0.54	–0.89	0.65	–0.99
CIS	0.99	–0.82	–0.83	0.70	–0.89	1.00	0.81
XSA	0.92	–0.89	–0.72	0.25	–0.76	0.90	0.91
CHN	0.93	0.88	–0.80	0.82	–0.84	0.80	–0.87
XSE	0.98	–0.89	–0.83	0.92	–0.76	0.98	0.91
XAF	1.00	–0.77	–0.81	0.74	–0.48	1.00	0.95
JPN	1.00	0.97	–0.83	0.75	–0.83	–0.77	–0.98
TUR	0.98	–0.97	–0.84	0.05	–0.78	0.99	0.99
XER	0.99	0.93	–0.80	NA	–0.95	0.99	–0.88
IND	0.99	–0.99	–0.93	0.38	–0.80	0.96	0.98
TUR	0.76	–0.86	–0.82	0.88	–0.78	0.85	0.90
USA	0.94	0.55	–0.87	0.90	–0.90	0.75	–0.54

2.9.3.2 Electricity demand of world megacities

Very few researchers have explored the relationship between electricity consumption in urban areas like megacities (Kennedy et al, 2015). Electricity is proven to be a strong determinant of urbanization (Liddle and Lung, 2014). The cities were selected on the basis of Brinkhoff's database for metropolitan areas available online at www.citypopulation.de/world/Agglomerations.html. We assumed each megacity fits inside the

half–degree grid. Although, city shape varies place to place, but, to establish a uniform criteria for all cities we made this assumption to define a city inside a most populous half–degree grid.

2.9.3.3 Electricity demand flow of megacities for 21st century

AIM model also provides future data for electricity demands. So, we downscaled the future electricity demands using the future GDP data from CGER, NIES datasets (Murakami and Yamagata, 2016). Similarly, after calculating GDP/capita in each city, we projected electricity demand flow for each megacity for various SSP scenarios.

2.9.3.4 Solar electric footprints of megacities

After knowing the electricity demands of each megacity, solar electric footprint, area needed to provide all energy from solar PV are estimated for each megacity. Solar PV resource previously calculated was used to estimate solar electric footprints. After calculating the solar electric footprint for each megacity, per–capita solar electric footprint of the corresponding megacity (i) is calculated by dividing the solar electric footprint by the population inside the city as expressed by Eq. (2.20).

$$\text{Per–capita solar electric footprint} = \frac{(\text{Solar electric footprint})_i}{(\text{Total Populatio})_i} \tag{2.20}$$

2.9.3.5 Roof top areas available with megacities

Finally, we worked out that how much electricity could be supported by covering the rooftops of each megacity. Wiginton et al, (2010) applied geographic information system (GIS) and also image recognition techniques to work out the on hand rooftop area for PV deployment in eastern Ontario. For solar PV fitting in Mumbai, pretty similar technique with the introduction of Building Footprint Area Ratio (BFAR), the ratio of built–up area by a building to total plot area is used by Singh and Banerjee, (2015). A methodology similar to the latter was used (Fig. 2.20) to work out the BFA for each megacity. This involves the data from Atlas of Urban Expansion, (2016) with global coverage of 200 cities. Parameters like urban built–up area, urban open area, area covered by roads and yearly changes (%) are provided for 1990, 2000, and 2014. More details are available at http://atlasofurbanexpansion.org/data. Urban built–up area for 2010

is obtained by using the annual change, and this is later subtracted from the area covered by roads to have the BFAR for each megacity. The prospective rooftop may be smaller because of i) shading from buildings, trees, and PV itself ii) roof area used for like ventilation, and heating/air conditioning and iii) roof area not appropriate for PV fixing because of uneven shape. To incorporate the influence of such parameters, a value of 0.4 for PV Available Roof Area Ratio (PVAR) as reported by Singh and Banerjee, (2015) was multiplied with BFAR to have the actual PV rooftop area available (PVA) as expressed in Eq. (2.21).

$$PVA = BFAR \times PVAR \tag{2.21}$$

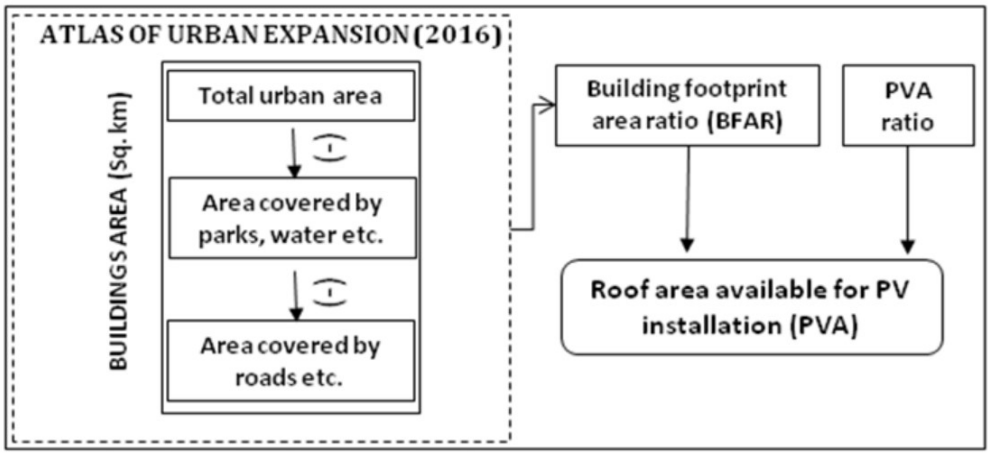

Fig 2.20: Scheme for megacities roof–top area calculation for 2010.

Chapter 3: RESULTS AND DISCUSSIONS

ENERGY

3.1 Temperature effects on solar PV efficiency reductions

Temperature increase increases the internal resistance amount of the solar cells and as a result, decreases the output of a system. Temperatures mainly the near-earth surface temperature affects the PV system, and eventually decreases the yield of a solar PV system. The sub–sections will discuss those factors in detail.

3.1.1 Solar PV module temperature T_m:

The first step towards the calculation of solar PV cell efficiency reductions is the calculation of solar PV module temperature (T_m). This is calculated by Eq. (2.2) and outputs for long-term mean of T_m are provided in Fig. 3.1. Daily T_m can reach up to 54.18°C and 54.45°C during the hot days of July and August in the regions like The Middle East and Sub–Saharan Africa when Ambient Temperature ($T_{a)}$ goes to a maximum of 45.21°C and 44.99°C for same days. However, seasonal maximum values for T_m are recorded as 48.85°C and 43.14°C for maximum T_a as of 40.4°C and 34.4°C for same regions during the season JJA and MAM respectively. Other areas, like parts of USA, South Asia, Southern Africa, and China also bear higher values for T_m during MAM and DJF. On the other side region like Australia bears very high temperature (~45°C) during the season DJF. Here the T_m reaches up to 53.75°C. For the calculations of T_m, we used coefficients ("a" and "b") for open mounted solar PV schemes which are similar to solar parks. In addition, near-earth surface temperature at 2m is considered as T_a along with wind speed at 10m is used in the derivation of T_m.

3.1.2 Solar PV cell temperature T_c:

After calculating T_m, we estimated the cell temperature (T_c) using Eq. (2.3), and outputs for long-term mean of T_m which are obtained from daily ones, is provided in Fig. (3.2). Most of

the researchers used T_m in the calculation of solar PV cell efficiency reductions for the temperature. However, as per experimental evidence from National Renewable Energy Laboratory (NREL) (King e al, 2004), T_c is a better predictor of such reductions. In addition, the solar PV module is sometimes covered with glass plates, etc., and also mounting does affect the T_c. Therefore in Eq. (2.3), we used coefficients like $\Delta Tcnd$ for open mounted solar PV schemes described earlier. Daily T_c goes up to up to maximum 57.18°C and 56.45°C during the hottest days of July and August in the areas like The Middle East and Sub–Saharan Africa. The seasonal maximum values for T_c are recorded as 49.81°C and 44.04°C for the seasons JJA and MAM respectively. Some parts of the USA, Southern America, South Asia, Southern Africa, and China also reach higher values for T_c during the same seasons. In contrast, Australia bears very high values for T_c (54.92°C) during DJF. To estimate T_c, the value of $\Delta Tcnd$ is obtained for an open mounted solar PV schemes in addition to the T_m calculated above.

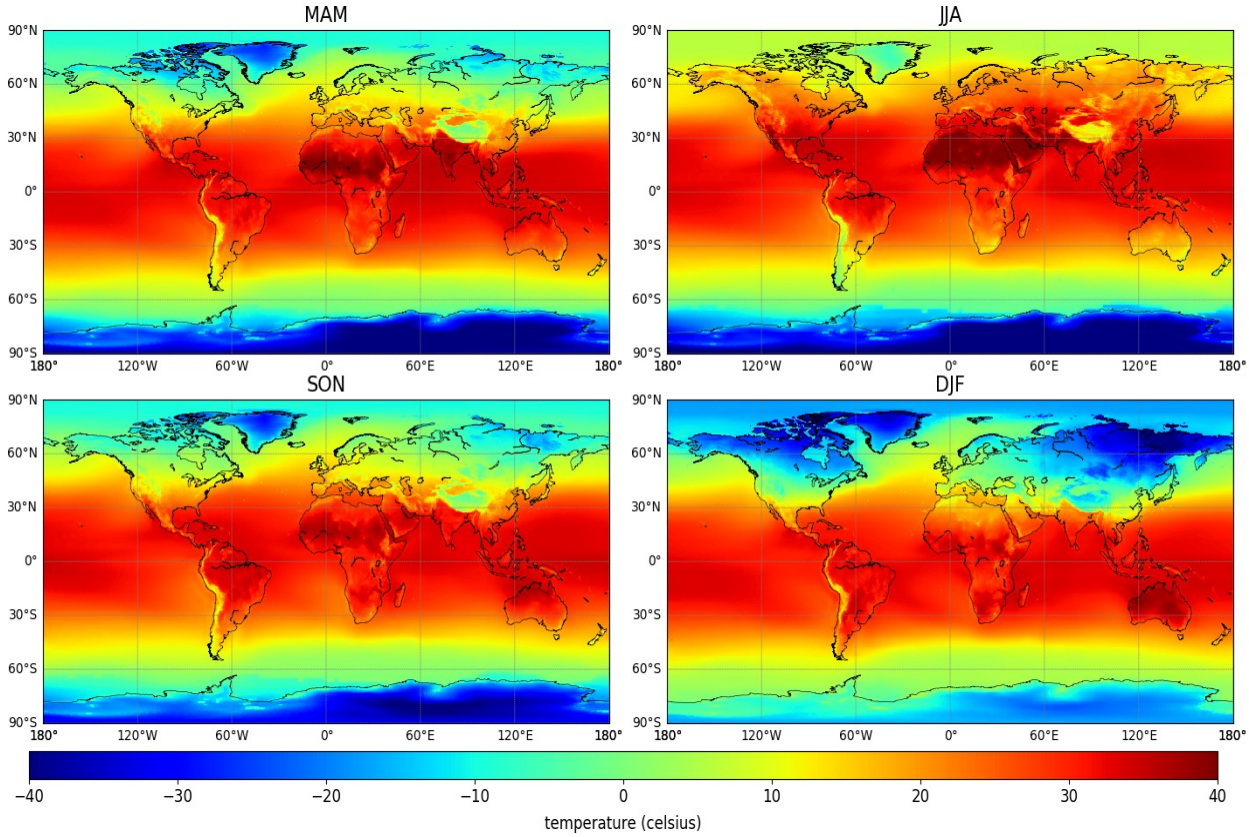

Fig 3.1: Long term mean of daily seasonal solar PV module temperature (T_m).

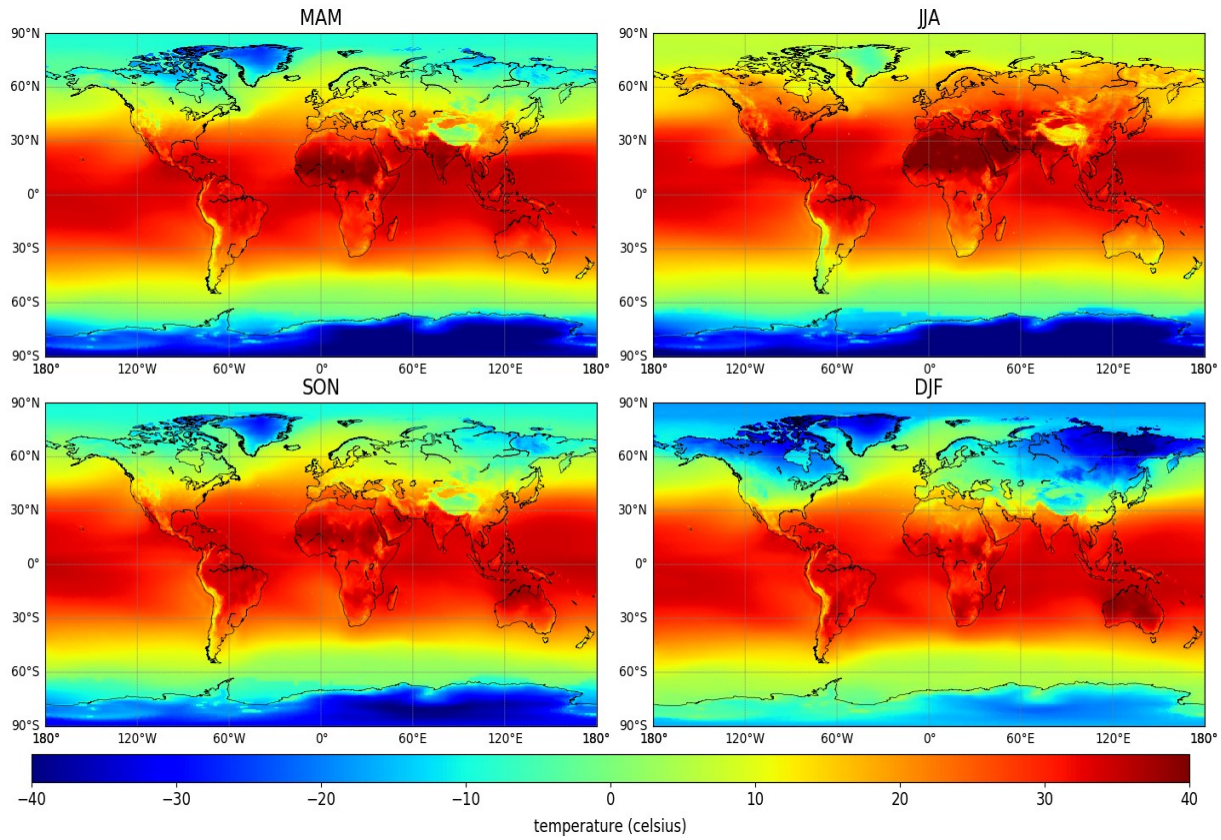

Fig 3.2: Long term mean of daily seasonal solar PV cell temperature (T_c).

3.1.3 Solar PV cell efficiency reductions due to the affect of temperature rise:

After estimating T_m and T_c, we used Eq. (2.1) to estimate the final efficiency reductions in the performance of solar PV cells due to the temperature increase. Results are in parallel to the above mentioned figure where areas undergoing high temperatures are severely affected by temperature losses. Daily losses from temperature increase ($\Delta\eta_T$) are recorded as 12.56% and 12.43% for Sub–Saharan Africa during the hottest days of July and August respectively. While seasonal maximum losses are obtained as 10.1% and 7.9% for JJA and MAM respectively. The annual maximum temperature loss is estimated as 5.23%. Similarly, areas in the Middle East, South Asia and parts of China also undergo high-temperature reductions. In contrast, Australia recorded the highest seasonal losses at 5.79% as shown in Fig. (2.3). Meanwhile, there are also areas that have negligible temperature effects include South America, South East Asia, Japan, and Turkey, etc.

T_a is initially used in this analysis since actual T_c data was not available for a longer time at global scale. The values for T_a are taken at 2m height to have a more realistic estimation of T_c and to avoid the effects of radiations coming back from the earth surface who are supposed to add to the uncertainties (Mildrexler et al, 2011). We believe that our results are more reliable however further investigations involving conversion of land surface temperature (LST) to air temperature (T_a) followed by calculation of T_c may be explored.

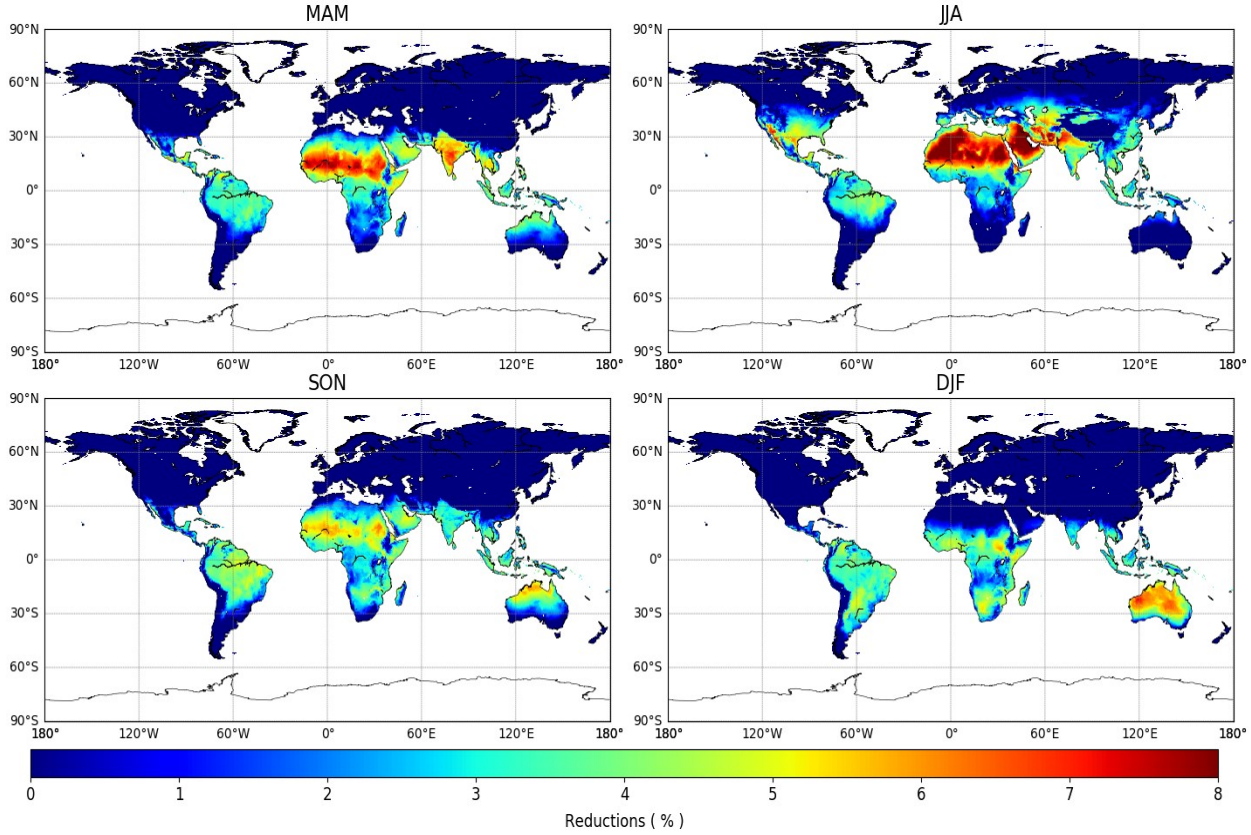

Fig 3.3: Long term mean of daily seasonal solar PV efficiency reductions due to the effect of temperature changes ($\Delta\eta_T$).

3.2 Dust effects on solar PV efficiency reductions

3.2.1 Loss factor for dust reduction (K_L):

The solar PV cell efficiency decrease due to dust covers ($\Delta\eta_D$) is directly proportional to the dust loss factor (K_L) described briefly in section 2.2.2. This factor mainly depends on the PV module tilt–angle (Sayyah et al, 2014) as dust particles try to roll on the surface for higher

angles. Therefore, K_L for optimum tilt angles (β_{opt}) is calculated by applying a curve fitting technique to the experimental data taken from Elminir et al, (2006). The relationship obtained is presented in Eq. (3.1)

$$y = -0.002*x + 0.245 \quad (3.1)$$

Where y is transmittance loss (K_L) and x is the tilt–angle.

Later this equation is applied to global tilt–angles obtained from Jacobson and Jadhav (2018) to estimated K_L globally as shown in Fig. (3.4)

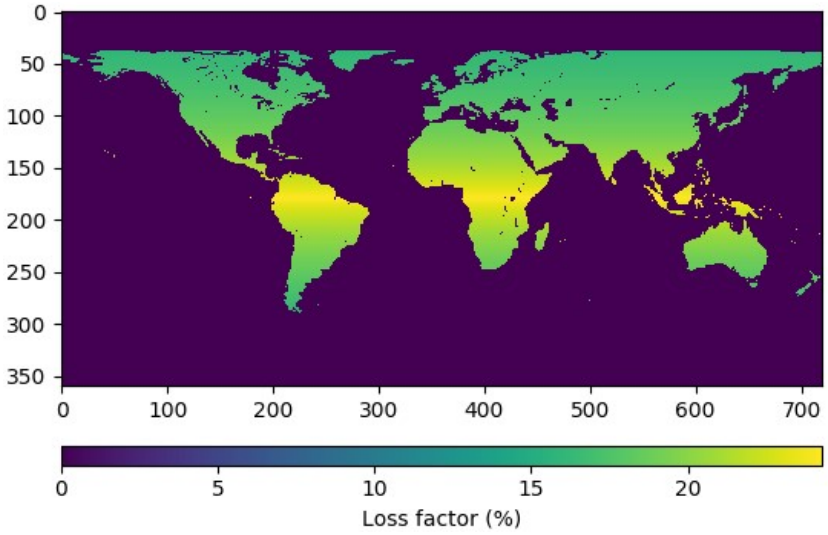

Figure 3.4: Transmittance Loss Factor ($K_{L)}$ at optimum tilt angles (Jacobson and Jadhav, 2018) is calculated globally by applying the curve fitting technique shown in Fig. (2.5).

3.2.2 Solar PV cell efficiency reductions due to the affect of dust deposition

We used AOT mask in Eq. (2.5) to calculate the decrease in solar PV cell efficiency for dust deposition for all seasons. The seasonal reductions are provided in Fig. (3.5). It is witnessed that Sub–Saharan Africa, The Middle East, a fraction of South America, South Asia, and China are badly affected by the dust cover reductions during the whole year. The maximum daily efficiency losses are recorded as 12.35%, 17.20%, 15.84%, and 13.53% for the season's MAM, JJA, SON, and DJB respectively in the above regions. However, seasonal reductions are 8.12% and 6.01% for JJA and SON respectively. The annual maximum dust loss is estimated as 5.90%. On the other hand, fewer efficiency losses (< 2%) are also seen for other parts of the world,

which include parts of North America, Central America, Europe, South Africa, and Southeast Asia, etc.

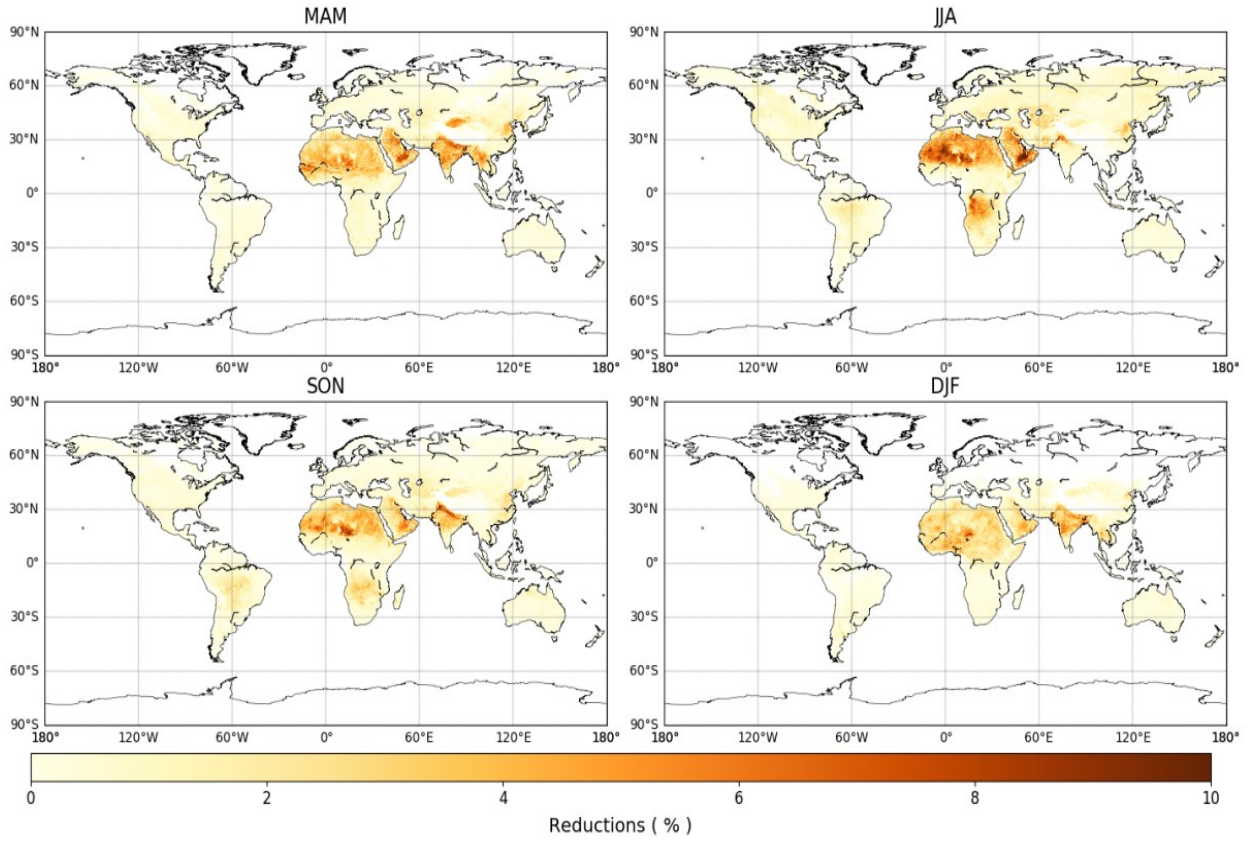

Fig 3.5: Long term mean of daily seasonal solar PV efficiency reductions due to the effect of dust ($\Delta\eta_D$).

We also checked PV module natural cleansing through precipitation. But, cleaning through rainfall is not significant in most parts. This is mainly due to the mismatch of dust deposition and precipitation timings. In contrast, there may be chances of light precipitation, which could have produced a sharp decline in the performance of solar cell by increasing the soil particles density by enhancing the adhesive forces that bind the particles more tightly to the surface (Paudyal et al, 2016). Therefore, we propose manual cleaning of the solar PV modules to improve the outputs. Available dry–cleaning procedures like silicone rubber brushes can offer water–free cleaning for solar PV arrays fitted in low–water–availability or desert locations (Parrott et al, 2018). Our analysis is in line with Li et al, (2020), who presented about 20% reductions for northern Africa and the Middle East, whereas we reported a maximum reduction of 17.20% for those areas. The variation may be due to the difference in study years and the data sets etc. Also, Schill et al, (2014) reported dust-related efficiency losses of >13% for Gran

Canary Island, Morocco. Our results for the same region show the mean seasonal efficiency reduction reaching 11%; however, daily losses are higher.

3.3 Snow effects on solar PV efficiency reductions

3.3.1 Seasonal snow depths

In colder climates, snow covers are among the prominent factors affecting solar PV cell efficiency by reducing transmittance. Daily snow depths (Sdp) are calculated from SWE, SCF, and snow density (ρ) using Eq. (2.6). Observation-based SWE data is used in our analysis which does account for daily sdp changes due to melts. Further, snow melts due to PV surface and sliding due to higher tilt–angles are provided with mass balance equation in section 2.2.2.3.

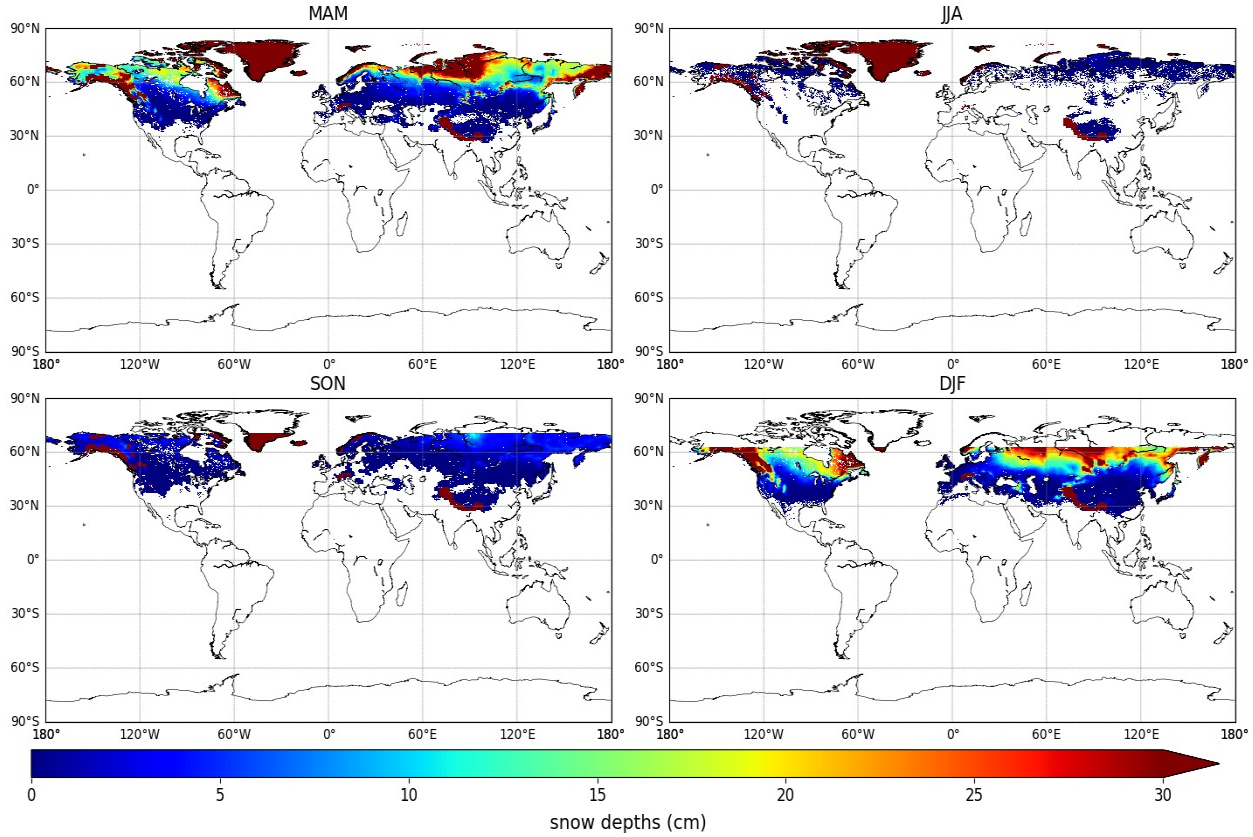

Fig 3.6: Long term mean of daily seasonal snow depth accumulated on top of solar PV modules.

Long term mean of daily seasonal snow depths in cm is provided in Fig. (3.6). it is seen that DJF has the maximum snow followed by MAM, where snow from previous months uses to stay for longer times due to higher temperatures. These higher snow depths (>10cm) are

witnessed for upper northern hemisphere includes Canada, Russia, Europe, and parts of the USA, China, and South Asia. It is also seen that the Himalayas, the upper part of Canada, and Russia are covered with thick snow throughout the year. Mild snow depths around 2cm are recorded for these regions during JJA and SON. In contrast, these snow covers are washed away for most regions in Europe, the USA, Canada, and China during higher temperature seasons like JJA and SON.

3.3.2 Solar PV cell efficiency reductions due to the affect of snow covers

The daily mean seasonal reductions in solar PV cell efficiency for snow covers are calculated using the algorithms provided in Eq. (2.7) & (2.8) respectively. The results (Fig. 2.9) of the curve–fitting for snow efficiency losses are calculated for transmittance, and snow depth and. This curve–fitting technique yielded a rational R^2 value of 0.91 and is expected to improve if more data points were available. The scarcity of fewer data points available was due to the reason that the experiment is done for just two winter seasons and no consistent data was reported during the seasons. Fig. (2.9) also verifies that even a very smaller snow depth (~1 cm) can reduce the efficiency by 50%. This is due to the reason that snow depth's effect on transmittance/loss of sunlight is too rigorous.

The results of daily seasonal snow efficiency reductions are provided in Fig. (3.7). it is seen that snow is the most dominant efficiency limiting factor among others. Mostly Canada, Russia, and the Himalayas have higher snow efficiency losses for MAM and DJF as solar PV modules are supposed to be under heavy snow covers throughout the seasons. The higher snowfall occurs during DJF and almost whole of the areas inside the upper northern hemisphere for Canada, Greenland, Russia, Europe, and the USA are covered by snow. Most of these areas have no power output as transmittance is totally blocked. This is in line with the Perovich. (2007) mentioning zero/no light transmittance for snow covers more than 12 cm. We don't recommend solar PV installations in those areas unless some snow removal technology is installed or any manual cleaning is possible. Though, lower parts of the USA, Canada, Europe, Russia, China, and Japan have a lesser amount of snow, where the annual losses go up to 20.1% maximum. Also, quite similar snow efficiency reductions are seen for the MAM as last season (DJF) snow stays in most of the areas. More or less, due to higher temperatures, it melts down in JJA, except Greenland, Antarctica, Himalayas, some parts of Canada, and Russia. Due to non–availability of

a global study on snow efficiency reductions, we compared our results with the existing regional study. During the winter season of 2010–11 and 2011–12, Marion et al, (2013) investigated PV module energy loss for snow in Colorado and Wisconsin, USA. They reported a maximum efficiency loss of 90%. Our findings for the Wisconsin area for DJF have a similar range of snow efficiency losses of 80−90%.

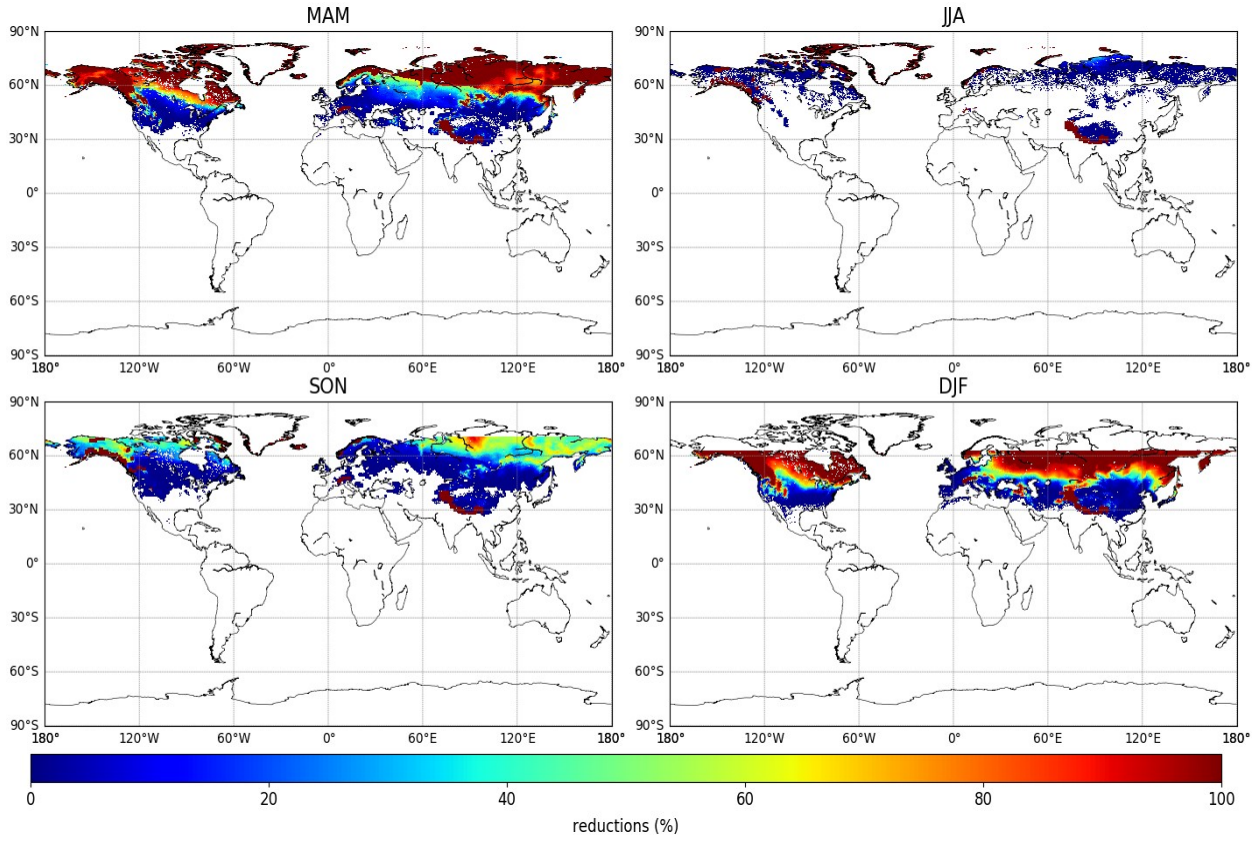

Fig 3.7: Long term mean of daily seasonal solar PV efficiency reductions due to the effect of snow covers ($\Delta\eta_S$).

3.4 Effects of geomorphologic parameter on Solar PV power output

3.4.1 Optimal Tilt angles

The power output of a solar PV system is the maximum at β_{opt}. Those angles are obtained from Jacobson and Jadhav, (2018) and presented in Fig. (3.8). It is seen that β_{opt} varies along the latitude. It increases while moving away from lower latitude and approaches zero or minimum at

the equator. The maximum angles (>30°) are recorded in the upper northern hemisphere, while lower angles (~10°) are seen for lower latitudes for optimum power generations.

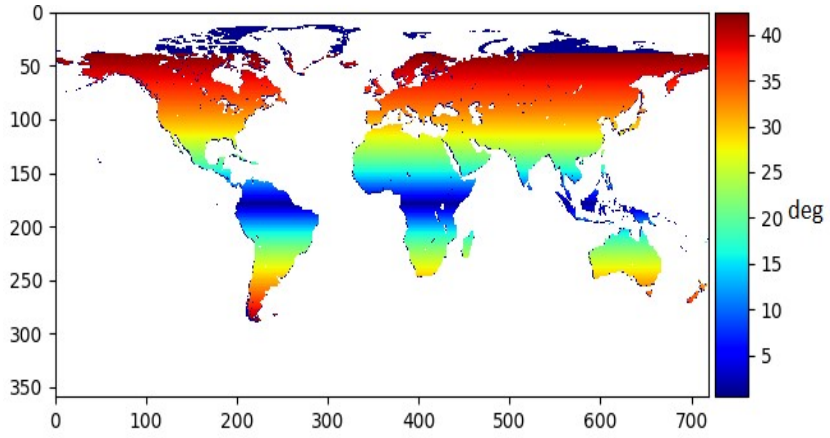

Fig 3.8: Global optimum tilt–angles (β_{opt}) taken from Jacobson and Jadhav, (2017). Higher tilts are observed for regions away from latitude.

3.4.2 Effective power ratio

The effective power ratio is calculated to see the difference between normal power and the optimum one. Normal power is calculated for solar PV modules at the horizontal surface, while optimum power is calculated at β_{opt}. The results are presented in Fig. (3.9) and it is seen that along the lower latitude, the effective power ratio is a bit lower in comparison to the upper-middle latitude where there is more increase in the effective power ratio for some of the areas due to higher β_{opt}.

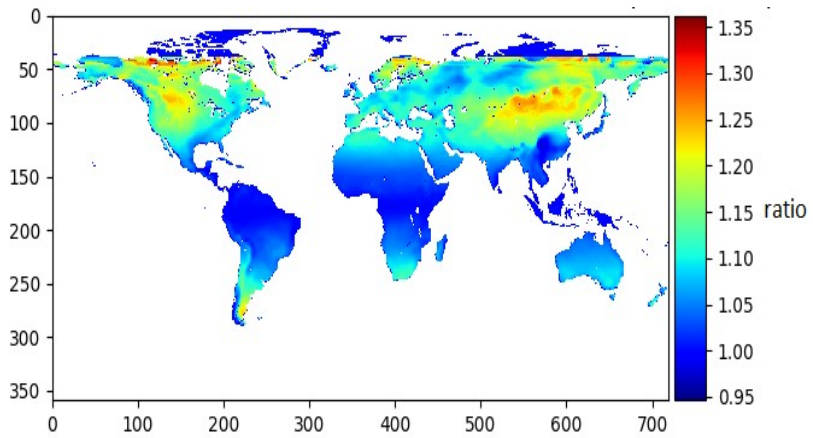

Fig 3.9: Global effective power ratio calculated for $\beta_{opt.}$

3.5 Effective power (P_{eff})

3.5.1 Performance ratio

Performance Ratio (PR) is defined as the fraction of actual estimated power (P_A) to the theoretical power (P_T). Individual solar PV cell efficiency reductions along with tilt angle variations are included to calculate the theoretical power, and PA is divided by PT to see the final PR available with the solar PV panels globally. The result for all seasons is presented in Fig. (3.10). It is seen that the PR at each place varies with the season as well as for geographical position. Mostly, the area from 30°N to 60°S show quite high values for PR for all seasons. It includes western America, South America, South Africa, Parts of South Asia and Southeast Asia, and Australia with PR values of more than 90%. These areas have some reductions due to the temperature changes as well as dust deposition. In contrast, areas in the upper northern hemisphere containing Canada, Europe, Russia, and the Himalayas have the least or zero PR values as they receive heavy snow during DJF and MAM which stays with some areas for longer time periods. Also, parts of China, South Asia, The Middle East and Japan show PR values range from 80–90% due to combining effect of snow, dust, and temperature changes.

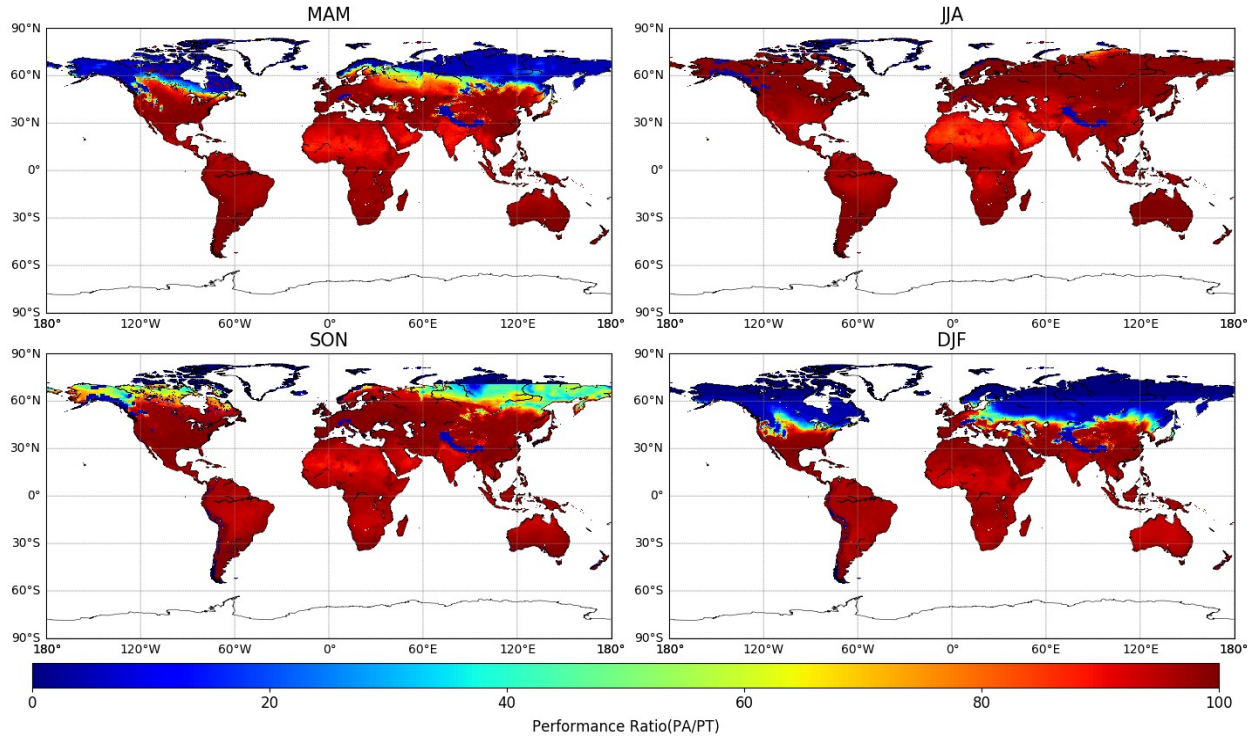

Fig 3.10: Final performance ratios (PR) calculated from all individual corrections and optimum tilt–angles.

3.6 Final solar PV resource

3.6.1 Actual estimated seasonal solar PV resources

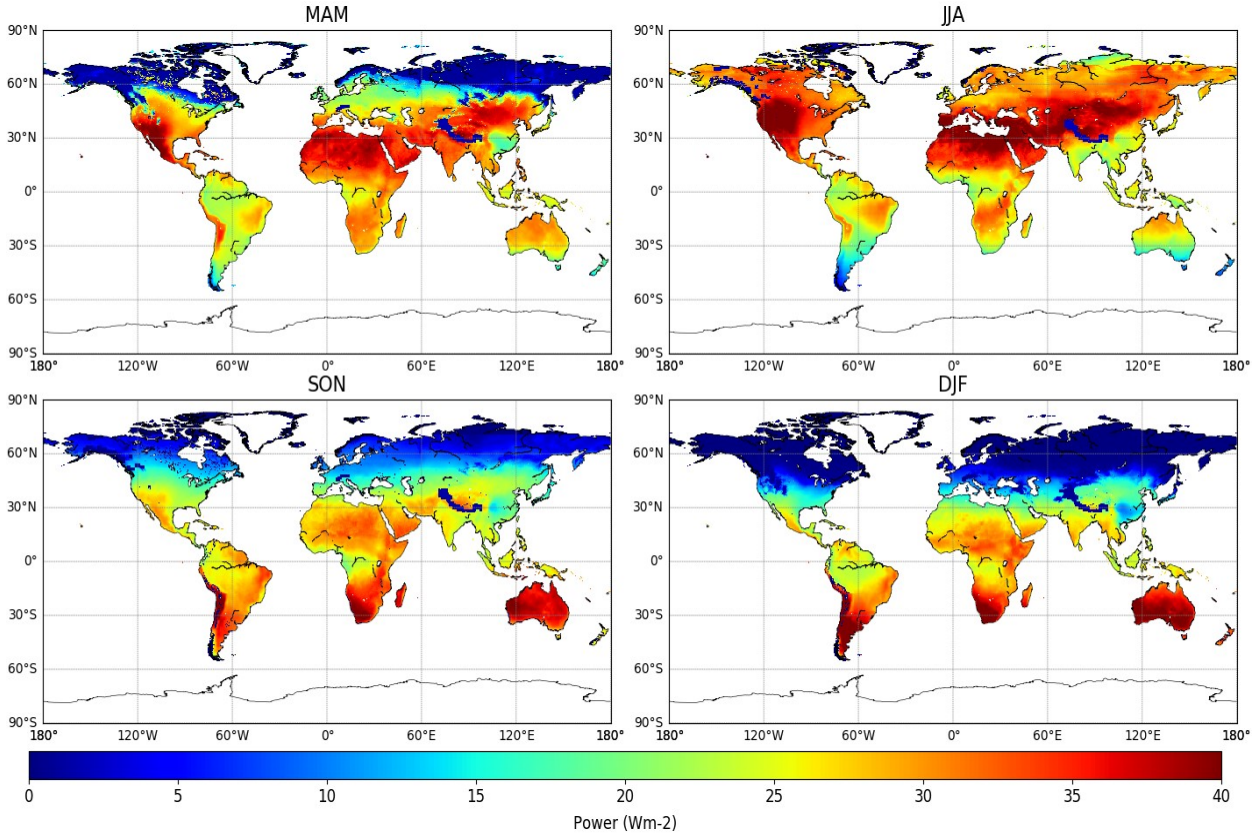

Fig 3.11: Global seasonal solar power resource in W/m^2. A solar cell efficiency of 15% is considered for final power output.

After incorporating losses from temperature, snow and dust, equation Eq. (2.9) is then used to calculate the η on global scale. These daily solar cell efficiencies, along with PR values are then 99 used in Eq. (2.10) to calculate final solar PV resource available globally for each season. The results are presented in Fig. (3.11). The most efficient continental locations comprise of western America, Sub-Saharan and South Africa, Middle East and Australia with annual PV resource is more than 30W/m2 .This pattern is generally in line with the prior assessment of solar PV power potential emphasizing temperature and wind corrections etc. (Adeh et al, 2019). Some other areas counting South America, South Asia, and Southeast Asia also contain a rational amount of PV resource ranging from 20-30W/m^2. In contrast, Russia, Canada, Europe, Russia, and Himalayas have the least or even no power output in DJF and MAM mostly due to thick snow

covers and less incoming SWR because of their geographic location. Significant solar cell efficiency drops are also seen for Sub-Saharan Africa, Australia, The Middle East, India, and Eastern China because of higher temperature and dust effects, however they still have plentiful power potential because of higher incoming SWR.

3.6.2 Actual estimated annual solar PV resources

Seasonal solar power resource at each place is averaged to know the annual solar PV resource globally. This is presented in Fig. (3.12a). It is seen that areas from the equator to Mid Latitudes in the South (50°S), as well as Mid Latitudes in the North (40°N), bear the highest power, >30 W/m^2. In addition, in the higher altitudes, containing parts of the USA and China also have a reasonable solar PV resource (~35 W/m^2). In the upper Northern Hemisphere, a lower solar PV resource of less than 20 W/m^2 is seen due to snow cover reductions in MAM and DJF as well as less incoming solar irradiance. The solar PV resource does vary along the latitudes and such seasonal and mean variations are shown in Fig. (3.12b). The lowest solar resource is seen for upper Northern Hemisphere for DJF shown by the red line, which is mainly due to thick snow covers. However, this resource is the maximum in the Southern Hemisphere. Likewise, for the Upper Northern Hemisphere, the maximum solar resource, 44.12 W/m^2 is seen for JJA due to fair weather and less snowfall.

Annual reductions in the theoretical power output along latitudes is seen due to the effect of temperature changes, dust and snow covers ,and are presented in Fig. (3.12c), (3.12d), and (3.12e) respectively. For temperature corrections, the maximum reduction is seen as 10.1% near the equator and attributed to the higher temperatures during MAM and JJA for Sub–Saharan Africa and the Middle East. For dust covers, the maximum reduction is seen as 8.12% for Sub–Saharan Africa and the Middle East. Snow covers have the most reductions among all other limiting factors, and it is estimated that about 20.1% theoretical power output is reduced in the Upper Northern Hemisphere. These final solar PV resource maps provide an insight of individual and the combined impacts of efficiency limiting factors, and one can see a better picture of which area is affected the most by these factors.

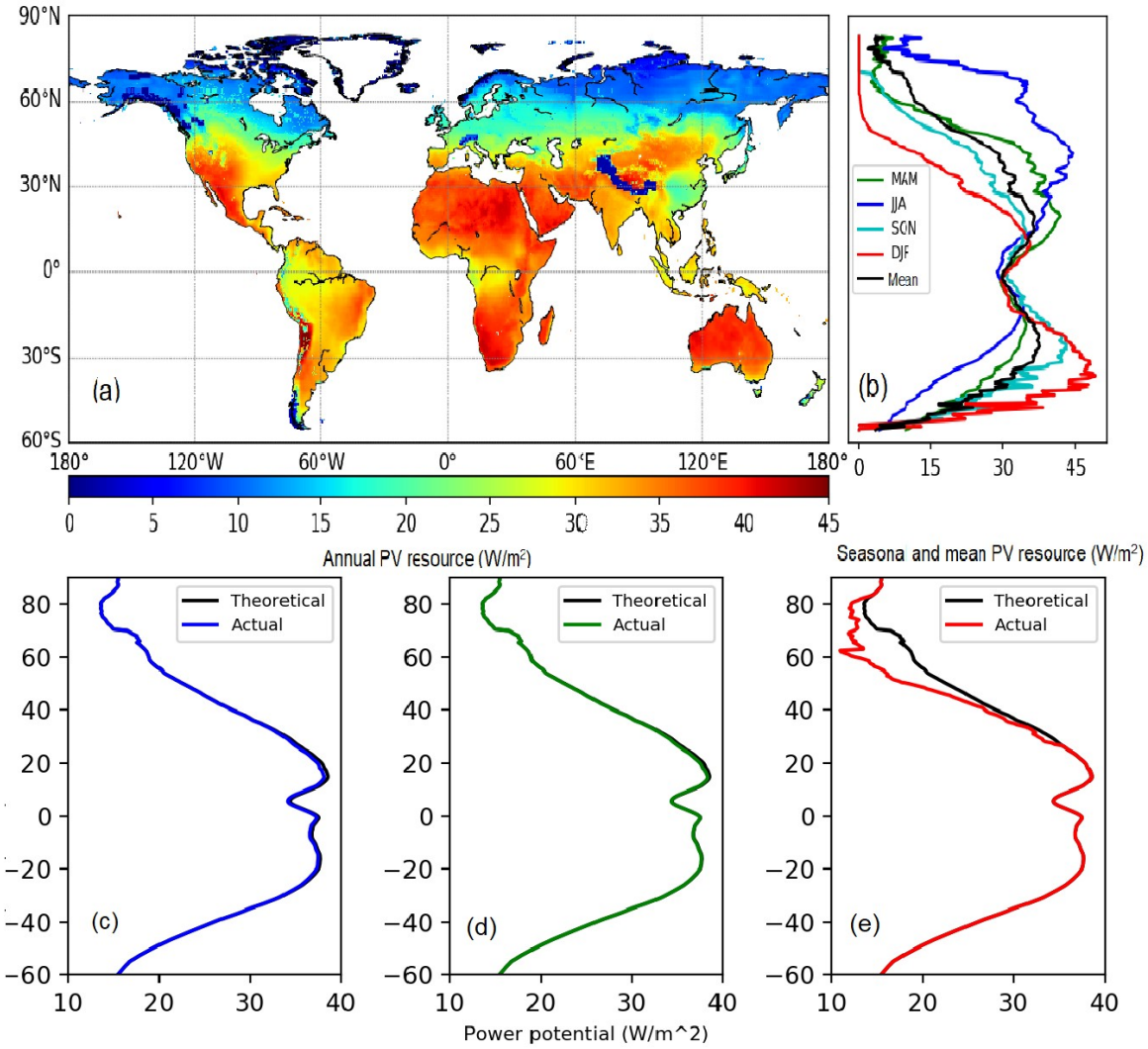

Fig 3.12: a) Global annual solar power resource (W/m^2) obtained by adding seasonal mean power resources. **b**) Variation of actual estimated seasonal and annual mean power resource along with the latitude **c**) Annual reductions in the mean power output along latitude due to the temperature affects **d**) Annual reductions in the mean power output along latitude due to the dust affects **e**) Annual reductions in the mean power output along latitude due to snow covers.

3.7 Validation of final power output

3.7.1 Global solar power plants output comparison

We compared our estimated solar PV resource with existing solar power plants globally. The validation data is taken from the Open Street Map (OSM) contribution, namely Wiki–Solar. This dataset comprises various global solar PV projects. It includes information like power

production (MW), geo–coordinates, the total area of a solar PV module (km^2), and the whole area covered by solar PV power plant (km^2), etc. Further details are available at https://wiki–solar.org/data/. We used 1374 globally existing solar PV power plant data for verification of our results. The location of these power plants along with the generation capacity is shown in Fig. (3.14a). From that map, it is obvious that we have a plentiful number of validation points for those regions affected by meteorological limitations like temperature, snow, and dust covers.

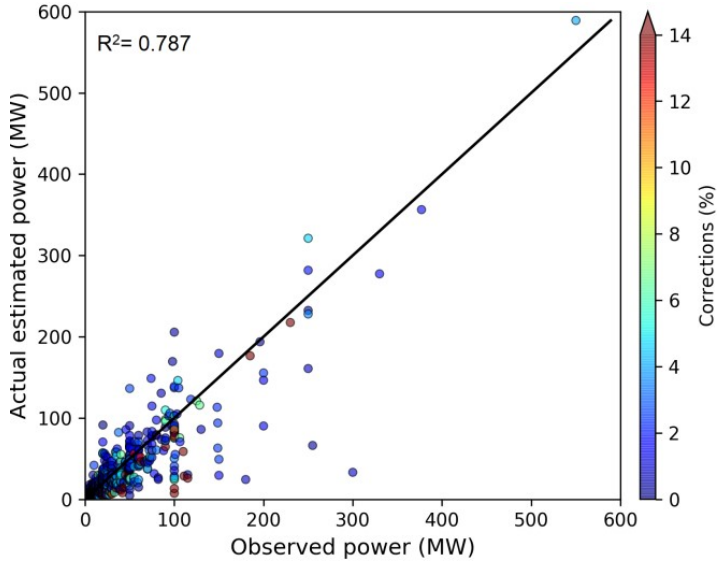

Fig 3.13: Scatter plot between observed power and the actual estimated power for all solar power plants globally. The coefficient of determination (R^2) is 0.787 while RMSE obtained is 17.12.

The comparison of observed and actual estimated power in Fig (3.13) shows quite a rational value of 0.787 for the coefficient of determination (R^2). This means the performance of our analysis is satisfactory. However, few of the power plants show a large differences, which is mainly due to the approximation of cell efficiency value. The cell efficiency is a function of material type. Since we do not have any such information; therefore, we used a harmonized value (15%) for all power plants. However, companies like Sunwaypv (https://www.sunwaypv.com/products) and Panasonic (https://panasonic.net/lifesolutions/solar/) claim higher values as 20.8% and 20.30% respectively.

3.7.2 Validation of regional solar power plants outputs

We also assessed the performance of our models for global nine regions as shown in Fig. (3.14b). Regions are selected based on their contribution to the global solar PV power generation

as well as those affected by various meteorological parameters. The 1st region (North America) contains The United States and Canada. Thick solar PV power plants are located in this region, where some of them are affected by the snow covers and very few with dust and temperature. The R^2 value of 0.86 shows quite a good performance of our estimation in the region. Region 02 (Europe) contains most solar power plants from France, Italy, and Spain, etc. Almost all of them are affected by snow covers and a few by dust deposition etc. Here, the performances of our models are rational, R^2= 0.69. Almost all meteorological factors like snow, dust, and temperature affected region 3 (China), where a good R^2 value of 0.69 is recorded. The region 4 contains Japan only, and mostly it is affected by snow covers. R^2 value of 0.75 shows better performance of our models in this region as well. Some differences are seen between observation and our estimation, and it seems that Japan is using higher cell efficiency as compared to our assumed one (15%). Among all, the region 5, Central America shows the best value of R^2 =0.87 as the region is surrounded by winds, causing the temperature to drop as well as areas with less snowfall and dust covers. A higher R^2 value of 0.83 is also recorded for Sub–Saharan Africa and the Middle East (region 6), where most of the reductions are due to dust and temperature increase. Likewise, in India and Pakistan (region 7) and parts of South America (region 8), power plants are affected by dust, and some temperature increase with a rational R^2 value of 0.76 and 0.85 respectively. Lastly in region 9 (South Africa and Australia), power plants are mainly affected by temperature increase, where our models show the lowest value for R^2=0.61 among others.

It is seen that performance of our models are quite good in almost all of the regions except Europe and China where few solar power plants are mostly affected by snow coverings. Hence, the reason can be mainly attributed to the performance of the snow model in those regions. As mentioned before, a curve fitting technique is applied for snow efficiency reductions, which may not be performing up to the mark as fewer number of data points were available from the experimental study (Perovich. 2007). Similarly, for temperature–related efficiency corrections, we used the earth's surface temperature at 2m height to calculate the T_c due to the non–availability of the global dataset for solar cell temperature. This may cause a minor change in the results, as the satellite–based temperature records are affected by existing structures and topography (Wan. 1999). Moreover, some of the power plants may have a cooling system during high temperatures in addition to manual/automatic cleansing which could lead to improve power

generations during heavy snow and dust covers. Lastly, Solar PV cell efficiency is an important contributor towards the final power output; most of the power plants in the developed regions like Europe, USA, China, Australia and Japan, etc are believed to be using higher efficiencies as compared to our assumed one which can cause underestimation of our results in those regions as well.

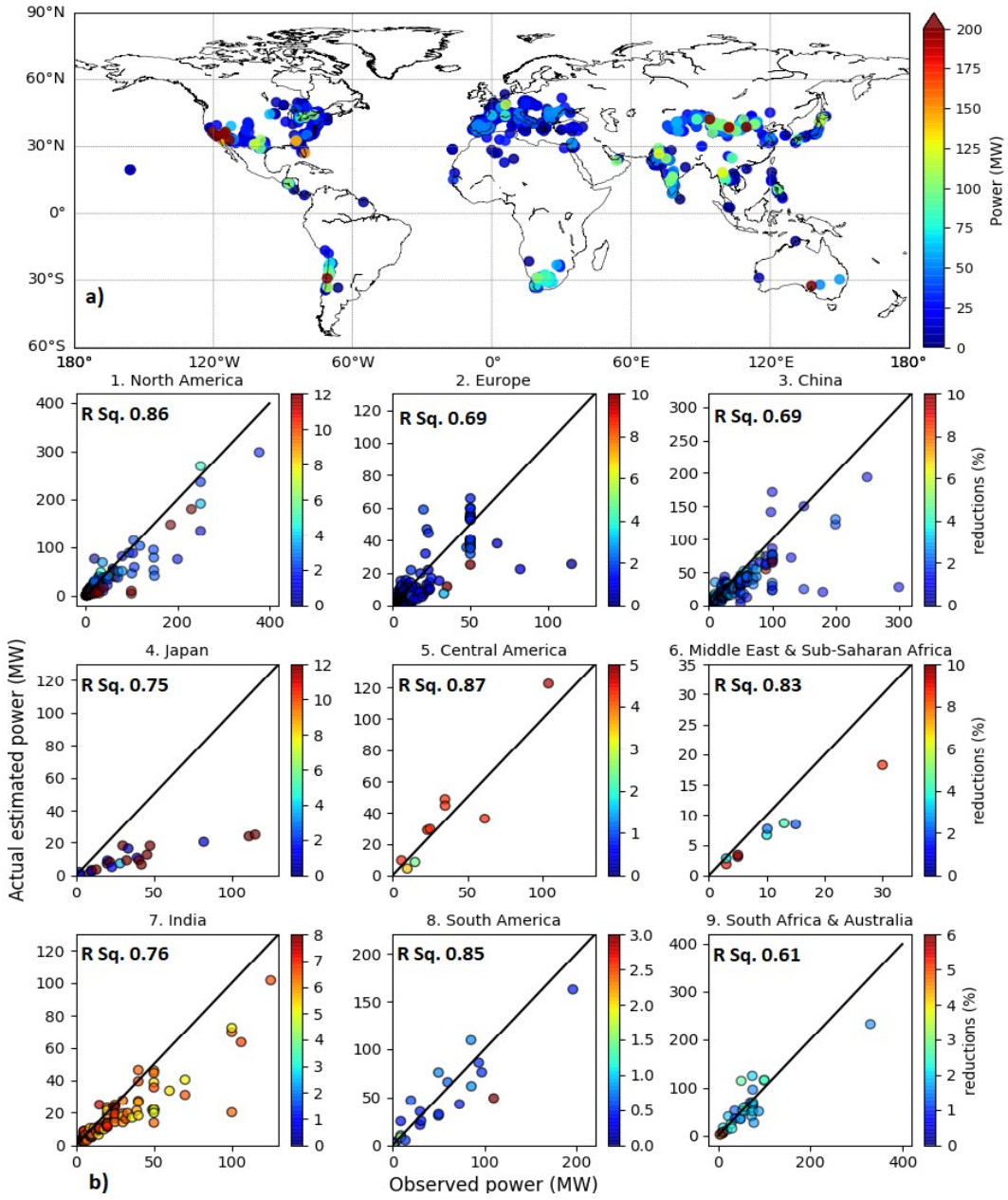

Fig 3.14a): Locations of existing solar power plants used in our validation, and taken from Wiki–Solar dataset. **b**) Scatter plot between observed power and the actual estimated power for global nine regions based upon their contribution to the total generation from solar PV.

3.8 Uncertainty analysis

3.8.1 Solar PV cell type

We used c–Si modules in our analysis because of the highest share in the market and the highest efficiency among all available solar cell materials commercially available. Though, bearing relatively similar characteristics, Polycrystalline silicon (p–Si) as well as another kind of technologies like the thin–film which includes cadmium telluride (cdTe) and amorphous silicon (a–Si) are also promising because of being less expensive as it uses fewer materials (Vrielink et al, 2012). In addition to cell efficiency, thermal resistances indicated by a power–temperature coefficient ($d\eta/dT$)of the entire cell types presented above are different. For p–Si and a–Si, it is reported as –0.4%/°C and –0.26%/°C respectively (Dubey et al,, 2012). While, cdTe has a lower value of –0.2%/°C (Strauss, 1977) as compared to others. With varying efficiencies like above, we checked the solar PV efficiency variation for all cell types. The results have shown some improvement in terms of R^2, and maximum value of 0.769 is observed for cdTe cell having the maximum resistance to the temperature changes for cell efficiency of 17%. In addition, we also proposed four virtual cells (VC1–VC4) with intermediate resistance to the temperature changes as compared to the normal cells. Their performance is someway close to the normal ones and a maximum R^2 value (0.769) is seen for virtual cell (IV) for cell efficiencies 17%, 18%, and 19%.

3.8.2 Solar PV cell efficiency

As stated earlier, for c–Si PV modules, we used a constant value of solar cell efficiency of 15% in the analysis. However, significant improvement in terms of solar PV cell efficiency is recently claimed by various manufacturers. Likewise, for commercial usage, Tyagi et al, (2013) reported the efficiency claimed by the c–Si PV modules manufacturer normally lies between 15% and 17%. As reported by Green et al, (2003) c–Si PV modules bear a cell efficiency of 20%, while Sampaio and Gonzalez (2017) reported a lower efficiency of 13%. Therefore, we performed a sensitivity analysis by using the varying efficiency (12%–20%) to see how it might affect the final outputs. The results in the shape of a heatmap are presented in Fig. (3.15). It is seen that cell types with higher resistance to temperature and high efficiencies have higher R^2 values. CdTe and VC–4 show the maximum values as 0.769 for 18% and 19% cell efficiency.

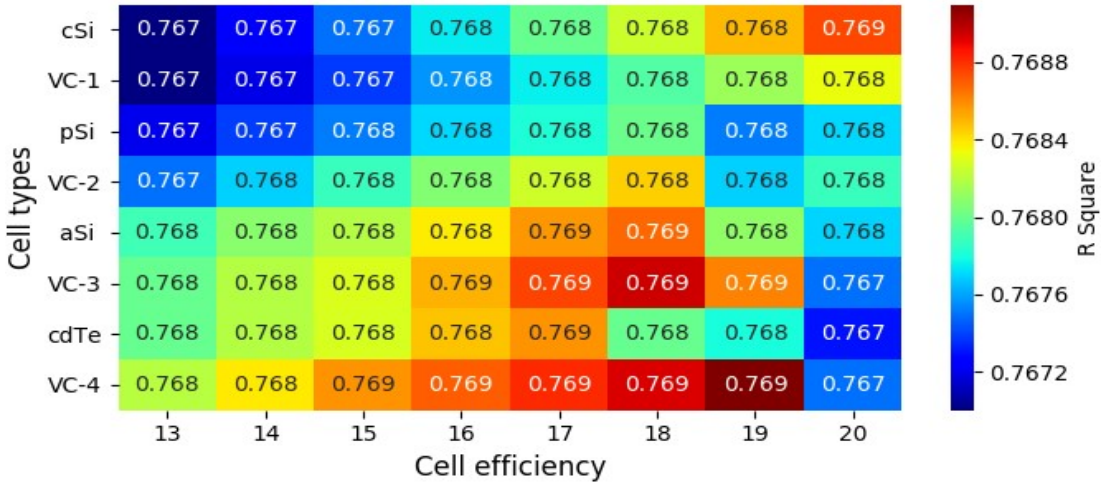

Fig 3.15: Heat map for R^2 values for varying cell efficiencies and available four cell types. In addition, we introduced four virtual cells (VC1–VC4) between the normal cells based upon temperature resistance coefficients.

3.8.3 Changes in Solar PV optimum tilt–angles

Both solar PV cell efficiency losses from dust and snow covers are proportional to the tilt–angles. Higher tilt–angle offers to roll of dust particles and helps to slide of falling snow. In our analysis, we used optimum tilt–angles to calculate such effects on power output. However, due to site conditions or topography, there are chances that such angles are not fully adopted. Therefore, we did the uncertainty analysis to check whether and how much it affects our results in terms of R^2. We selected four additional positions (–5°, –2.5°, +2.5°, and +5°) in accordance with the optimum tilt–angles. The results show variations in terms of R^2 values which decreases for lower angles (–5° and –2.5°) and slightly improved for higher tilt–angles (+2.5° and +5°) due to the changes in dust and snow loss factors. A maximum R^2 value of 0.795 is recorded for maximum tilt–angle change (+5°) for cdTe, while the lowest is 0.774 at the lowest angle change (–5°) for c–Si solar cell type (Fig. 3.16a). Similarly, a regional heatmap in Fig. (3.17) demonstrates the variations on the regional basis.

3.8.4 Data source

The results are also verified and cross–checked using different data set to see how it affects the output. For this purpose, WATCH Forcing Data applied to ERA–Interim reanalysis

data (WFDEI) is used. The temporal and spatial resolution of WFDEI is the same as that of GSWP3, for example, 0.5 º and daily from 2001–2014. The details of the data set can be seen from Weedon et al, (2014). The final output using the new forcing data set is compared with that of the output from GSWP3 and presented in Fig. (3.16b). It is seen that a high R^2 value =0.99 exists between the power outputs of both datasets. Hence, it provides satisfaction overusing the GSWP3 data set with no considerable change by moving to another data set.

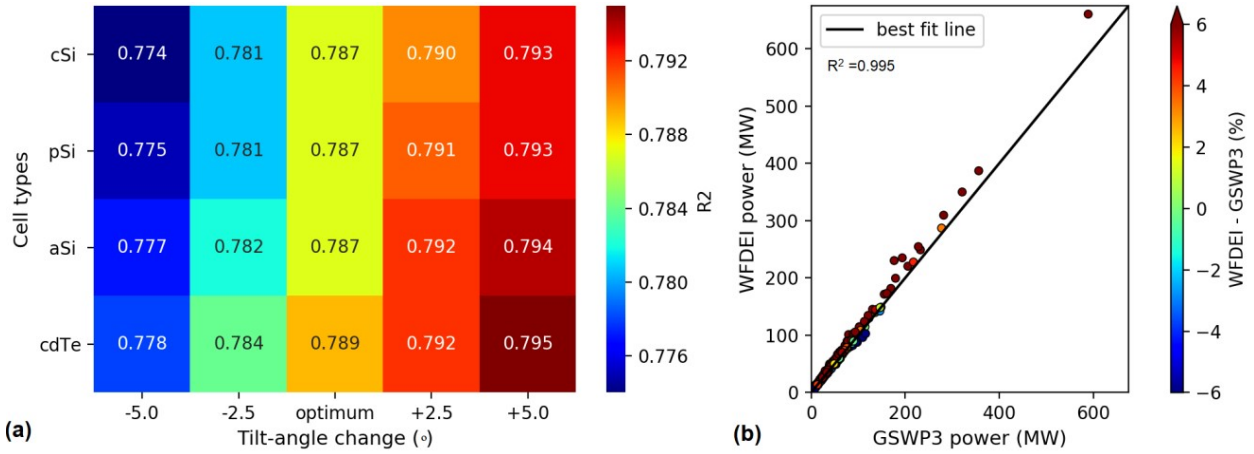

Fig 3.16a) Heat map for R^2 for changing tilt–angles in comparison to optimum ones for four cell types. **b**) Scatter plot for final power output for GSWP3 dataset and WFDEI dataset. A rational R^2 value of 0.99 is obtained between both of them.

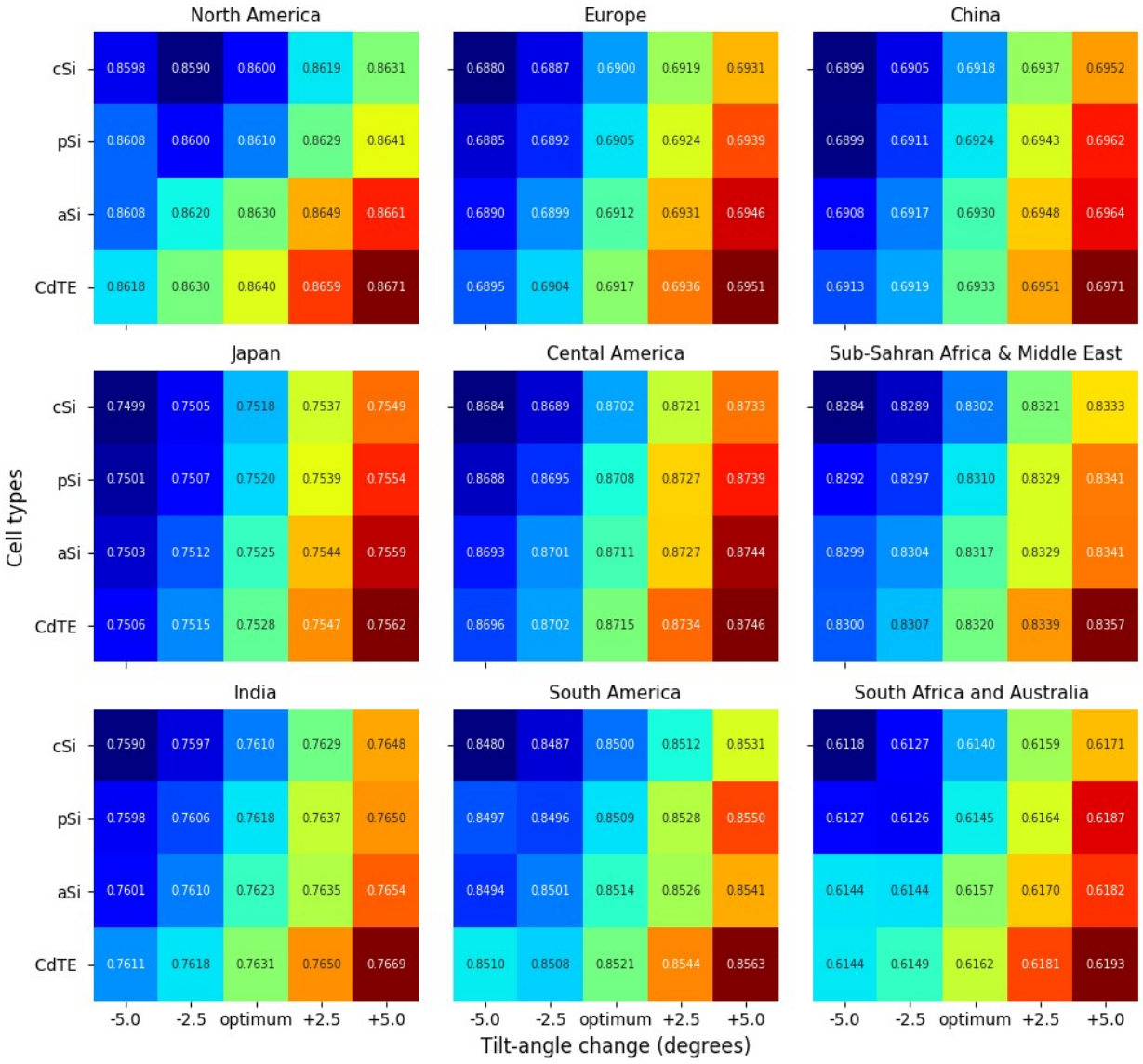

Fig 3.17 Regional heatmap for R^2 values for changing tilt–angles in comparison to the optimum ones for four cell types.

3.9 The economic analysis of solar PV electricity

3.9.1 The cost of PV electricity for centralized scheme

The global gridded cost of the centralized scheme is provided in Fig. (3.18) using the relationship provided in section 2.6.2. The estimates show that cost is lower in areas with higher technical potential or good solar resources. The cost is lower (<0.08$/KWh) in areas like Eastern USA, Western South America, Sub–Saharan Africa, the Middle East, parts of China, and Australia as they have reasonable solar resource. These areas if containing a bigger population with higher electricity demands can be provided with big solar parks to fulfill their electricity demands. Likewise, Western USA, Eastern North America, South Africa, South Asia also has a fair cost for solar PV installation, ~0.12$/KWh. The costs are somehow higher (~0.135$/KWh) for parts of the Middle East, Western China, India, and Japan due to less technical potential of solar PV. Other areas like Europe, USSR, and Canada have a very high cost and not in competition with conventional energy technologies.

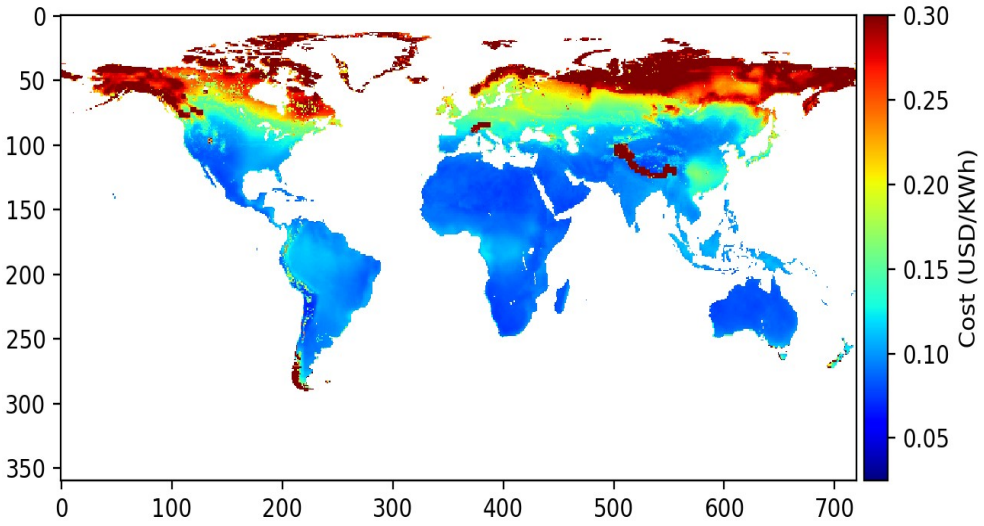

Figure 3.18: Grid-scale spatial distribution of the centralized solar PV electricity generation costs at a global scale for 2015

3.9.2 Cost supply curves of PV electricity for centralized scheme

In addition to the gridded electricity estimates, cost supply curves for main regions are also drawn and presented in Fig. (3.19). At a global level as well as for world-main regions, the

figure contains the technical potential (PWh/yr) in association with their electricity production costs for solar PV. Australia has the maximum potential, approaching 50 PWh/yr, while Sub-Saharan Africa has the least cost, 0.065$/KWh among all other prominent regions. Quite close to Australia, Northern Africa also show a lower cost, 0.07$/KWh with a large potential of 47.9 PWh for 2015. In addition, Other Africa has more potential with lower costs. While other regions show very small potential and higher costs. Europe has the least potential, 3.25 PWh, and a higher cost of >0.235 USD for the same year. For decentralized schemes, the cost–supply curves are similar; however, the supply is about 50 times less. The most attractive regions concerning the techno–economic potential of PV electricity include Northern, and Southern Africa, the Middle East, and Oceania. Where an amount of electricity is equivalent to the current world electricity consumption and can be produced at costs below 0.065$/kWh.

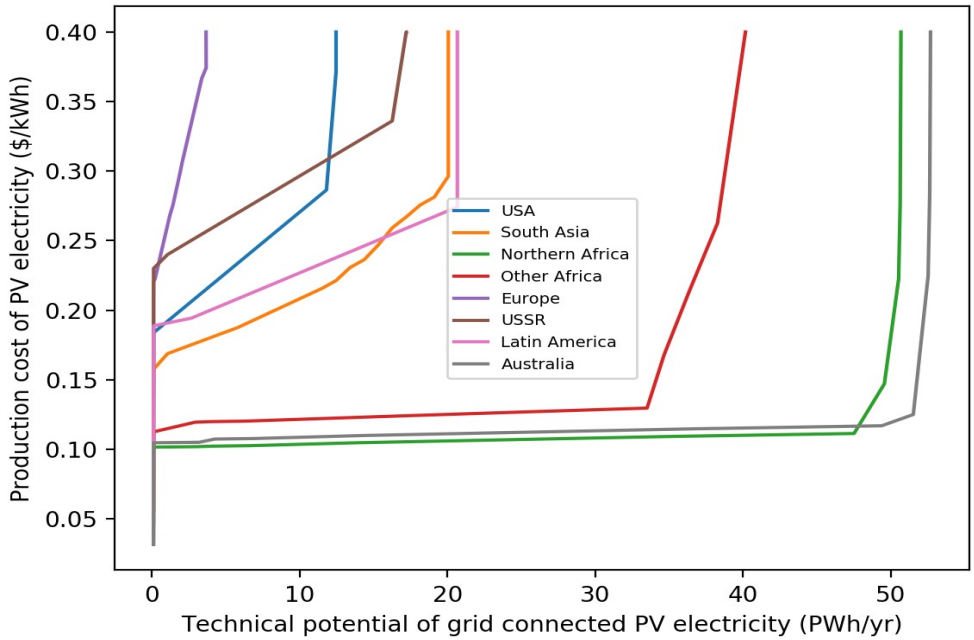

Figure 3.19: Global and regional cost–supply curves for centralized PV scheme for 2015. The Northern Africa has the least cost while Australia has the maximum solar PV potential,

3.9.3 The cost of PV electricity for decentralized scheme

The global gridded cost of the decentralized scheme is also calculated and provided in Fig. (3.19). The estimates show that cost is lower for most areas with good technical potential, The cost is lower (~0.09 $/KWh) in areas like the USA, South America, Sub–Saharan Africa,

South Africa, the Middle East, Southeast Asia, and Australia. In these regions, Western USA, South Asia, Western China, and Japan have big urban population clusters which can be provided with centralized solar PV system to fulfill their electricity demands. In contrast parts of China, Russia, Europe, and Canada have higher PV costs (>0.20 $/KWh) due to less available solar resources. But still, they can be used for small-scale levels like charging small devices, running small motors for pumping, etc.

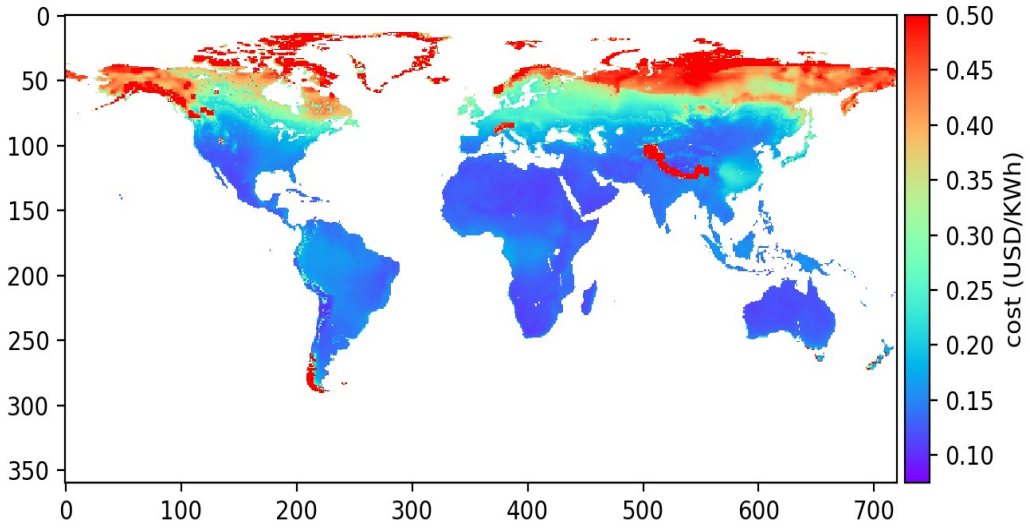

Figure 3.20: The global grid-scale spatial distribution of decentralized solar PV electricity generation costs.

3.10. Summary and conclusions for solar PV cost analysis

In this research, we have examined the theoretical, geographical, and techno–economic potential of solar PV electricity globally and regionally as well. Globally, the technical potential of both centralized (On–grid) and decentralized (Of–grid) PV schemes is estimated at a value of ~4.02× 10^2 PWh/yr, or about 21.9 times the current global electricity consumption. For most areas, 95.2% consists of a centralized PV schemes. For a cut–off price of 0.4 $/ kWh, the present technical potential is around 3.9× 10^2 PWh/yr. The current global electricity consumption can be produced at prices around 0.130 $/kWh. It should be kept in mind that this number does include costs involved in grid–connection, transmission, and distribution but not the storage costs. The solar PV potential greatly depends on the existing area for its fixation, which at a regional scale can be smaller than 1% of the overall area, and the conversion rate (efficiency) of PV cells, and

the PR value of a PV system. Depending on potential growth in technology development, i.e., an improvement in the PV cell conversion efficiency or an increase in the PR values of PV scheme, the technical potential of an On–grid PV schemes may increase with a factor twice as of current. Likewise, the technical potential of the decentralized scheme may even boost because of an amplified rooftop area. It is also approximated on the basis of likely future price reduction that it may become feasible to produce the required consumption at a cost competing for the conventional energy technologies. This would involve that regions like Sub–Saharan and Northern Africa, the Middle East, and Australia would produce and export huge amounts of electricity. Though, it will involve the high transmission and infrastructural costs which may be estimated carefully to have a real picture of the economic potential of solar PV electricity.

Chapter 4: RESULTS AND DISCUSSIONS

WATER

4.1 Water Scarcity

4.1.1 WTA for H08

WTA provides the map of water scarcity on a global level for various stress limits. Fig. (4.1) shows the output for the H08 model for GCM HadGEM2–ES and MIROC5 along with their ensemble mean. All of them shows quite similar trends, where parts of the USA, Europe, Sub–Saharan Africa, The Middle East, South Asia, and China show severe scarcity. Similar areas have higher proportions of higher stress regions as well. All of these have more withdrawals in comparison to the available freshwater resources. However, in comparison to stressed areas, there are many areas (blue ones) with no or zero scarcity as well. The areas with a white color contain regions with no population.

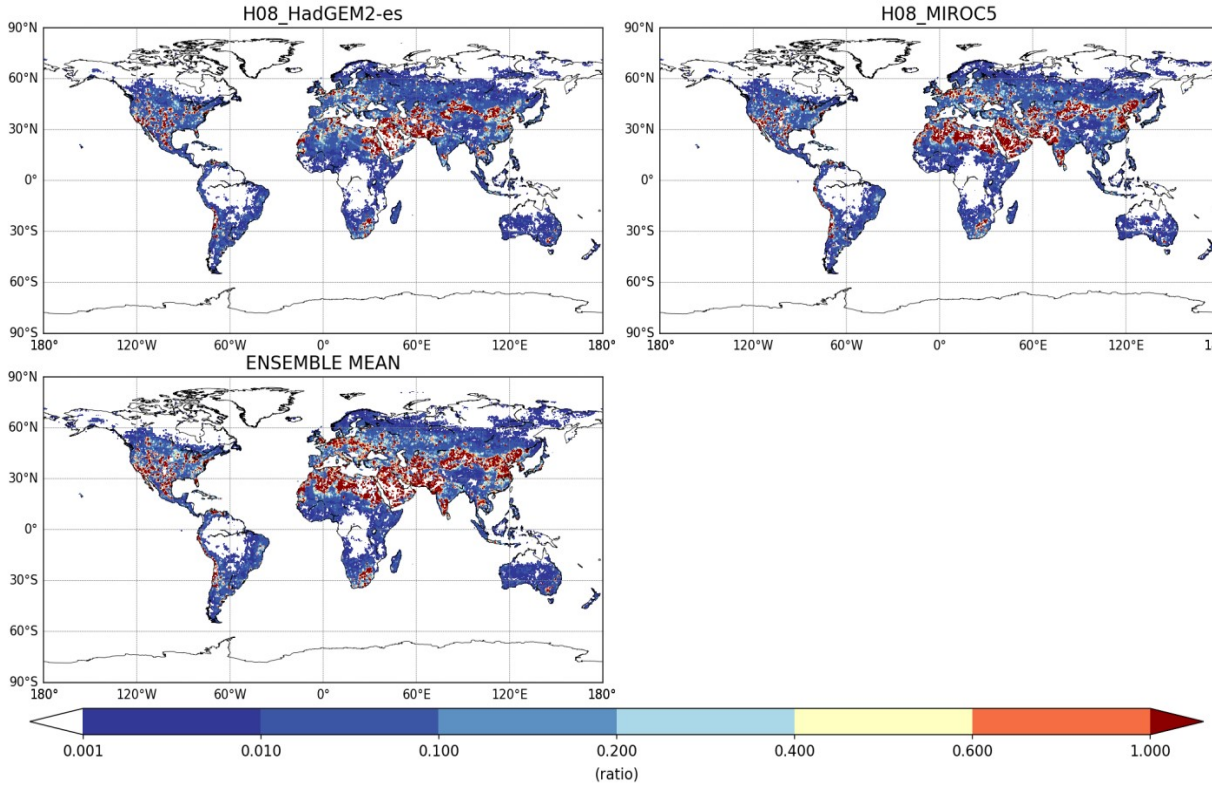

Fig 4.1: Water scarcity maps obtained while using WTA for H08 model along with two GCMs, HadGEM2–ES and MIROC5. The ensemble mean is also calculated for both GCMs.

4.1.2 WTA for WATERGAP2

WTA provides the map of water scarcity on a global level for various stress limits. Fig. (4.2) shows the output for the WATERGAP2 model for GCM HadGEM2–ES and MIROC5 along with their ensemble mean. GCM MIROC5 has more scarcity however, mostly they show quite similar trends, where parts of the USA, Europe, Sub–Saharan Africa, The Middle East, South Asia, and China show severe scarcity. Similar areas have higher proportions of higher stress regions as well. All of these have more withdrawals in comparison to the available fresh water resources. However, in comparison to stresses areas, there are many areas (blue ones) with no or zero scarcity. The areas with no or least population are shown with white color.

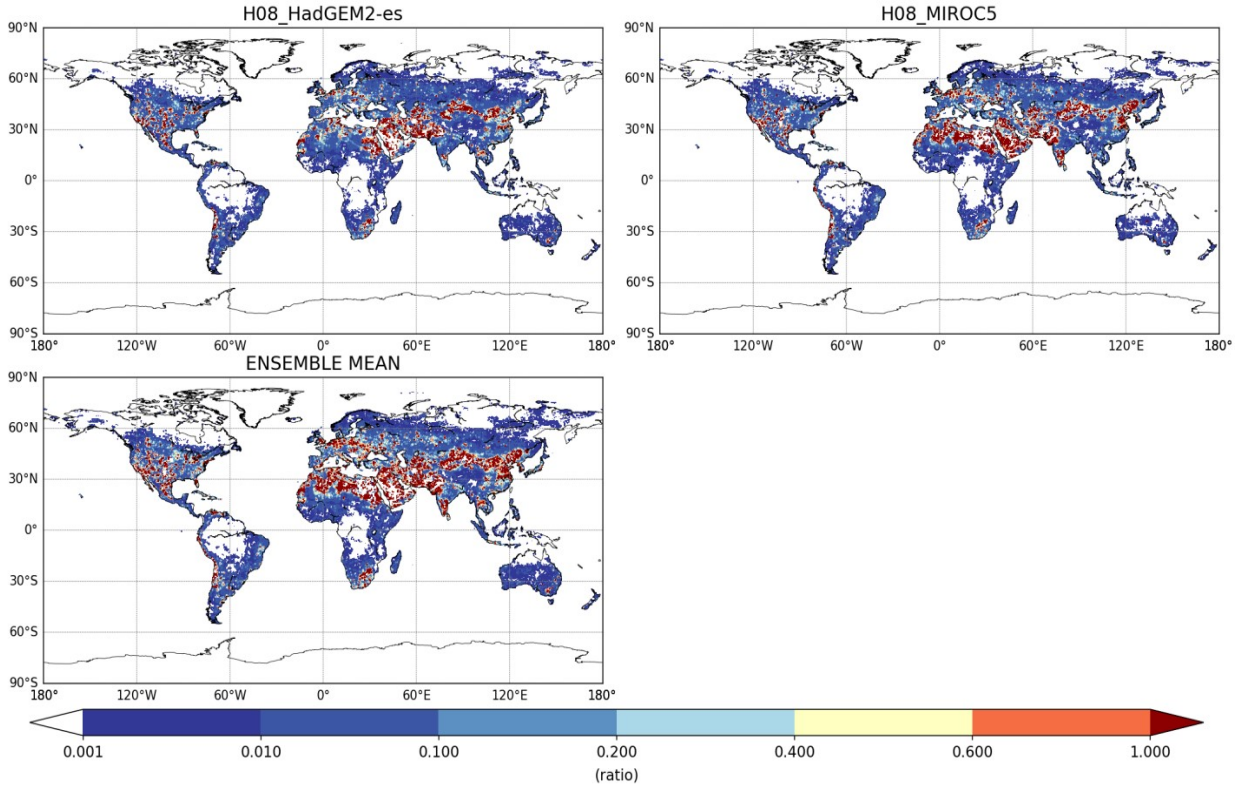

Fig 4.2: Water scarcity maps obtained while using WTA for WATERGAP2 model along with two GCMs, HadGEM2–ES and MIROC5. The ensemble mean is also calculated for both GCMs.

4.1.3 People under various stress limits

4.1.3.1 H08

Since from WTA, we have grid-wise population under various stress limits on a global scale. Then using AIM regional raster map, we aggregated the population in each region to see

the number of people under various stress limits in each region for the H08 model and shown in Fig. (4.3). For Low-stress limits, most of the population in each region falls in this category. For medium stress, maximum peoples are recorded for Europe, China, India, and the Rest of Southeast Asia regions. A similar situation is seen for high-stress limits. While for severe stress limits, regions like China, India, the Middle East, and the Rest of Latin has a bigger population. The numbers are recorded 235.5mill, 140.2mill, 78.59mill, and 77.59mill respectively. Similar regions have 120.7mill, 70.8mill, 18.2mill, and 25.59mill population under the High-Stress situation as well.

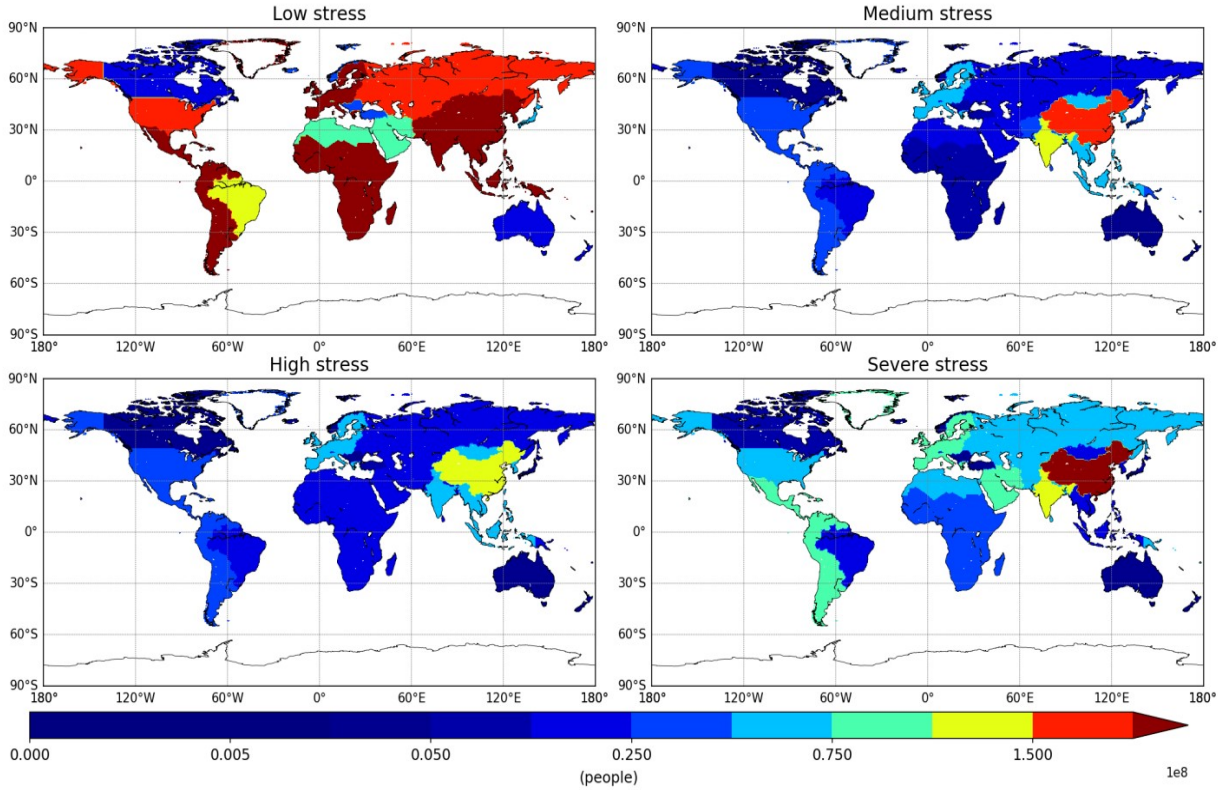

Fig 4.3: Population (numbers) under various stress limits for the ensemble mean of H08 for AIM regions globally.

4.1.3.2 Percentage population under stress levels for H08

After calculating the population under various stress limits in each AIM region, we checked their percentage in association to the total population in a region for the H08 model and shown in Fig. (4.4). For Low-stress limits, almost more than 40% of the total population in each region falls in this category. For medium stress, about 10–20% of the total population is seen for

USA, Europe, China, Middle East, and Australia, and New Zealand. While other regions have less than 10% of their total population under this stress limit. About 10–20% of the total population of Europe and Turkey falls in high stress limit category. For severe-stress limits, regions like The Sub–Saharan Africa, and The Middle East has 30–40% of total population in this category; the USA, South America, and Russia have 20–30%; however, Canada, Europe, China and India have 10–20% of the total population under severe limits. While other regions have 0–10% of their total population under this stress limit

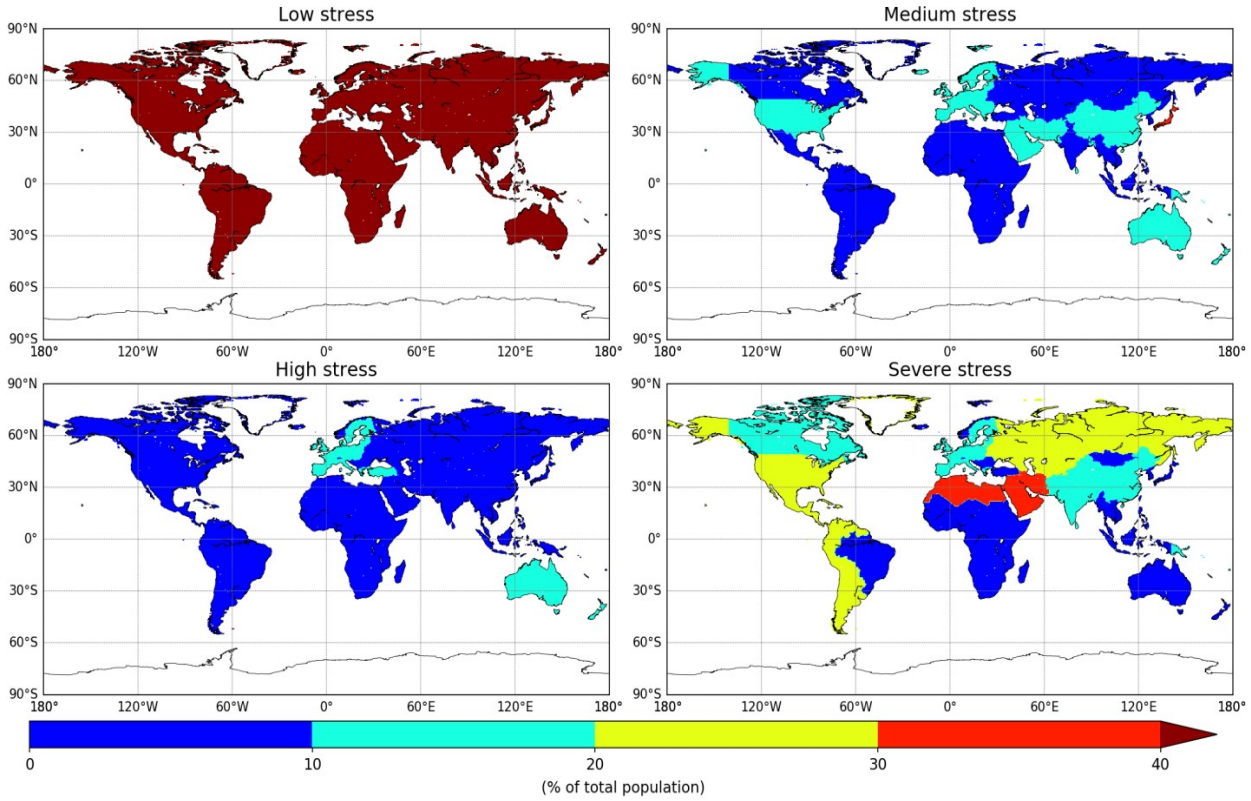

Fig 4.4: Percentage of population (%) with respect to the total population under various stress limits for the ensemble mean of H08 for AIM regions globally.

4.1.3.3 WATERGAP2

Like the H08, we also applied WTA to know the grid-wise population under various stress limits on a global scale. This number is aggregated to AIM regions to see the number of people under various stress limits in each region for the WATERGAP2 model and shown in Fig. (4.5). For Low-stress limits, most of the population in each region lies in this category. For medium stress, maximum peoples are recorded for Europe, China, India, and Rest of South and

East Asia regions. A similar situation is seen for high-stress limits. While for severe-stress limits, regions like The USA, South America, Europe, Sub–Saharan Africa, South Africa, The Middle East, China, India, and the Rest of Southeast Asia has a huge population. The statistics are quite similar to that of the H08.

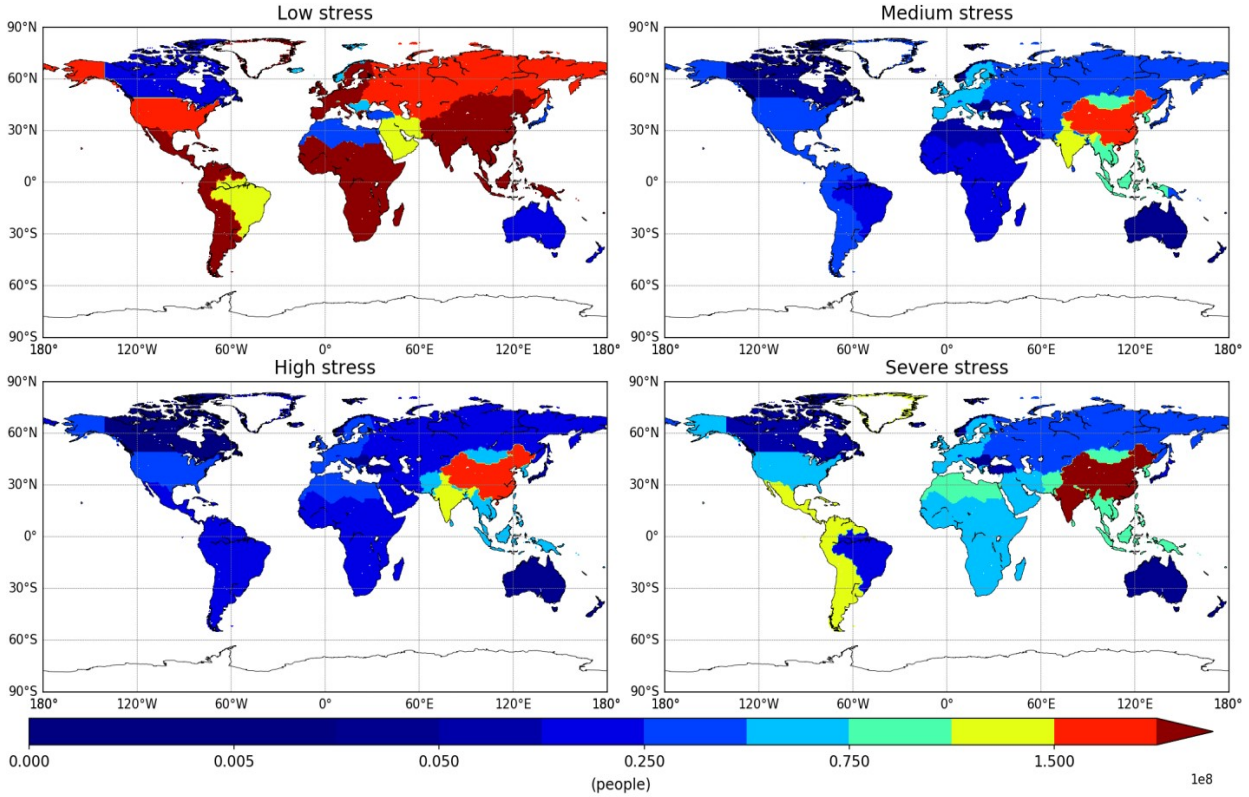

Fig 4.5: Population (numbers) under various stress limits for the ensemble mean of WATERGAP2 for AIM regions globally.

4.1.3.4 Percentage population under stress levels for WATERGAP2

After calculating the population under various stress limits in each AIM region, we also checked their percentage in association to the total population in a region for WATERGAP2 model and shown in Fig. (4.6). For Low-stress limits, almost all regions except Sub–Saharan Africa, more than 50% of the total population falls in this category. For medium-stress, about 10–20% of the total population is seen for USA, Europe, China, Middle East, and Australia and New Zealand. While other regions has less than 10% of their total population under this stress limit. About 10–20% of the total population of USA, Sub–Saharan Africa, Turkey, Other Asia, China and Australia, and New Zealand falls in the high-stress limit category For severe stress

limits, regions like Sub–Saharan Africa has 40–50% of the total population; The Middle East has 30–40% of the total population; USA, South America and Russia has 20–30%; Canada, South America, India, and China has 20–30%; however, Russia, Europe, the Rest of South and East Asia, and Australia and New Zealand 10–20% of the total population under severe-stress limits. While other regions have 0–10% of their total population under this stress category.

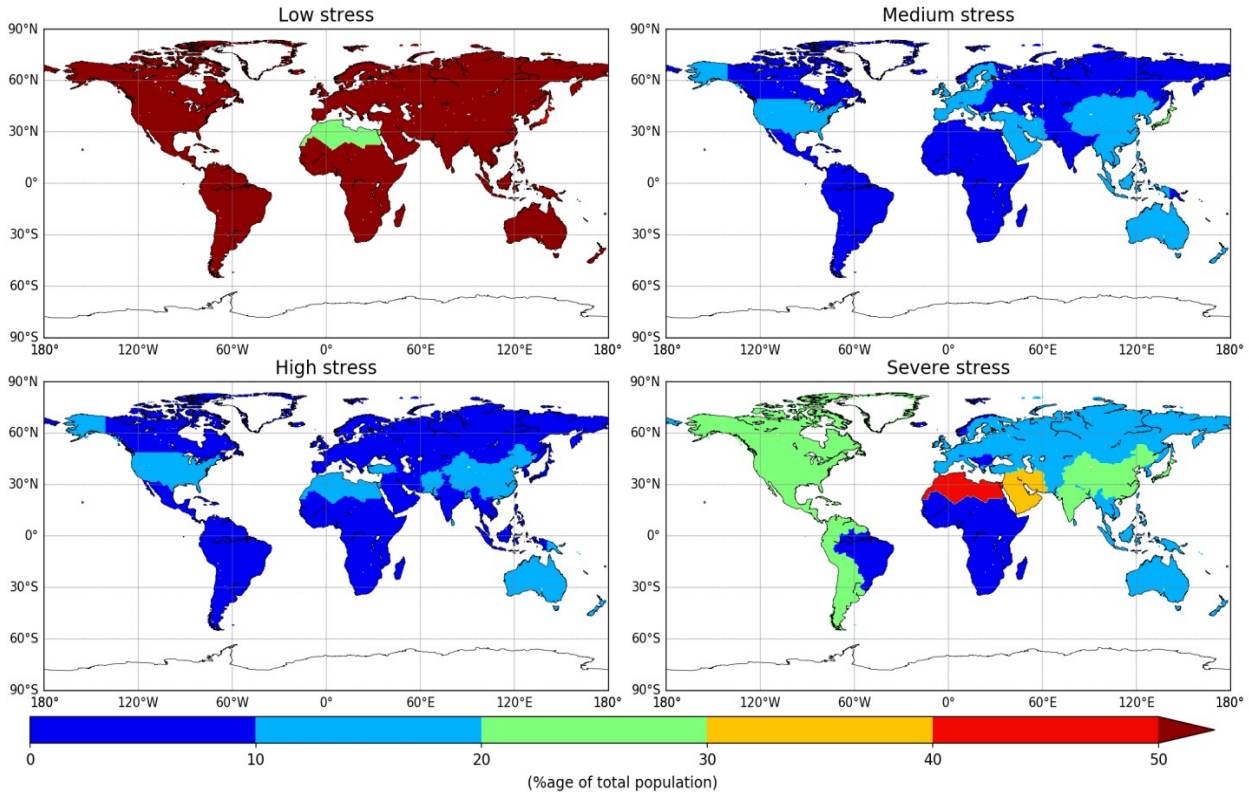

Fig 4.6: Percentage of population (%) with respect to the total population under various stress limits for the ensemble mean of WATERGAP2 for AIM regions globally.

4.2 Electricity generation

4.2.1 Thermoelectric Power Plants

Globally 80% of electricity is supplied by the TEPPs. Therefore we considered their four major kinds including Coal, Oil, Gas, and Nuclear based upon their contribution to the total generation by fossil-fuelled power plants. As of 2015, the maximum contributions for Coal power plants are seen in the total generation, which is $9.59X10^6$ GWh, equals 52% of the total generation. While the least one, 4.83% is for Oil power plants. The distribution of TEPPs is available in Fig. (4.7) where it is seen that most of the Gas fuelled plants are located in China, India, and Russia. In contrast, Coal fuelled plants are available in the USA, South America, and The Middle East. While Oil fuelled plants are in the USA, Europe, and China. Water withdrawals by such plants are highly dependent upon their generation technology, and cooling types. Thus such distributions are supposed to highly affect the regional water withdrawals to cool the TEPPs.

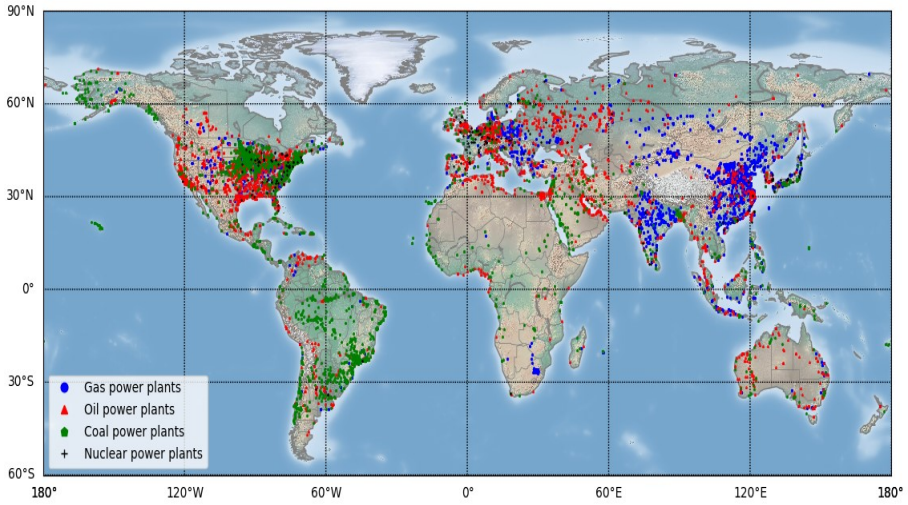

Fig 4.7: Geographic location of all TEPPs (Coal, Oil, Gas and Nucl) as obtained from World Resources Institute (WRI. 2018).

4.2.2 Electricity demands by TEPPs

We used TEPPs database provided by WRI (WRI. 2018) for the first time to model the electricity consumptions for AIM regions using the methodology provided in section 2.7. The results are presented in Fig. (4.8). It is seen that regions like China, The USA, and Europe are generating more electricity from TEPPs, which are 13.40EJ, 12.35EJ, and 7.22EJ respectively.

While, regions like Rest of Asia, Brazil, Turkey, and Canada are generating least powers from TEPPs which are 0.46EJ, 0.54EJ, 0.69EJ, and 0.87EJ respectively.

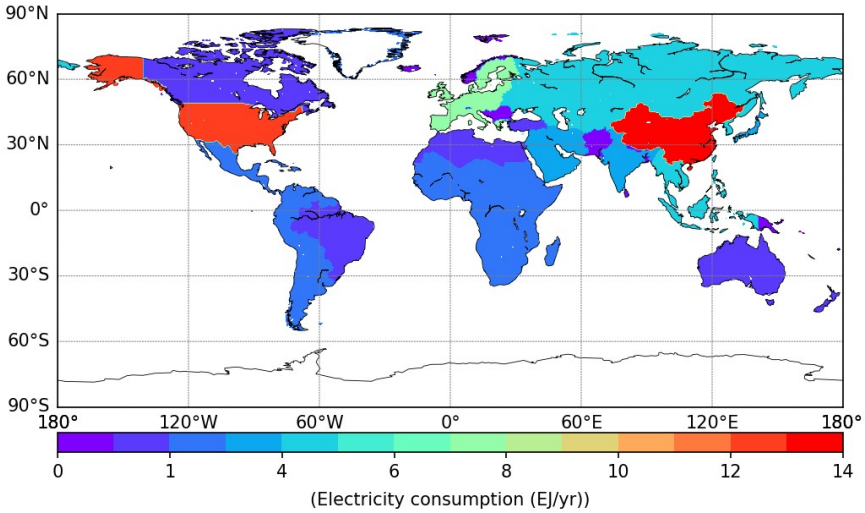

Fig 4.8: Electricity demands for AIM regions by TEPPs (Coal, Oil, Gas and Nucl).

4.2.3 Comparison of electricity estimates with literature

Electricity generation by our methodology using WRI dataset (WRI. 2018) is then compared with the existing estimates from AIM model. The results are presented in Fig. (4.9). Scatter plot shows quite high R^2 value (0.931) between our estimate and AIM model outputs. This shows satisfactory performance of our methodology and high global coverage (>80%) of WRI. (2018) database for TEPPs as claimed by their developers.

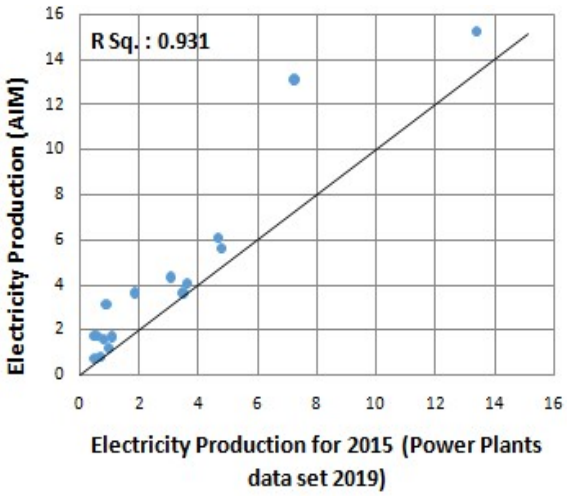

Fig 4.9: Scatter plot between electricity generations by our method with the AIM model outputs. A rational R^2 value= 0.931 shows higher coverage of our database globally.

4.2 Water withdrawals

4.2.1 Cooling water for TEPPs

Using the above electricity generation estimates, and WUI for each cooling technology type, we calculated water withdrawals by TEPPs for each AIM region. The methodology has already been provided in section 2.7.3. The maximum cooling water withdrawals (CWW) are seen for the USA, China, Europe, Russia, and India, which are 218.4Km^3, 131.78 Km^3, 83.3Km^3, 79.84Km^3, and 56.11Km^3 respectively. Most electricity generation was seen for China, but, interestingly, more CWW are witnessed for the USA. There are two main reasons, first is the cooling technology type which uses different WUI, and second is the seawater shares, which vary among both countries. More power plants from coal and oil are witnessed for the USA, while, China has gas power plants the most. Such differences are making the variations in the CWW among these two regions. Likewise, the lowest CWW are seen for regions like the Rest of Asia, Brazil, Australia and New Zealand, North Africa, Other Africa, and Canada, which are 1.76 Km^3, 3.68 Km^3, 3.82 Km^3, 4.86 Km^3, and 4.89 Km^3 respectively.

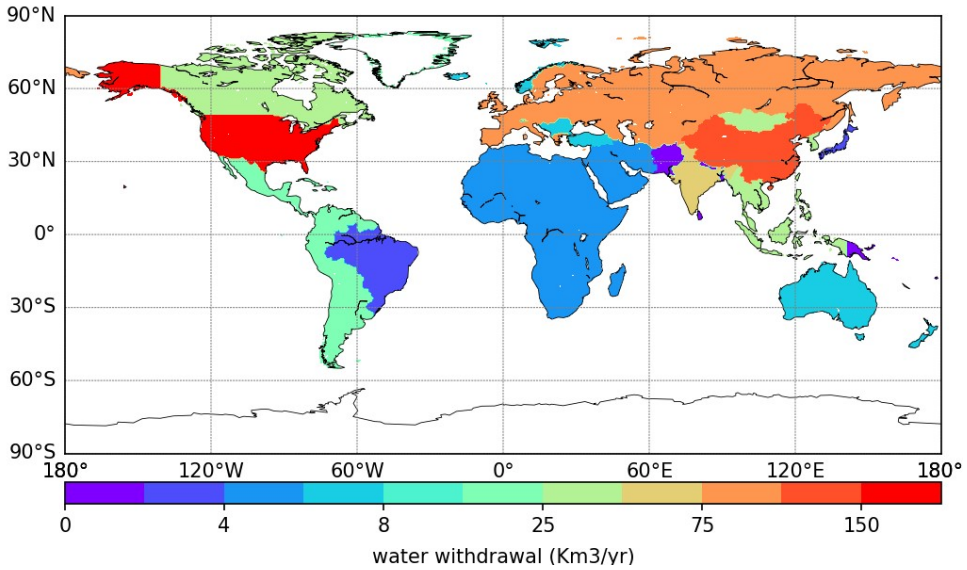

Fig 4.10: Water withdrawals (Km^3/yr) while generating electricity by TEPPs for AIM regions using the WRI database.

4.2.2 Comparison of water withdrawal estimates with literature

The CWW estimates for electricity generation are very scarce. Food and Agriculture Organization (FAO) provides some country statistics, but it is for total IWW, not the CWW by

the TEPPs. In addition, the data is scarce, not covering too many countries, and temporal resolution is not harmonized as well. Recently, there is one global study by Huang et al, (2017), who calculated the CWW by using some downscaling methods. Therefore, we compared our methodology with that study. The results are presented in Fig. (4.11). The scatter plot shows a quite high R^2 value (0.942) between our estimate and those by Huang et al, (2017). This shows an adequate performance of our methodology and high global coverage of WRI. (2018) database for TEPPs.

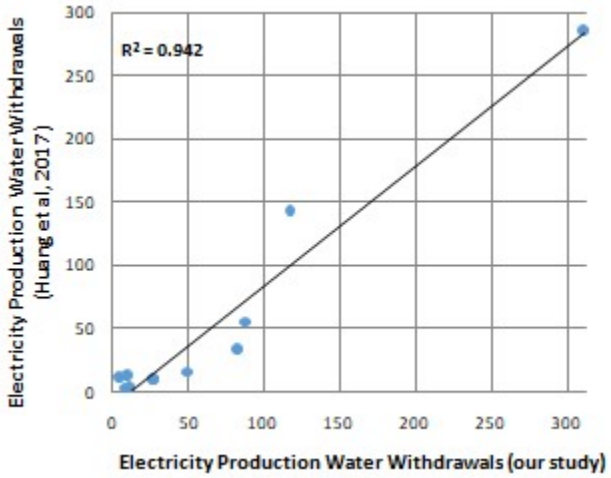

Fig 4.11: Scatter plot between electricity water withdrawals (Km^3/yr) by our method with Huang et al, (2017). A rational R^2 value= 0.942 is obtained between both studies.

Chapter 5: RESULTS AND DISCUSSIONS

ENERGY–WATER NEXUS (EW–nexus) FOR FUTURE SUSTAINABILITY

5.1 Future solar PV resource

Similar to the current analysis, future solar PV resources are calculated in the same manner at a global scale. It should be kept in mind that cell efficiency is changing (improving) with time, however, to have a comparison for current and future resources; it is kept constant with time. The daily mean annual solar PV resource for 2050 and 2100 is presented in Fig. (5.1). For all SSPs and RCPs, the most efficient continental locations consist of western America, Sub–Saharan and South Africa, The Middle East and Australia with annual PV resources are more than 300W/m^2. This pattern is generally in line with the earlier assessment of solar PV power potential (Adeh et al, 2019). Some other areas counting South America, South Asia, and Southeast Asia also contain a rational amount of PV resource ranging from 20–30W/m^2. On the contrary, Russia, Canada, Europe, Russia, and the Himalayas have the least or even no power output in DJF and MAM mostly due to thick snow covers and less incoming SWR because of their geographic location. Significant solar cell efficiency drops are also seen for Sub–Saharan Africa, Australia, The Middle East, India, and Eastern China because of higher temperature and dust covers; however they still have plentiful resources because of higher incoming SWR.

The difference of current and future solar PV resources is also calculated for all SSPs and RCPs and presented in the bottom of Fig. (5.1). For SSP1–RCP2.6, most areas have shown a reduction in the total resource. They include Sub–Saharan Africa, The Middle East, Europe, USSR, and Australia, etc. A maximum decrease of 6.23% is seen in Europe due to the climate change impact. However, some regions like South America, South Africa, parts of China, and Australia have also shown an increase (5.91% max) in the solar PV resource. Similarly for SSP2–RCP4.5, regions like South and North America, Sub–Saharan Africa, The Middle East, Europe and USSR, etc have witnessed a decrease in the solar PV resource. A maximum decrease of 6.41% is seen in Europe. While parts of South Africa, India, USSR, and Australia have shown

an increase in the solar PV resource, and a maximum of 5.79% is seen for Europe. Lastly, the variation in the solar PV resource for SSP3–RCP.0 is observed quite similar to the SSP1–RCP2.5. Where, an increase of solar PV resource is noted for South and North America, South Africa, India, parts of China, and Australia. While, a drop in solar PV resource (6.78% max), is also observed for parts of North America, Europe, USSR, and China, etc. These future estimates provide an insight that how important and prominent is climate change impact in the assessment of solar PV resources.

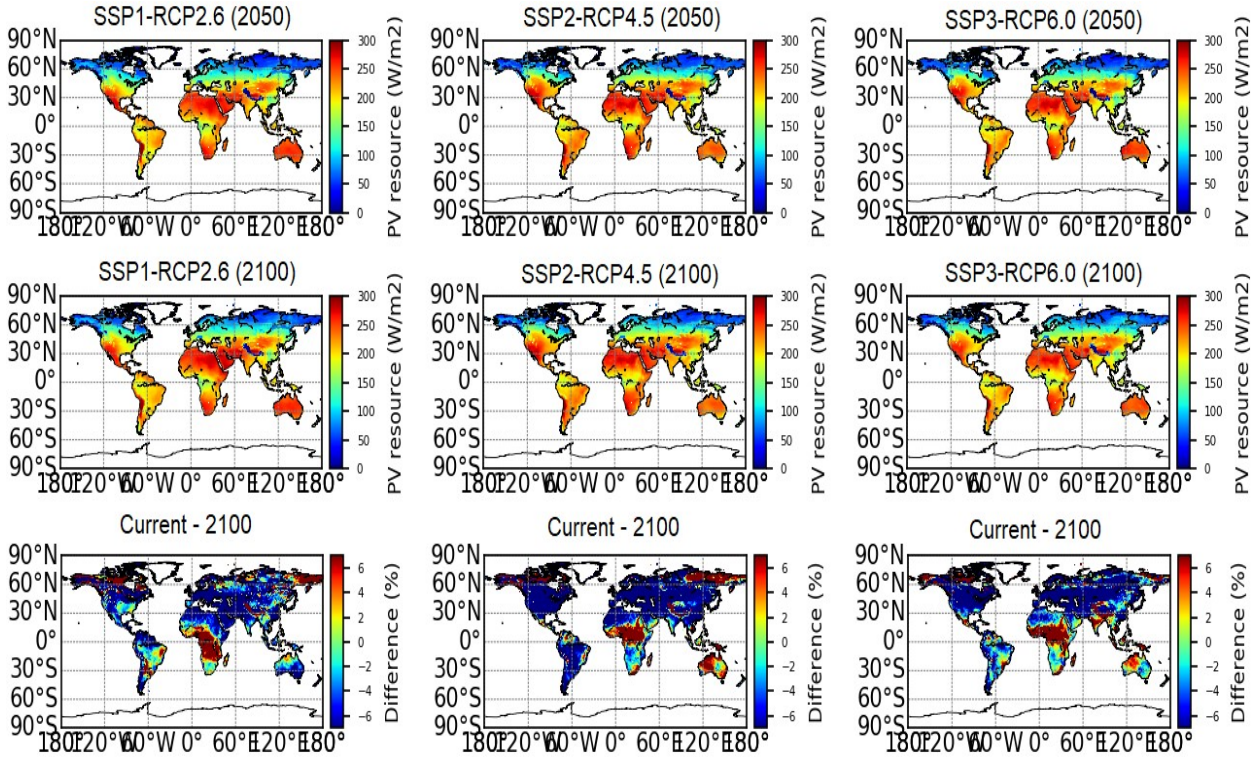

Fig 5.1: Future solar PV resource (W/m^2) and difference (%) of current and future PV resources for various SSP and RCP scenarios.

5.2. Future water withdrawals for BAU scenarios

AIM model outputs for various SSP and RCP scenarios are used as a representative of the BAU scenario. Using the similar methodology, provided in section 2.7.3, CWW are estimated for the future (2050 and 2100) for all such SSPs and RCPs. The outputs for all corresponding scenarios are presented in Fig. (5.2).

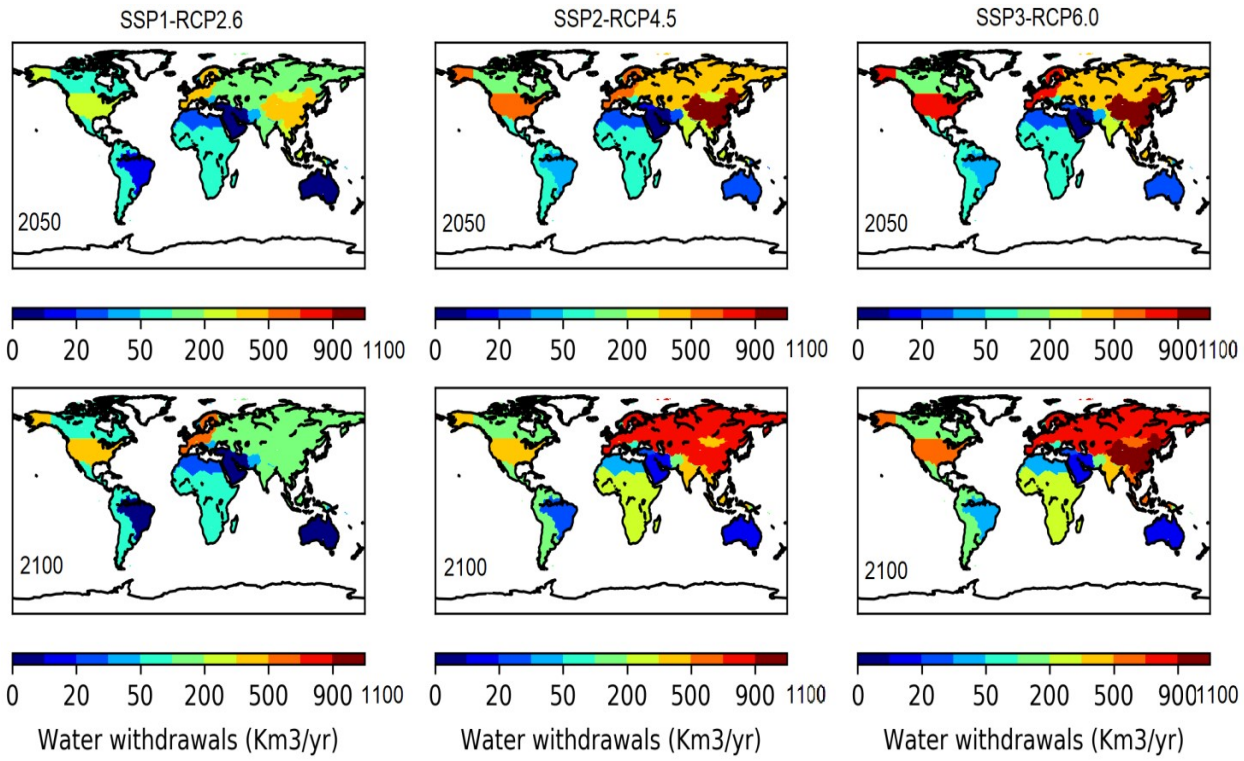

Fig 5.2: Future water withdrawals (Km3/yr) for the BAU case for various SSP and RCP scenarios.

For almost all scenarios, the maximum CWW are seen for the USA, China, Europe, Russia, and India, etc. due to their higher electricity demands. For SSP1–RCP2.6, a maximum CWW of 438.07Km^3 and 626.14Km^3 a year are seen for Europe for 2050 and 2100 respectively. Moving from 2050 to the end of the century, an increase in CWW is seen for Europe and the USA, whereas, a decrease in CWW is noted for the Rest of Asia and China, mainly attributed to the technological shifts and efficiency improvements. Also, more electricity generation was seen for USA, but, interestingly, more CWW are witnessed for Europe. There are two main reasons, first is the cooling technology type which uses different WUI, and second is the seawater shares, which vary among both countries. More power plants from coal and oil are witnessed for the USA, while, Europe has gas power plants the most. Such differences are making the variations in the CWW among these two regions. For SSP2–RCP4.5, a maximum CWW of 990.9Km^3 and 826.09Km^3 are seen for China for 2050 and 2100 respectively. By the end of the century, an increase in CWW is seen for USSR and India, whereas, a decrease in CWW is noted for the USA and China. Lastly, for SSP3–RCP6.0, a maximum CWW of 1094.9Km^3 and 945.7Km^3 are observed for China for 2050 and 2100 respectively. By the end of the century, an increase in

CWW is seen for South America, USSR and India, whereas, a decrease in CWW is noted for the USA only. Among all above three scenario combinations, a maximum CWW of 1094.9Km^3 is observed for China for SSP2–RCP4.5 scenario for 2100.

5.3 Solar PV area needed for PV_{enh} scenarios

The major concern about solar PV is the area needed to fulfill the needed electricity. Keeping in view the current technology growth, higher inputs for solar PV (PV_{enh}) in comparison to existing SSP and RCP scenarios are designed as most of IAM seem to be underestimating future PV input in the total system. Based upon the available solar PV resource in each region, solar PV sitting areas for all PV_{enh} scenarios are calculated for the future. The solar PV areas in terms of km^2 for all corresponding scenarios are presented in Fig. (5.3).

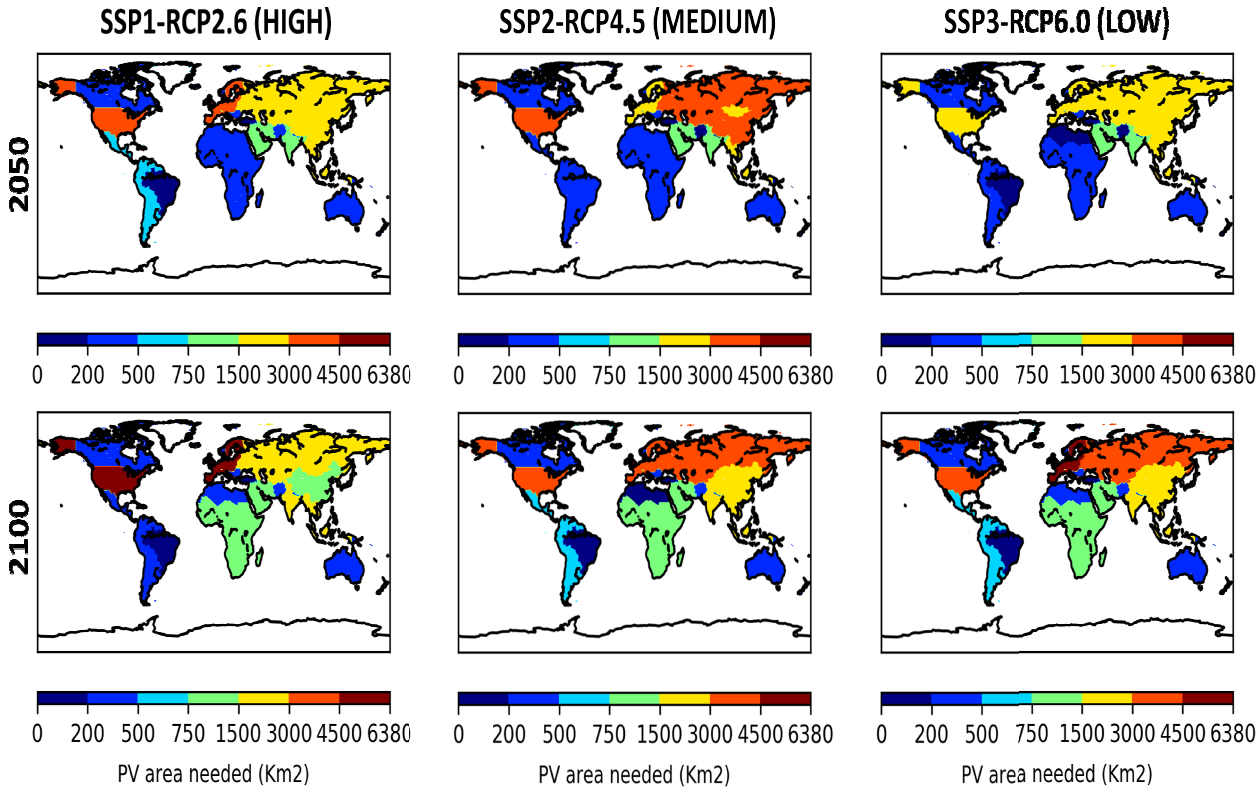

Fig 5.3: Solar PV area (km^2) needed for PV_{enh} scenarios for AIM regions globally.

For HIGH scenario, a maximum solar PV area equals 3774Km^2 and 6370.14Km^2 is seen for Europe for 2050 and 2100 respectively. Going to the end of the century, an increase in solar PV area is seen for most of the regions due to their higher electricity demands for 2100.

Whereas, USSR and China witnessed lower PV sitting areas by the end of the century due to smaller electricity demands associated with decline population. For MEDIUM scenario, a maximum area of 3613Km^2 and 3567Km^2 is seen for China and Europe for 2050 and 2100 respectively. Lastly, for the LOW scenario, a maximum PV area of 2760Km^2 and 4520Km^2 is noted for the USA and Europe for 2050 and 2100 respectively. Among all the above three PV_{enh} scenario combinations, a maximum PV area equals 6370Km^2 is seen for Europe for the HIGH scenario for 2100.

Such areas may be availed by providing solar power plants of various capacities like 1MW, 10MW, 20MW, or more, etc. based upon the electricity demand of concerned areas. The maximum areas needed for all scenarios would be highest for the China, USA, Europe, Russia, the Rest of East & South Asia, India, and Japan. These areas are larger due to their higher anticipated electricity. However, Europe and Russia need bigger area due to less solar PV resource available in addition to their higher electricity demands. However, they are still quite small (<0.1 %) in comparison to their total available land areas.

5.3.1 Water withdrawals for PV_{enh} scenarios

After knowing the potential areas for the application of solar PV power plants, we calculated the revised CWW for PV_{enh} scenarios by replacing TEPPs with solar PV. The outputs for CWW (Km^3) are presented in Fig. (5.4). All regions show a reduction in the usage of CWW due to substitution of TEPPs with solar PV.

For the HIGH scenario, a maximum CWW equals 284Km^3 and 233Km^3 is seen for China and the USA for 2050 and 2100 respectively. Going to the end of the century, a decrease in CWW is seen for most of the regions due to higher PV inputs, higher solar PV resources owing to efficiency improvement and technological changes. For the MEDIUM scenario, a maximum CWW equal to 792Km^3 and 536Km^3 is seen for China for 2050 and 2100 respectively. Also, for the LOW scenario, China has the maximum CWW equal to 984Km^3 and 662Km^3 for 2050 and 2100 respectively. Among all above three PV_{enh} scenario combinations, a maximum CWW equals 984Km^3 is seen for China for the HIGH scenario for 2100.

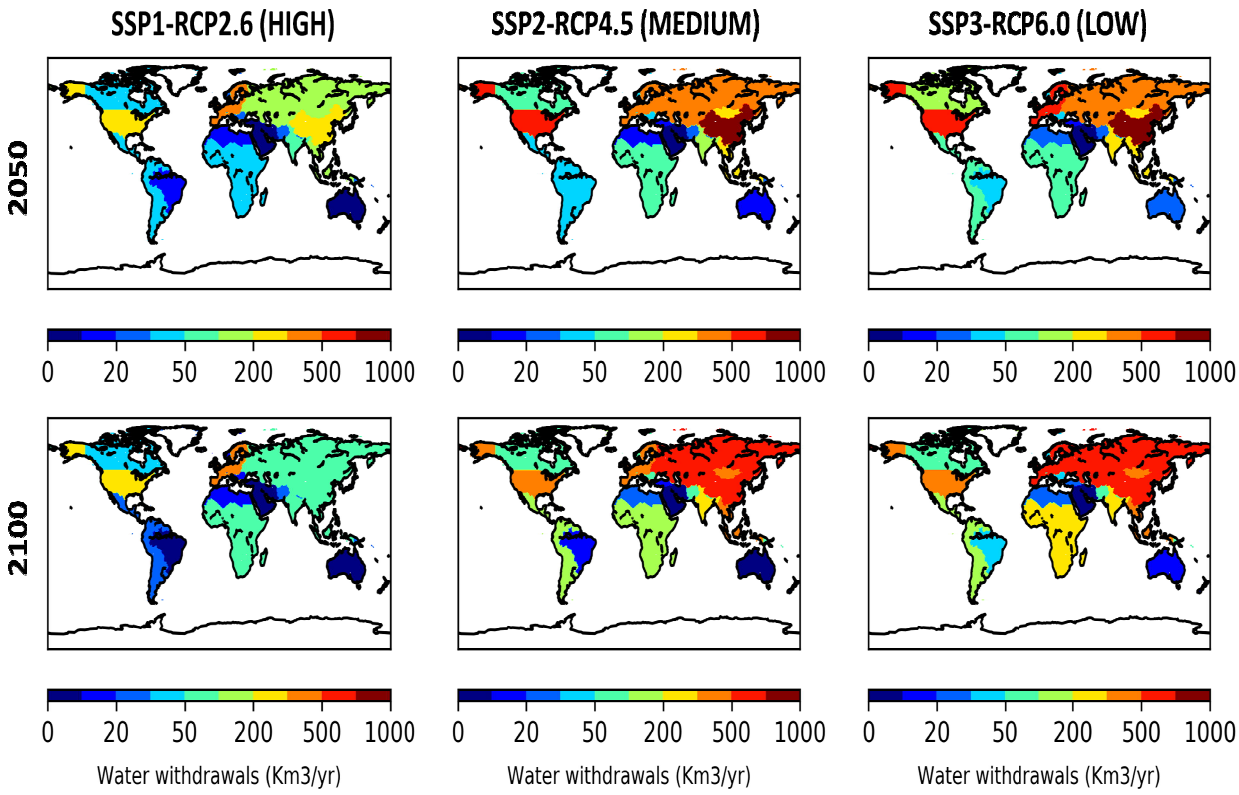

Fig 5.4: New water withdrawals (km^3) for PV_{enh} scenarios for future for AIM regions globally.

5.3.2 Freshwater savings for PV_{enh} scenarios

As witnessed from the above section, CWW have reduced for all regions due to the substitution of TEPPs with solar PV plants. For the HIGH scenario, a maximum CWW saving equals 131.4Km^3 and 281.8Km^3 is seen for Europe for 2050 and 2100 respectively. By the end of the century, higher CWW savings are seen for all of the regions except China and Brazil. These two have lower electricity production by TEPPs in the future and mainly correspond to technological shift. For the MEDIUM scenario, maximum CWW savings equal to 198Km^3 and 289.1Km^3 is seen for China for 2050 and 2100 respectively. Also, for the LOW scenario, China has the maximum savings for CWW equal to 109Km^3 and 279Km^3 for 2050 and 2100 respectively. Among all above three PV_{enh} scenario combinations, a maximum CWW saving equals 289.1Km^3 is seen for China for the MEDIUM scenario for 2100.

It is witnessed that all of the global 17 regions show significant savings in terms of freshwater withdrawals. Higher savings are seen for countries with electricity demands and reliance on TEPPs who withdraw a lot of freshwaters. The validation of such freshwater savings for the current could not be done due to non–existence of such statistics at a global or regional level.

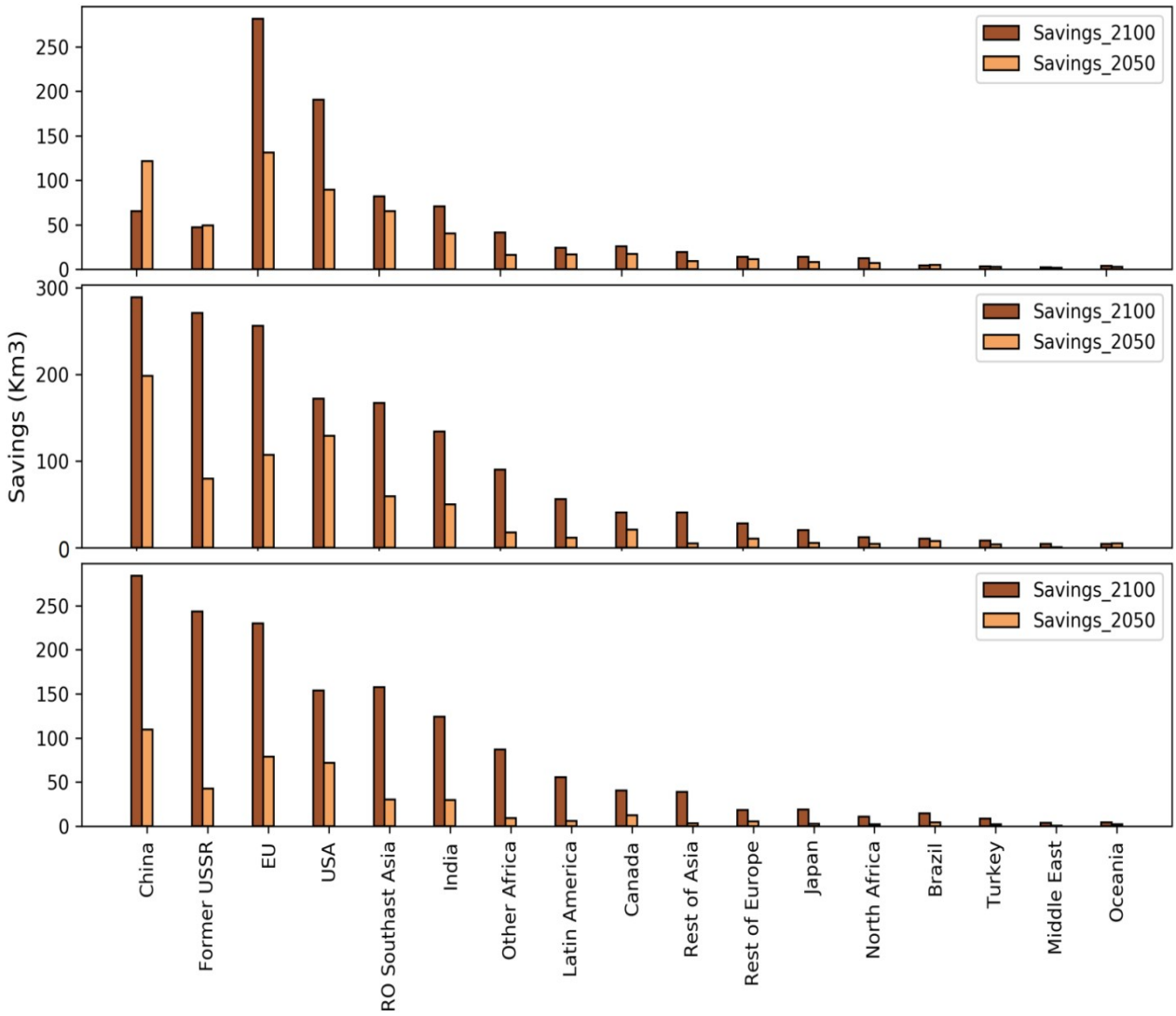

Fig 5.5: Fresh water savings (Km^3/yr) for each region for PV_{enh} scenarios in comparison to the BAU scenario.

Table 5.1: Summary of AIM regional water savings (km^3) for PV_{enh} scenarios globally.

Regions	Name	HIGH (2050)	HIGH (2100)	MEDIUM (2050)	MEDIUM (2100)	LOW (2050)	LOW (2100)
1	Latin America	16.35844	24.28198	11.74468	56.30582	6.1266	55.566
2	USA	89.54438	190.7657	129.3859	171.8953	72.03565	153.666
3	Middle East	1.328916	2.363586	0.641952	4.459026	0.49522	4.0974
4	Oceania	2.457677	3.847619	4.78183	4.244067	2.51225	4.365
5	North Africa	7.00832	12.21768	4.272827	12.23529	2.4956	10.9995
6	EU	131.4222	281.7648	107.4588	256.0624	79.0566	229.6965
7	Former USSR	49.40664	46.90732	79.59266	270.6874	42.5659	243.0675
8	Rest of Asia	9.062902	19.3616	5.062014	40.58675	3.2125	38.865
9	China	121.7979	65.37691	198.19	289.1334	109.4255	279
10	RO Southast Asia	65.29059	81.72324	59.53062	166.8788	30.3985	157.665
11	Other Africa	15.87334	41.11036	17.3561	90.33232	9.2568	87.066
12	Japan	8.164782	14.09675	5.543395	20.35572	2.8952	18.7698
13	Turkey	2.617075	3.245276	3.732867	8.438502	2.12355	8.7966
14	Rest of Europe	11.33299	13.73519	10.36386	28.25148	5.5265	18.3669
15	India	40.02862	70.48234	49.90919	133.8711	29.55662	124.275
16	Brazil	4.686458	4.403142	7.746544	10.34906	4.25658	14.8686
17	Canada	17.24369	25.94566	20.97951	40.88233	12.522	40.686

Chapter 6: RESULTS AND DISCUSSIONS

ELECTRICITY DEMANDS: MEGACITIES CASE STUDY

6.1 Global gridded electricity demands map

Electricity is the major form of energy needed for all types of development. In addition to supply–side analysis like solar PV resource maps, demand analysis for electricity is equally important to know the potential areas for the offset of solar PV power plants with conventional power generation facilities especially TEPPs. The electricity demand map developed by using the methodology explained in section 2.8.3 is shown in Fig. (6.1). The high electricity demand areas include Eastern and Western USA, Europe, Middle East, India, Western China, parts of Japan, and Southeast Asia regions. In such areas, electricity demands are greater than 0.01EJ/year. These higher demand areas are mostly hub of industrialization/economical activities in addition to the higher population residing in those areas. Also, parts of Latin America. North Africa, Europe, The Middle East, USSR, India, and Oceania have fair electricity demands, i.e. ~0.01 EJ/yr.

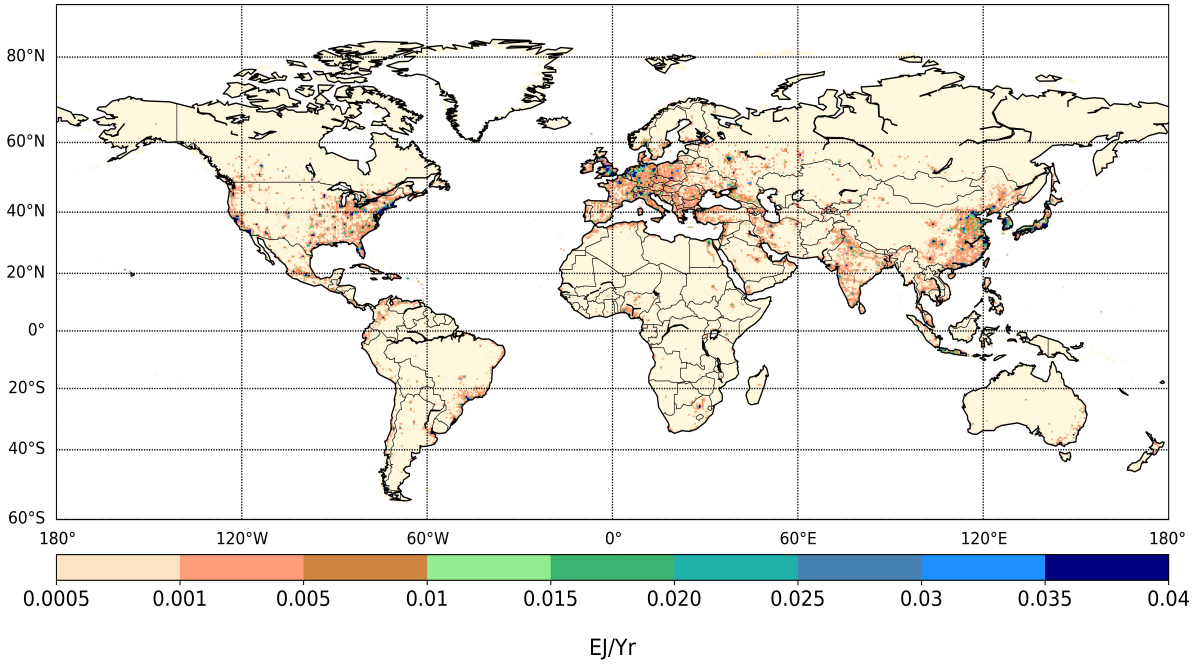

Fig 6.1: Global gridded (0.5°) electricity demand map for 2010. Using grid–based GDP, AIM regional electricity demands are downscaled to draw the above map.

6.2 Megacities electricity demands

6.2.1 Electricity flow for world megacities for 21st century for SSP3 scenario

From the above figure, it is clear that highly populous areas are demanding more electricity which is mainly due to the bigger population and economic activities. These areas have provoked the development of megacities. We extracted the electricity demands of such highly populous areas using their geo–coordinates. Moreover, their electricity demand flow in comparison to GDP/cap is also estimated and presented in Fig. (6.2). All 27 megacities show different behavior in their future electricity demands. For 2010, the maximum electricity demand is seen as 1.07EJ for Shanghai. While Lagos has the minimum electricity demand noted as 0.019EJ. For the future, all of the 27 megacities show increasing electricity demands for SSP3 scenario due to an expected bigger population. Where, cities like Shanghai, New York, Guangzhou, Jakarta, Tokyo, and Cairo have the maximum demands among others. Shanghai, Guangzhou, Jakarta, Tokyo, and Cairo show increasing electricity demands trend until 2070, which is then decreased until 2100. However, a city like New York shows an increasing trend until the end of the 21st century. It is also pertinent to mention that megacities with higher GDP have higher electricity demands as confirming for Shanghai, New York, Guangzhou and Tokyo etc.

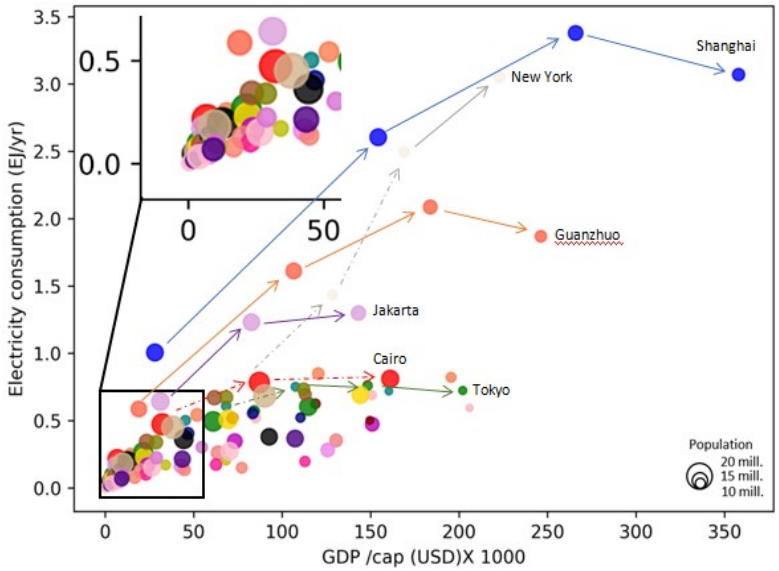

Fig 6.2: Electricity demand and GDP/cap flows for 27 megacities for 21st century.

6.2.2 Comparison of electricity estimates with existing

There are not many studies, which estimate the electrical energy demands for all megacities. However, Kennedy et al, (2015) presented the electricity demands of some of the megacities for 2011. Due to the non–existence of any estimate for 2010, we compared our electricity estimates with that of Kennedy et al, (2015). We assumed that the electricity demand estimates for 2011 are not so different from 2010. A high correlation of determination (R^2= 0.76) shows a quite satisfactory performance of our methodology to estimate the megacities electricity. For most of the cities, our estimates are highly correlated with that of Kennedy et al, (2015). However, some cities like Tokyo, Seoul, Guangzhou, and Manila, show significant deviation (~10–25%) which is mainly attributed to the difference of assumed areas for those megacities for both studies.

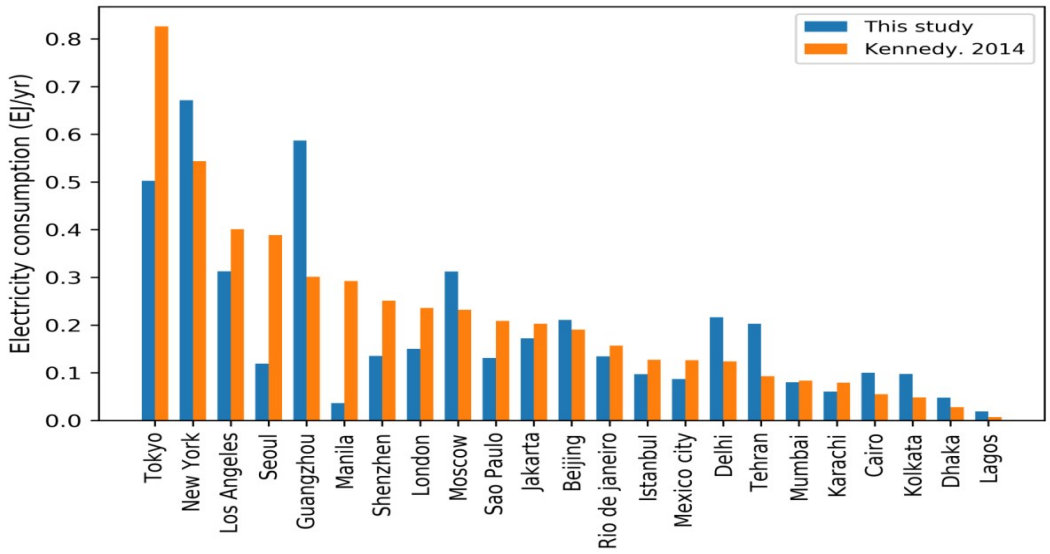

Fig 6.3: Comparison of electricity estimates for megacities for our study and Kennedy et al, (2015)

6.2.3 Solar PV resource for megacities

Seasonal PV resources available for each megacity (Fig. 6.4) are estimated by extracting the values of each megacity using its geo–coordinates. Most of the cities have a quite high solar resource, i.e., >25 W/m^2 through all four seasons with Cairo, Buenos Aires, and Tehran showing exceptionally high values (~40 W/m^2). It is worth mentioning that such values are daily means; however, diurnal values especially during the daytime would be many times higher and could be

used during peak hours. In addition, if battery storage is available then extra storage can also be stored for cloudy or non–sunny days. For cities lying in Northern Hemisphere, like Paris, Moscow, London, and Istanbul, solar PV resource is less during the winter seasons which is mainly due to the snow covers. However, for other seasons, they still have plenty of resources to fulfill their demands.

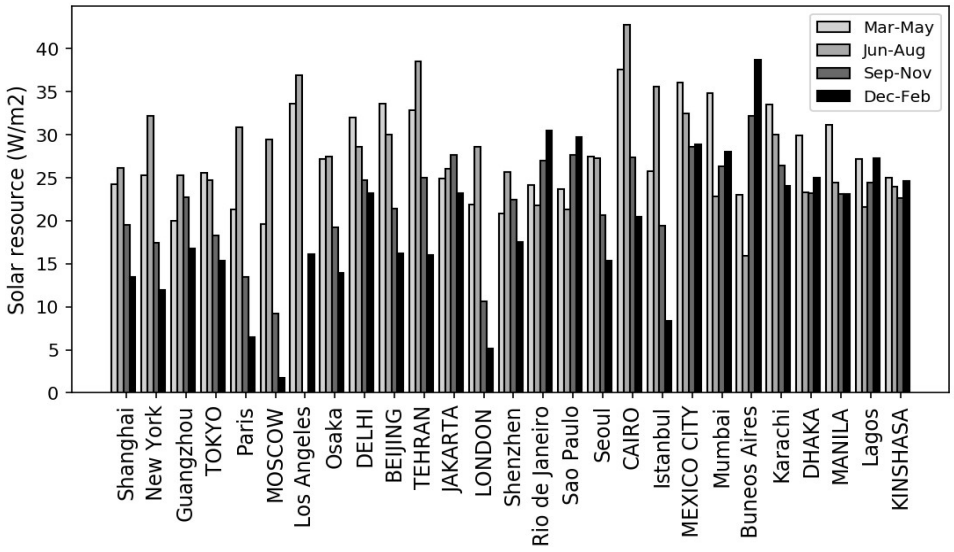

Fig 6.4: Seasonal solar PV resource available for all megacities. Most of them have good PV resource during all seasons, but, during SON and DJF, cities like Paris, Moscow, London, and Istanbul have less resource due to snow covers

6.2.4 Solar electric footprints of megacities

Solar electric footprints of world megacities are calculated using the Eq. (2.20) and provided in Fig. (6.5). It is seen that solar electric footprints are highly dependent upon the available solar PV resource in addition to the electricity demands. For 2010, the maximum solar electric footprints are calculated as 1324 km^2 and 1264 km^2 for Moscow and New York respectively. Now York has bigger PV footprints due to higher electricity demands, whereas, Moscow needs more area solar PV as it lies in a region with the less annual solar resource. Similar to Moscow, London and Paris also shows larger footprints due to fewer resources available. While, cities like Shanghai, Guangzhou, Los Angeles, and Tokyo have bigger footprints because of their higher electricity demands. Some African cities like Lagos and Kinshasa has the least footprints (<50km^2) due to smaller per capita and total electricity demands.

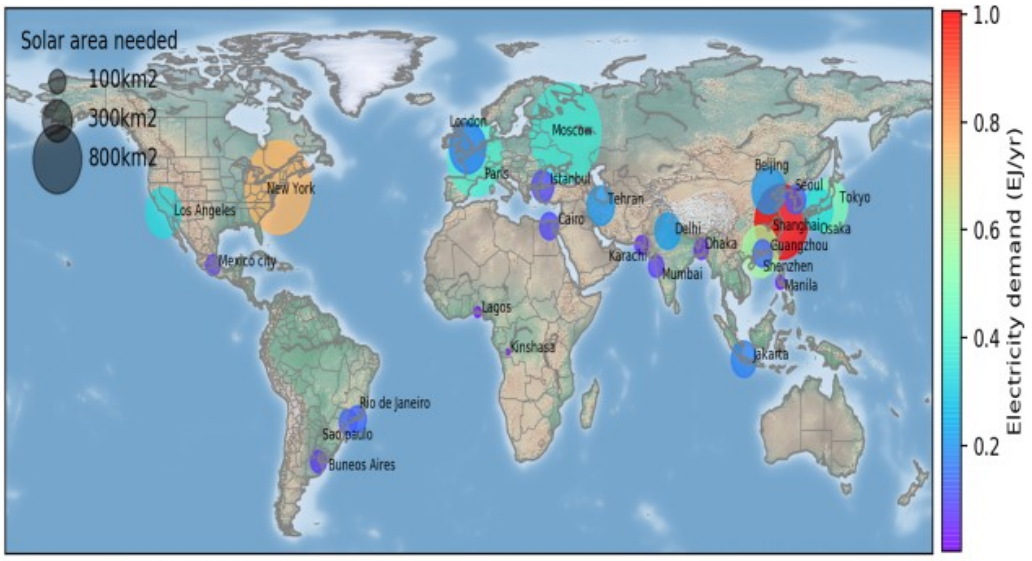

Fig 6.5: Solar electric footprints of world megacities derived from electricity demands and solar PV resources for each city for 2010.

6.3 Solar PV rooftop scheme

6.3.1 Solar PV area available Vs needed

After knowing the solar electric footprints of each megacity, we used the methodology presented in Fig. (2.20) to calculate the rooftop areas available for solar PV to each megacity. Such rooftop areas available are then plotted against solar electric footprints of each megacity for 2010 and shown in Fig. (6.6). For 11 out of 24 mega, whole electricity demand can be met if all available rooftops are covered with solar PV, while for the remaining 13 cities (bottom figure) can produce around 40–50% of their required electricity. Our estimates do not include any penetration ratio, which is the willingness of the owner towards covering his rooftop with solar PV. In addition, our rooftop estimates only consider the building tops, while including facades and support structures as demonstrated in the decentralized PV scheme, such available areas may subject to an increase. For cities that are unable to fulfill their all electricity demands by covering rooftop, areas can get additional electricity by providing on–grid (centralized scheme) solar parks in the neighboring areas depending upon policymakers and planners.

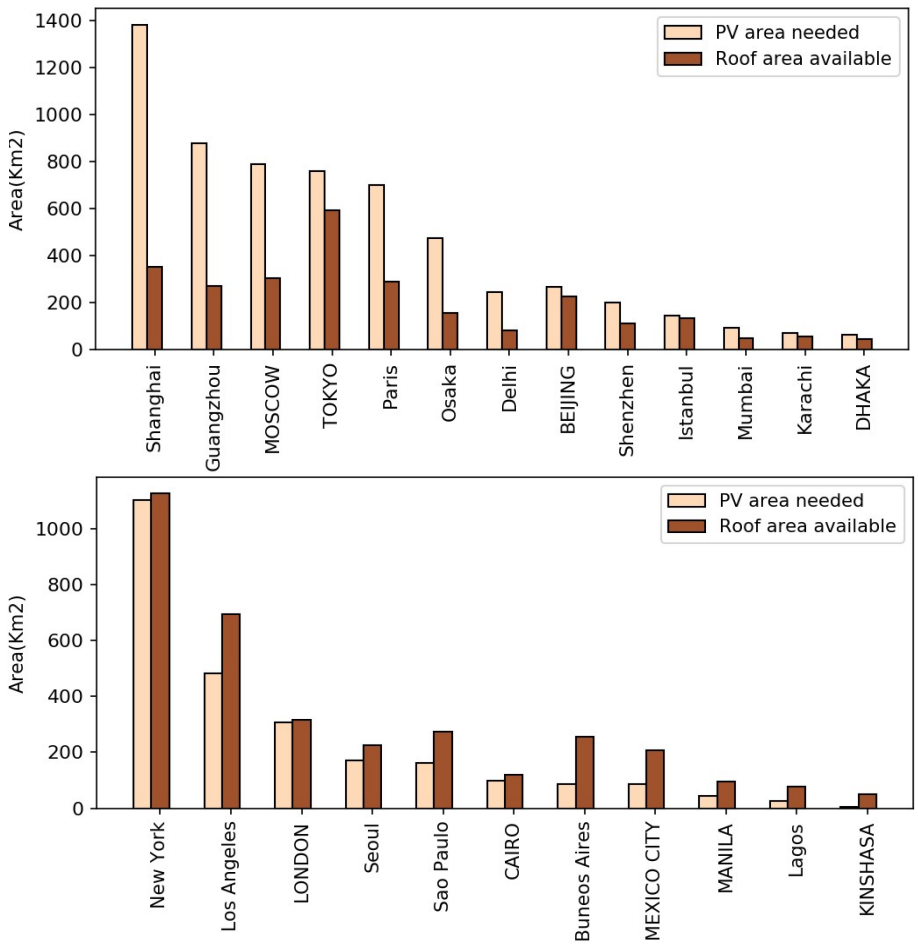

Fig 6.6: Solar electric footprints vs. rooftop area available for 2010. For 11 out of 24 cities (top), the entire electricity demand can be met if all available rooftops are covered with PV while the remaining 13 cities (bottom) can produce around 40–50% of their required electricity.

6.3.2 Comparison of rooftop estimates with existing studies

The rooftop area estimates are also compared with some existing roof–top areas previously calculated. These contain the research done by Singh et al, (2015) for Mumbai, India, Byrne et al, (2016) for Seoul, and Kabir et al, (2010) for Dhaka and OECD. (2013) for some other megacities using various GIS techniques. The results are available in Fig. (6.8), and it is evident our study is well correlated with old studies with R^2=0.85. In addition, other studies used different criteria for the calculation of rooftops area. But, we used a harmonized scheme for all megacities to assess their areas and suppose our methodology has still a worth among others.

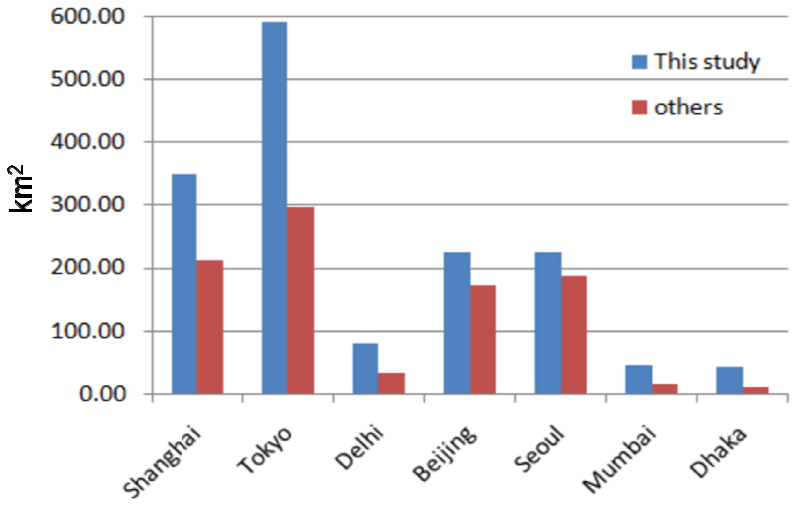

Fig 6.7: Comparison of estimates for roof area availability (km^2) with existing studies for some of the megacities.

6.4. Conclusion of solar electric footprints of world megacities:

Solar energy is among the abundantly available renewable energy reserves, which can be adopted for sustainable development. International Energy Agency (IEA) in its report (IEA. 2014) for World Key Energy Statistics mentioned that the world annual potential for solar energy is 1,575 (EJ). However, the maximum projected total world energy demand for 2100 is about 506 EJ (IEA. 2009). Therefore, all energy requirements could easily be accomplished with the plentiful available solar energy. Considering the fact that over 50 % of global population is living in the urban environment (IEA. 2009) and covering electricity demand part of the total energy requirements, solar electric footprints of world megacities case study has been conducted to estimate that how much electricity could be generated using their rooftops for 2010, and how much area inside/around them is required to satisfy their growing electricity needs. The rooftop scheme will also minimize the cost of electricity by avoiding lengthy transmission lines and the infrastructure involved. It is seen that in most cities, 11 out of 24 are capable of supporting their entire electricity demands by just covering the rooftops with solar PV and no additional areas are needed by them. Other city's rooftops can support ~40% of their electricity demands.

Besides, provision of neat & clean energy, solar energy from solar farms can alter the land surface properties; resulting in increased precipitation with enhanced vegetation cover as

witnessed for the Sub–Saharan Desert (Li et al, 2018). Although, the effect of solar panels seen for global mean earth temperature & precipitation is negligible, but, when installed on a massive scale, it can result in an increase in local temperature (+0.4◦C) as well as changes in regional wind patterns (Millstein et al, 2011). This will help in keeping the growing world temperature well below the Paris Agreement (2 °C).

Another worthy fact for solar PV energy generation system is that it could be installed over abandoned land like mines (Choi et al, 2013) or even on the area affected by nuclear radiations as seen recently from 1MW Chernobyl Solar Park (Ukraine) built over 1.6 hectares affected area from nuclear power plant meltdown in1986. Besides the provision of neat and clean energy, it could contribute to the country's economy effectively (Song et al, 2015). Also, with every passing day, the solar PV technology is improving and the installation costs are decreasing likewise. Lastly, it has noteworthy implications for megacities in terms of climate protection through GHG reductions, managing and saving cities resources like freshwater being used by TEPPs will be no more needed if they are replaced with PV. Hence, such footprint maps will potentially contribute towards UN SDG Goal No. 07– Affordable and Clean Energy – and Goal No. 13 – Climate Action in a quantitative manner.

Chapter 7: CONCLUSION

1. Considering meteorological & geomorphologic limiting factors, reliable solar PV resource maps are developed globally which does consider various uncertainties involved in the shape of cell efficiency, cell types, variations in the optimum tilt-angles, and using another data set. Based upon learning from various local experimental investigations, dust and snow algorithms are improved. They include information like tilt angle effect as well as the snow melts from solar PV surface due to an increased temperature. The comparison of our estimates with existing studies shows the better performance of our models (R^2=0.787). Maximum reductions are seen for snow covers during the winter season in the upper Northern Hemisphere. While temperature and dust participated in the solar cell efficiency reductions particularly for mid and lower latitude areas for summer seasons and throughout a year respectively.

2. These PV resource map, through EW–nexus, can lead to future sustainability in terms of energy & water, while replacing TEPPs to fulfil the electricity demands of potential areas. Various scenarios (PV_{enh}) set for the future are in line with country policies and initiatives towards limiting the GHGs and global temperature rise under Paris Agreement. All PV_{enh} scenarios show freshwater savings. However, more saving are seen for those regions that are withdrawing more water for cooling purposes. The China witnessed the maximum freshwater savings for the MEDIUM scenario (SSP2–RCP4.5) for 2100, which is recorded as 289Km^3 (35.3% of total CWW).

3. Global economic analysis is done at a grid–scale level and it is seen that solar PV costs are decreasing with an increase in cell efficiency, and decreasing module costs, etc. The lowest solar PV cost of 0.065$/KWh is seen for Sub-Saharan Africa which is quite competitive to the conventional one. Although, for some areas, solar PV is still not in competition with existing energy options, however, with each passing day, it is getting closer to conventional technologies.

4. Global gridded electricity demand maps show that electricity consumption is highly linked with urban areas with bigger population and more input to the economy. It

includes parts of the USA, Europe, China, Japan, and South Asia mainly with electricity demand of more than 0.01EJ/year. . These regions have provoked the development of sheer population hubs, megacities. A novel methodology to calculate electricity demands and solar electric footprints of such megacities have revealed that megacities like Shanghai, Guanzhou, and New York, etc. have bigger solar electric footprints and therefore will be requiring more PV area to fulfil their electricity needs. On the other hand, the rooftop scheme has proven to be a viable solution for most of the cities for their current electricity needs.

5. This study provides a valuable dataset for understanding global solar irradiance and for determining the most effective deployments schemes for solar PV arrays. Therefore, this study should be of wide interest to scientists and engineers, as well as to those involved in sustainable development.

6. These solar PV resource maps, EW–nexus along with solar electric footprints of world megacities are helpful for resource planning, policymaking, and investments. Such studies are also beneficial to various global models like Earth system models (ESMs), Impact assessment models (IAM), and Energy economy models (EEMs). In addition, these are useful towards decarbonising policies on the country as well as regional/global scale.

7. This study is potentially contributing to UN SDGs, Clean Water and Sanitation (Goal 06), Affordable and Clean Energy (Goal 07), Sustainable Cities and Communities (Goal 11), and Climate Action (Goal 13) in a quantitative manner.

RECCOMMENDATIONS:

a) Solar PV resources are developed using daily mean values, diurnal values, especially during the day time could be many times higher. These can be analyzed in the future for studies dealing with hourly or sub-daily variations.

b) We used fixed PV modules (non–tracking) types for similarity and ease of handling the meta–data in our analysis. However, Li et al, (2020) reported different losses to single–axis, double–axis tracking PV modules. In the future, such provisions could be adopted to have a more detailed analysis.

c) The combination of rainfall and dust affects the yield of the solar PV systems. Depending on rainfall intensity, it can either promote or slow down the dust accumulation on PV modules. Kimber et al, (2006) recommended a minimum of 20mm/day rainfall to remove the dust from a PV system. Meanwhile, fewer rainfalls can distribute dust particles in a more uniform manner than that of a coarser one thus decreasing the voids (spaces) between dust particles through which sunlight can pass (El–Shobokshy & Hussein, 1993). Such dust and rainfall categorization should therefore be included in details in future assessments.

d) Due to very high annual losses from snow in the upper Northern Hemisphere, we recommend cleaning the solar PV modules on regular basis. This can be done either by manual cleaning or with thermostatically controlled, insulated electric heat tape on the backsides of solar PV modules. The later one seems to be a safer choice in comparison to the manual cleaning which can cause additional problems like damaging the module surface or even breaking the entire panel (Brearley, 2015).

e) We did not consider smaller losses in the converter, wiring, etc. which could be added to have more detailed estimates of solar PV resources in the future.

f) Water scarcity assessments scale maps are coarse (AIM regions) due to non–availability of individual power plants cooling technology statistics. In the future, methodologies should be sought to develop those datasets which can help to map freshwater scarcity at a finer scale.

g) Defining megacities shape in a unified format was quite challenging and we assumed that each megacity lies inside a grid of 0.5– degrees. Such assumptions may limit the

accuracy of our estimates as well. We also calculated potential rooftop areas which are independent of resident's attitude towards covering rooftop with solar PV, penetrated area. Such social issues may also be considered in the future to have a better representation of the real world.

Bibliography:

1. Abdullah, K. B (2006), Use of water and land for food security and environmental sustainability, Irrig. Drain, 55, 219–222.
2. Afraz, S (2020). Valuing Water Use at Different Sectors with Considering Socio–Economic Development: Global Scale Assessment [PhD thesis]. The University of Tokyo, Japan. Available at: http://hydro.iis.u–tokyo.ac.jp/Mulabo/thesis.html.
3. Alcamo, J., M. Flörke, & M. Märker (2007). Future long–term changes in global water resources driven by socio–economic and climatic changes. Hydrological Sciences–Journal–Des Sciences Hydrologiques, 52(2). http://doi/pdf/10.1623/hysj.52.2.247
4. Alcamo J. & T. Henrichs (2002) Critical regions: A model–based estimation of world water resources sensitive to global changes. Aquat Sci 64, 352– 362.
5. Andenaes, E., B. P. Jelle, K. Ramlo, T. Kolas, J. Selj, S.E. Foss (2018) The influence of snow and ice coverage on the energy generation from photovoltaic solar cells. Solar Energy, 159, 318–328. https://doi.org/10.1016/j.solener.2017.10.078.
6. Andrews, R. W., A. Pollard, and J. M. Pearce (2013) The Effects of snowfall on solar photovoltaic performance. Solar Energy, 92, 84–97. https://doi.org/10.1016/j.solener.2013.02.014.
7. Alcamo, J., P. Döll, T. Hanrichs, F. Kaspar, B. Lehner, T. Rösch, S. Siebert (2003) Global estimates of water withdrawals and availability under current and future "business–as–usual" conditions. Hydrol. Sci. J. 48, 339–348.
8. Alley, R. B., J. Marotzke, W. D. Nordhaus, J. T. Overpeck, D. M. Peteet, R. A. Pielke Jr., R. T. Pierrehumbert, P. B. Rhines, T. F. Stocker, L. D. Talley, J. M. Wallace (2004) Abrupt climate change. Scientific American, 291, 62–69.
9. Alsayed, M., M. Cacciato, G. Scarcella and G. Scelba (2013) Multicriteria Optimal Sizing of Photovoltaic–Wind Turbine Grid Connected Systems. IEEE TRANSACTIONS ON ENERGY CONVERSION, 2, 370–379.
10. Alsema, E. and M. van Brummelen (1993) Het potentieel van pv–systemen in OECD landen, Utrecht University, Department of Science, Technology and Society, pp: 53.
11. Ascencio–Vásquez, J., K. Brecl, and M. Topič (2019) Methodology of Köppen–Geiger–Photovoltaic climate classification and implications to worldwide mapping of PV system performance. Solar Energy, 191, 672–685. https://doi.org/10.1016/j.solener.2019.08.072.
12. Asif, M and T. Muneer (2007) Energy supply, its demand and security issues for developed and emerging economies. Renewable and Sustainable Energy Reviews, 11, 1388–1413
13. Asl–Soleimani, E., S. Farhangi, M. S. Zabihi (2001) The effect of tilt angle, air pollution on performance of photovoltaic systems in Tehran. Renewable Energy, 24, 459–468. https://doi.org/10.1016/S0960–1481 (01)00029–5.
14. Barasa, M., D. Bogdanov, A. S. Oyewo and C. Breyer (2018) A cost optimal resolution for Sub–Saharan Africa powered by 100% renewables in 2030. Renewable & Sustainable Energy Reviews, 92, 440–457.

15. Bartos, M. D. and M. V. Chester, (2015) Impacts of climate change on electric power supply in the Western United States. Nat. Clim. Change, 5, 748–752. Doi: 10.1038/nclimate2648.
16. Bauer, N., K. Calvin, J. Emmerling, O. Fricko, S. Fujimori, J. Hilaire, J. Eom, V. Krey, E. Kriegler, I. Mouratiadou, H. S. de Boer, M. van den Berg, S. Carrara, V. Daioglou, L. Drouet, J. E. Edmonds, D. Gernaat, P. Havlik, N. Johnson, D. Klein, P. Kyle, G. Marangoni, T. Masui, R. C. Pietzcker, M. Strubegger, M. Wise, K. Riahi& D. P. van Vuuren (2017) Shared Socio–Economic Pathways of the Energy Sector – Quantifying the Narratives. Global Environmental Change–Human and Policy Dimensions, 42, 316–330.
17. Bayu, T., H. Kim, & T. Oki (2020). Water governance contribution to water and sanitation access equality in developing countries. Water Resources Research, 56, e2019WR025330. https:// doi.org/10.1029/2019WR025330
18. Berkhout, F. & R. Howes (1997) The adoption of life–cycle approaches by industry: Patterns and impacts. Resources Conservation and Recycling, 20, 71–94
19. Biswas, W.K., P. Bryce & M. Diesendorf (2001) Model for empowering rural poor through renewable energy technologies in Bangladesh. Environmental Science and Policy, 4, 333–344.
20. Blanco, J., S. Malato, P. Fernandez–Ibanez, D. Alarcon, W. Gernjak & M. I. Maldonado (2009) Review of feasible solar energy applications to water processes. Renewable and Sustainable Energy Reviews, 13, 1437–1445.
21. Bogenrieder, J., C. Camus, M. Huttner, P. Offermann, J. Hauch and C. J. Brabec (2018) Technology–dependent analysis of the snow melting and sliding behavior on photovoltaic modules. Journal of Renewable and Sustainable Energy, 10, 1– 15.
22. Braff, W.A., J. M. Mueller, and J. E. Trancik (2016) Value of storage technologies for wind and solar energy. Nat. Clim. Change 6, 964–970.
23. Carter, N, T. (2010) Energy's water demand: trends, vulnerabilities, and management. Congressional Research Service, Washington, D.C., USA. Available online: http://www.fas.org/sgp/crs/misc/R41507.pdf
24. Chander, S., A. Purohit, A. Sharma, A. Arvind, S. P. Nehra and M. S. Dhaka (2015) A study on photovoltaic parameters of mono–crystalline silicon solar cell with temperature. Energy Rep. 1, 104–109. https://doi.org/10.1016/j.egyr.2015.03.004
25. Chang, A. T. and A. Rango (2000) Algorithm Theoretical Basis Document (ATBD) for the AMSR–E Snow Water Equivalent Algorithm. [Online]. Available: https://nsidc.org/sites/nsidc.org/files/technical–references/amsr_atbd_snow.pdf. Accessed 19 December 2019].
26. Chen, S. T., H. I. Kuo, & C. C. Chen (2007) The relationship between GDP and electricity consumption in 10 Asian countries. Energy Policy, 35, 2611–2621.
27. Comprehensive Assessment of Water Management in Agriculture (IWMI, 2007). Water for Food, Water for Life: A Comprehensive Assessment of Water Management in Agriculture. London: Earthscan, and Colombo: International Water Management Institute.
28. Clarke L. E., J. A. Edmonds, H. D. Jacoby H. M. Pitcher J. M. Reilly, and R. G. Richels (2007) Scenarios of greenhouse gas emissions and atmospheric concentrations. Report 2.1 A. Washington: US Climate Change Science Program and the Subcommittee on

Global Change Research, Office of Biological and Environmental Research, US Department of Energy; 2007.
29. Creutzig, F., G. Baiochhi, R. Bierkandt, P–P. Pichler (2015) Global typology of urban energy use and potentials for an urbanization mitigation wedge Proceedings of the National Academy of Sciences of the United States of America, 112, 6283–6288.
30. Dankers, R., N. W. Arnell, D. B. Clark, P. D. Falloon, B. M. Fekete, S. N. Gosling, J. Heinke, H. Kim, Y. Masaki, Y. Satoh, T. Stacke, Y. Wada and D. Wisser (2014) First look at changes in flood hazard in the Inter–Sectoral Impact Model Intercomparison Project ensemble. Proceedings of the National Academy of Sciences of the United States of America, 111, 3257–3261.
31. Darwish. Z.A., H. Kazem, K. Sopian, M. Al–Goul and H. Alawadhi (2015) Effect of dust pollutant type on photovoltaic performance. Renewable and Sustainable Energy Reviews, 41,735–744.
32. Davies, E. G. R., P. Kyle, and J. A. Edmonds (2013) An integrated assessment of global and regional water demands for electricity generation to 2095, Adv. Water Resour., 52, 296–313. Doi:10.1016/j.advwatres.2012.11.020.
33. DeAngelis, A., F. Dominguez, Y. Fan, A. Robock, M. Deniz Kustu, and D. Robinson (2010) Evidence of enhanced precipitation due to irrigation over the Great Plains of the United States. J. Geophys. Res.115, D15115. Doi: 10.1029/2010JD013892.
34. Denholm, P. & R. M. Margolis (2007) The Regional Per–Capita Solar Electric Footprint for the United States. Technical Report NREL/TP–670–42463. Available online: https://www.nrel.gov/docs/fy08osti/42463.pdf
35. Delucchi, M. A. and M. Z. Jacobson (2011) Providing all global energy with wind, water, and solar power, Part II: Reliability, system and transmission costs, and policies. Energy Policy, 39, 1170–1190.
36. DOE. SunShot vision study. Washington DC: US department of energy (DOE). 2012. Doi: SunShot, Energy Efficiency and Renewable Energy, U.S. Department of Energy. NREL Report No. BK5200e47927; DOE/GO–102012–3037.
37. Duffie, J., and W. Beckman, Solar Energy Thermal Processes, Toronto: John Wiley & Sons, 1974.
38. Eakins, B., and P.R. Grothe, (2014) Challenges in Building Coastal Digital Elevation Models. Journal of Coastal Research, 30, 942–953.
39. Elminir, H. K., A. E. Ghitas, R. H. Hamid, F. El–Hussainy, M. M. Beheary and K. M. Abdel–Moneim (2006) Effect of dust on the transparent cover of solar collectors. Energy Conversion and Management, 47, 3192–3203.
40. El–Shobokshy, M., and F. Hussein (1993) Degradation of photovoltaic cell performance due to dust deposition on its surface. Renewable Energy, 3, 585–590.
41. Energy Information Administration (2009a). Annual Energy Outlook 2009, DOE/ EIA–0383(2009), US Department of Energy, Washington, DC, March. Available from: /www.eia.doe.gov/oiaf/aeo/index.html.
42. EPRI (2002). Comparison of Alternate Cooling Technologies for California Power Plants: Economic, Environmental, and Other Tradeoffs, Consultant Report to EPRI and California Energy Commission 2002; EPRI: Palo Alto, CA; California Energy

Commission: Sacramento, CA. Available online: www.energy.ca.gov/reports/2002–07–09_500–02–079F.PDF.
43. Eyring, V., S. Bony, G. A. Meehl, C. A. Senior, B. Stevens, R. J. Stouffer & K. E. Taylor (2016) Overview of the Coupled Model Intercomparison Project Phase 6 (CMIP6) experimental design and organization. Geoscientific Model Development, 9, 1937–1958.
44. European Commission, Eurostat (2010). Available online: https://ec.europa.eu/eurostat (accessed on 25 October 2020).
45. Falkenmark M (1989) The massive water scarcity now threatening Africa: Why isn't it being addressed? Ambio, 18, 112–118.
46. Faurès, J. M. J. Hoogeveen and J. Bruinsma (2002) The FAO irrigated area forecast for 2030, Food and Agric. Organ., Rome. Available online: http://www.fao.org/3/I9278EN/i9278en.pdf (accessed on 29 October 2020).
47. Food and Agriculture Organization of the United Nations (FAO, 2016a). AQUASTAT – FAO's Information System on Water and Agriculture. Available online: http://www.fao.org/nr/water/aquastat/water_use/index.stm
48. FAO (1997) Statistics on prices paid by farmers for means of production, Rome.
49. Faundez, P (2003) Potential cost of four short–rotation silvicultural regimes used for the production of energy, Biomass and Bioenergy, 24, 373 – 380.
50. Feeley, T. J., J. S. Timothy, G. J. Stiegel, A. McNemar, M. Nemeth, B. Schimmoller, J. T. Murphy, and L. Manfredo (2008) Water: A critical resource in the thermoelectric power industry. Energy, 33, 1–11. https://doi.org/10.1016/j.energy.2007.08.007.
51. Fischer, G., F. N. Tubiello, H. V. Velthuizen, & D. A. Wiberg (2007) Climate change impacts on irrigation water requirements: Effects of mitigation, 1990–2080. Technol. Forecasting Soc. Change, 74, 1083–1107.
52. Freydank, K., and S. Siebert (2008) Towards mapping the extent of irrigation in the last century: A time series of irrigated area per country. Frankfurt Hydrol. Pap., 08., Univ. of Frankfurt, Frankfurt, Germany.
53. Fthenakis, V., J. E. Mason, K. Zweibel (2009). The technical, geographical, and economic feasibility of solar energy to supply the energy needs of the US. Energy Policy 37, 387–399.
54. Fuentes, M. K (1985) A Simplified Thermal Model of Photovoltaic Modules," Sandia National Laboratories Report, SAND85–0330, 1985.
55. Fujimori, S., N. Hanasaki & T. Masui (2017) Projections of industrial water withdrawal under shared socioeconomic pathways and climate mitigation scenarios. Sustainability Science, 12, 275–292.
56. Fujimori S, T. Masui, and Y, Matsuoka (2012) AIM/CGE (basic) manual, http://www.nies.go.jp/social/dp/pdf/2012–01.pdf: Center for Social and Environmental Systems Research, National Institute Environmental Studies
57. GEA, 2012: Global Energy Assessment – Toward a Sustainable Future, Cambridge University Press, Cambridge, UK and New York, NY, USA and the International Institute for Applied Systems Analysis, Laxenburg, Austria.
58. Global Energy Observatory, Google, KTH Royal Institute of Technology in Stockholm, Enipedia, World Resources Institute. 2018. Global Power Plant Database. Published on

Resource Watch and Google Earth Engine; http://resourcewatch.org/ https://earthengine.google.com/
59. Goldemberg, J (2000) World Energy Assessment, New York, United Nations Development Programme, United Nations Department of Economic and Social Affairs. World Energy Council, pp: 508.
60. Goossens, D., Z. Y, Offer, and A. Zangvil (1993) Wind tunnel experiments and field investigations of eolian dust deposition on photovoltaic solar collectors. Sol. Energy, 50, 75–84. https://doi.org/10.1016/0038–092X(93)90009–D.
61. Green, M. A., K. Emery, D. L. King, S. Igari, and W. Warta, W (2003) Solar cell efficiency tables (Version 21). Progress in photovoltaics research and applications, 11, pp: 39 – 45, https://doi.org/10.1002/pip.4782003.
62. Griggs, D., M. Stafford–Smith, O. Gaffney, J. Rockstrom, M. C. Ohman, P. Shyamsundar, W. Steffen, G. Glaser, N. Kanie & I. Noble (2013) Sustainable development goals for people and planet. Nature, 495, 305–307.
63. Grübler, A (1998), Technology and global change, Laxenburg, Cambridge University Press.
64. Hanasaki, N., Kanae, S., Oki, T., Masuda, K., Motoya, K., Shirakawa, N., Shen, Y., and Tanaka, K (2008a) An integrated model for the assessment of global water resources – Part 1: Model description and input meteorological forcing. Hydrol. Earth Syst. Sci., 12, 1007–1025, doi: 10.5194/hess–12–1007–2008.
65. Hasan, A., and A. Sayigh (1992) The effect of sand dust accumulation on the light transmittance, reflection, and absorbance of the PV glazing, Oxford: Pergamon Press, 1992.
66. Hawker, L., J. Rougier, J. Neal, P. Bates, L. Archer and D. Yamazaki (2018) Implications of simulating global digital elevation models for flood inundation studies. Water Resour. Res., 54, 7910–7928.
67. Hejazi, M., J. Edmonds, V, Chaturvedi, E, Davies, & J, Eom (2013). Scenarios of global municipal water use demand projections over the 21st century. Hydrological Sciences Journal–Journal Des Sciences Hydrologiques, 58, 519–538. https://doi.org/10.1080/02626667.2013.772301
68. Hertwich, E. G., T. Gibon, E. A. Bouman, A. Arvesen, S. Suh, G.A. Heath, J.D. Bergesen, A. Ramirez, M. I. Vega, and L. Shi (2015) Integrated life–cycle assessment of electricity–supply scenarios confirms global environmental benefit of low–carbon technologies. Proc. Natl. Acad. Sci. USA 112, 6277–6282.
69. Heugens E. H. W., A. J. Hendriks, T. Dekker, S. N. M. Van, and W. Admiraal (2002) A review of the effects of multiple stressors on aquatic organisms and analysis of uncertainty factors for use in risk assessment Crit. Rev. Toxicol, 31, 247–84.
70. Hightower, M., and S. Pierce (2008) The energy challenge. Nature 452, 285–286. https://doi.org/10.1038/452285a
71. Hirabayashi, Y., and S. Kanae (2009) First estimate of the future global population at risk of flooding. Hydrological Research Letters 3, 6 –9.
72. Hirt, C (2016) Digital Terrain Models, in Encyclopedia of Geodesy, Switzerland. Springer International Publishing, 1–6.

73. Hoekstra, A, Y., and A.K. Chapagain (2007) Water footprints of nations: water use by people as a function of their consumption pattern. Water Resour. Manage, 21, 35–48.
74. Holmstrup, M., A–M. Bindesbøl, G. J. Oostingh, A. Duschl, V. Scheil, H–R. Köhler, S. Loureiro, A.M.V.M. Soares, A. L.G. Ferreira, C. Kienle, A. Gerhardt, R. Laskowski, P. E. Kramarz, M. Bayley, C. Svendsen, & D. J. Spurgeon (2010) Interactions between effects of environmental chemicals and natural stressors: A review. Science of The Total Environment, 408, 3746–3762. https://doi.org/10.1016/j.scitotenv.2009.10.067.
75. Honsberg, C., and S. Bowden (2018) Solar Radiation on a Tilted Surface. Available online: https://www.pveducation.org/pvcdrom/properties–of–sunlight/solar–radiation–on–a–tilted–surface. [Accessed 20 October 202].
76. Hoogwijk, M., 2004. On the global and regional potential of renewable energy sources. Utrecht University /http://www.library.uu.nl/ digiarchief/dip/diss/2004–0309–123617/full.pdfS.
77. Hsu, N. C., S.–C. Tsay, M. D. King and J. R. Herman (2004) Aerosol Properties Over Bright–Reflecting Source Regions. IEEE Transactions on Geoscience and Remote Sensing, 42, 557–569, 2004.
78. Hussey, K (2010) Interconnecting the Water and Energy Cycles: Identifying and Exploiting the Synergies. Australian National University.
79. International Energy Agency (2018) World Energy Outlook, 2018. Available online: https://www.iea.org/reports/world–energy–outlook–2018
80. International Energy Agency (2017) Key World Energy Statics. Available online: https://telegra.ph/World–energy–statistics–2017–pdf–01–28.
81. International Energy Agency (2012) World Energy Outlook 2012. OECD/IEA, Paris, France, 690, 2012.
82. International Energy Agency (2010). Energy balances of OECD countries 1960– 2008. Paris: International Energy Agency; 2010.
83. IPCC WGII AR5. (2012) WGIIAR5–Chap3. Available online: https://library.harvard.edu/collections/ipcc/docs/AR5_WG2_n_SREX_chapters_and_review/i_WG2/b_1st_order_draft_ch_1_to_20_part_A/WGIIAR5– Chap3_FODall.pdf
84. IEA/OECD (2002a) World energy Outlook 2002, Paris, pp: 523.
85. IEA/OECD (2001a) Potential for building integrated photovoltaics, Paris, pp: 11.
86. Jacobson, M. Z., and V. Jadhav (2017) World estimates of PV optimal tilt angles and ratios of sunlight incident upon tilted and tracked PV panels relative to horizontal panels. Solar Energy, 169, 55–66. https://doi.org/10.1016/j.solener.2018.04.030.
87. Jalal, K. A., A. Asmat and N. Ahmad (2015) Aerosol Optical Depth (AOD) Retrieval Method using MODI. Proceeding of the 2015 International Conference on Space Science and Communication (IconSpace), Langkawi, 2015.
88. Jones, C., J. Hughes, N, Bellouin, S. Hardiman, G. Jones, J., Knight, et al, (2011) The HadGEM2–ES implementation of CMIP5 centennial simulations. Geoscientific Model Development, 4, 543–570. Doi: 10.5194/gmd–4–543–2011, 2011.
89. Kabir, Md. H., W. Endlicher & J. Jägermeyr (2010) Calculation of bright roof–tops for solar PV applications in Dhaka Megacity, Bangladesh. Renewable Energy, 35, 1760–1764. https://doi.org/10.1016/j.renene.2009.11.016

90. Kaldellis, J. K., M. Kapsali and K. A. Kavadias (2014) Temperature and wind speed impact on the efficiency of PV installations. Experience obtained from outdoor measurements in Greece. Renewable Energy, 66, 612–624.
91. Kennedy, C. A., I. Stewart, A. Facchini, I. Cersosimo, R. Mele, B. Chen, M. Uda, A. Kansal, A. Chiu, K. G. Kim, C. Dubeux, E. L. La Rovere, B. Cunha, S. Pincetl, J. Keirstead, S. Barles, S. Pusaka, J. Gunawan, M. Adegbile, M. Nazariha, S. Hoque, P. J. Marcotullio, F. G. Otharan, T. Genena, N. Ibrahim, R. Farooqui, G. Cervantes & A. D. Sahin (2015) Energy and material flows of megacities. Proceedings of the National Academy of Sciences of the United States of America, 112, 5985–5990.
92. Kenny, J.F., N.L. Barber, S.S., Hutson, K.S. Linsey, J. K. Lovelace, & M.A. Maupin (2009) Estimated use of water in the United States in 2005, US Geological Survey Circular 1344, Reston, Virginia, United States of America, 52. http://pubs.usgs.gov/circ/1344/pdf/c1344
93. Kerr, R. A (2006), No Doubt About It, the World Is Warming. Science, 312, 825.
94. Kerr, R. A (2006) A Worrying Trend of Less Ice, Higher Seas. Science, 311, 1698– 1701.
95. Khater, A (2001) Intensive groundwater use in the Middle East and North Africa. In: Llamas, Ramon, Custodio, Emilio (Eds.), Intensive Use of Groundwater: Challenges and Opportunities
96. King, D. L., W. E. Boyson, and J. A. Kratochvil (2004) Photovoltaic Array Performance Model. SAND2004–3535. Albuquerque, NM: Sandia National Laboratories, August 2004.
97. King, D., W. Boyson, and J. Kratochvil (2002) Analysis of Factors Influencing the Annual Energy Production of Photovoltaic Systems. 29th IEEE PV Specialists Conference, 2002.
98. Kikuchi, M., H. Murakami, K. Suzuki, T. M. Nagao and A. Higurashi, (2018)Improved Hourly Estimates of Aerosol Optical Thickness Using Spatiotemporal Variability Derived from Himawari–8 Geostationary Satellite. IEEE Transactions on Geoscience and Remote Sensing, 56, 3442–3455, 2018.
99. Kim, H (2017) Global Soil Wetness Project Phase 3 Atmospheric Boundary Conditions (Experiment 1) [Data set]. Data Integration and Analysis System (DIAS). https://doi.org/10.20783/DIAS.501.
100. Kimber, A., L. Mitchell, S. Nogradi, and H. Wenger (2006) The Effect of Soiling on Large Grid–Connected Photovoltaic Systems in California and the Southwest Region of the United States. IEEE 4th World Conference on Photovoltaic Energy Conference, Waikoloa, HI, 2006, 2391–2395. Doi: 10.1109/WCPEC.2006.279690, 2006.
101. King, D. L., W. E. Boyson, and J.A. Kratochvil (2004) Photovoltaic Array Performance Model. SAND2004–3535. Albuquerque, NM: Sandia National Laboratories, August 2004.
102. Koberle, A.C., D. E .H .J. Gernaat, and D. P. van Vuuren (2015) Assessing current and future techno–economic potential of concentrated solar power and photovoltaic electricity generation. Energy, 89, 739–56.
103. Kurokawa, K (2003) Energy from the desert: feasibility of very large scale photovoltaic power generation (VLS–PV) systems, London, James & James.

104. Kyle, P., E. G. Davies, J. J. Dooley, S. J. Smith, L. E. Clarke, J. A. Edmonds, and M. Hejazi (2013) Influence of climate change mitigation technology on global demands of water for electricity generation. Int. J. Greenh. Gas Con., 13, 112–123. Doi: 10.1016/j.ijggc.2012.12.006.
105. Levy, R. C., S. Mattoo, L. A. Munchak, L. A., Remer, A. M. Sayer, F. Patadia, and N. C. Hsu (2013) The collection 6 MODIS aerosol products over land and ocean. Atmos. Meas.Tech., 6, 2989–3034. Doi: 10.5194/amt–6–2989–2013.
106. Li, X., D. L. Mauzerall, and M. H. Bergin (2020) Global reduction of solar power generation efficiency due to aerosols and panel soiling. Nat. Sustain, 3, 720–727. https://doi.org/10.1038/s41893–020–0553–2.
107. Liao, X. W., J. W. Hall, and N. Eyre (2016) Water use in China's thermoelectric power sector. Glob Environmental Change, 41, 142–52.
108. Liddle B & S. Lung (2014) Might electricity consumption cause urbanization instead? Evidence from heterogeneous panel long–run causality tests .Glob Environ Change, 24, 42–51. https://doi.org/10.1016/j.gloenvcha.2013.11.013
109. Lobell, D. B., K. G. Cassman, & C. B. Field (2009) Crop Yield Gaps: Their importance, Magnitudes, and Causes. Annual Review of Environment and Resources, 34, 179–204
110. Lohrmann, A., J. Farfan, U. Caldera, C. Lohrmann, C. Breyer (2019) Global scenarios for significant water use reduction in thermal power plants based on cooling water demand estimation using satellite imagery. Nature Energy, 4 (2019), 1040–1048
111. Lu, W. C (2017) Electricity Consumption and Economic Growth: Evidence from 17 Taiwanese Industries. Sustainability, 9.
112. Lv, J., Y. P. Li, B. G. Shan, S. W. Jin, and, C. Suo (2018) Planning energy–water nexus system under multiple uncertainties – a case study of Hebei province. Applied Energy, 229, 389–403.
113. Margat, J., & S. Treyer (2004). L'eau des Méditerranéens: situation et perspectives. Technical Report 158, UNEP–MAP (Mediterranean Action Plan).
114. Mathiesen, B. V., H. Lund & K. Karlsson (2011) 100% Renewable energy systems, climate mitigation and economic growth. Applied Energy, 88, 488–501.
115. Maghami, M. R., H. Hizam, C. Gomes, M. A. Radzi, M. I. Rezedad and S. Hajighorbani (2016) Power loss due to soiling on solar panel: A review. Renewable and Sustainable Energy Reviews, 1307–1316.
116. Mani M., and R. Pillai (2010) Impact of dust on solar photovoltaic (PV) performance: research status, challenges and recommendations. Renewable and Sustainable Energy Reviews, 9, 3124–3131.
117. Mekonnen, M. M., and A. Y. Hoekstra (2010) The Green, Blue and Grey Water Footprint of Crops and Derived Crop Products. Value of Water Research Report Series, Delft, The Netherlands: UNESCO. Available at: https://waterfootprint.org/media/downloads/Report47–WaterFootprintCrops–Vol1_1.pdf
118. Meneses–Rodríguez, D., Horley, P. P., González–Hernández, J., Vorobiev, Y. V., and Gorley, P. N (2005) Photovoltaic solar cells performance at elevated temperatures. Solar Energy, 78, 243–250, https://doi.org/10.1016/j.solener.2004.05.016.

119. Mildrexler, D. J., M. Zhao and S. W. Running (2011) A global comparison between station air temperatures and MODIS land surface temperatures reveals the cooling role of forests. Journal of Geophysical Research Biogeosciences, 116, 1–15.
120. Millennium Ecosystem Assessment (2005) Ecosystems and Human Well–Being: Wetlands and Water Synthesis. World Resources Institute, Washington, DC, USA.
121. Milly, P. C. D., R. T. Wetherald, K. A. Dunne & T. L. Delworth (2002) Increasing risk of great floods in a changing climate. Nature, 415, 514–517.
122. Mohanty, A. & D. Chaturvedi (2015) Relationship between Electricity Energy Consumption and GDP: Evidence from India. International Journal of Economics and Finance, 7, 9710–9728.
123. Moran, D., K. Kanemoto, M. Jiborn, R. Wood, J. Tobben and K. C. Seto (2018) Carbon footprints of 13 000 cities. Environmental Research Letters, 13, 6.
124. Mulder, E. & F. Kraas (2008) Megacities of tomorrow. A World of Science 6(4):2–10.
125. Müller Schmied, H., S. Eisner, D. Franz, M. Wattenbach, F.T. Portmann, M. Flörke, and P. Döll (2014) Sensitivity of simulated global–scale freshwater fluxes and storages to input data, hydrological model structure, human water use and calibration. Hydrol. Earth Syst. Sci., 18, 3511–3538. Doi: 10.5194/hess–18–3511– 2014.
126. Murakami, D. & Y. Yamagata (2016) Estimation of gridded population and GDP scenarios with spatially explicit statistical downscaling, ArXiv, 1610.09041. Available online: URL: https://arxiv.org/abs/1610.09041. Accessed Nov 11, 2019.
127. National Research Council, Committee on Health, Environmental, and Other External Costs and Benefits of Energy Production and Consumption, 2010. Hidden Costs of Energy: Unpriced Consequences of Energy Production and Use. The National Academies Press, Washington, DC /www.nap.edu/catalog/12794.html.
128. Neverre, N., & P. Dumas (2015). Projecting and valuing domestic water use at regional scale: A generic method applied to the Mediterranean at the 2060 horizon. Water Resources and Economics, 11, 33–46. https://doi.org/10.1016/j.wre.2015.06.001
129. Newell, B., D. M. Marsh, and D. Sharma (2011) Enhancing the resilience of the Australian National Electricity Market: taking a systems approach in policy development. Ecology and Society 16(2):15.
130. Oki, T. and S. Kanae. (2006). Global Hydrological Cycles and World Water Resources. Science, 313, 1068–1072. https://doi.org/10.1126/science.1128845
131. Oki. T., Y. Agata, S. Kanae, T. Saruhashi, D. Yang, and K. Musiake (2001) Global assessment of current water resources using total runoff integrating pathways. Hydrol. Sci. J. 46, 983–995.
132. Oliver, M. and T. Jackson (2001) Energy and economic evaluation of building–integrated photovoltaics, Energy, 26, 431 – 439.
133. Oliver, M. and T. Jackson (2000) The evolution of economic and environmental cost of crystalline silicon photovoltaics, Energy Policy, 28, 1011 – 1021.
134. O'Neill, B. C., E. Kriegler, K. Riahi, K. L. Ebi, S. Hallegatte, T. T. Carter, R. Mathur and D. P. van Vuuren (2014a) A new scenario framework for climate change research: the concept of Shared Socioeconomic Pathways. Climate Change, 122, 387–400. https://doi.org/10.1007/s10584–013–0905–2.

135. Pachauri, R. K., M. R. Allen, V. R. Barros, J. Broome, W. Cramer, R. Christ, J. A. Church, L. Clarke, Q. Dahe, P. Dasgupta, N. K. Dubash, O. Edenhofer, I. Elgizouli, C. B. Field, P. Forster, P. Friedlingstein, J. Fuglestvedt, L. Gomez–Echeverri, S. Hallegatte, G. Hegerl, M. Howden, K. Jiang, B. Jimenez Cisneroz, V. Kattsov, H. Lee, K. J. Mach, J. Marotzke, M. D. Mastrandrea, L. Meyer, J. Minx, Y. Mulugetta, K. O'Brien, M. Oppenheimer, J. J. Pereira, R. Pichs–Madruga, G. –K. Plattner, H. O. Pörtner, S. B. Power, B. Preston, N. H. Ravindranath, A. Reisinger, K. Riahi, M. Rusticucci, R. Scholes, K. Seyboth, Y. Sokona, R. Stavins, T. F. Stocker, P. Tschakert, D. van Vuuren, and J. –P.van Ypserle (2014) Climate Change 2014: Synthesis Report. Contribution of Working Groups I, II and III to the Fifth Assessment Report of the Intergovernmental Panel on Climate Change / R. Pachauri and L. Meyer (editors), Geneva, Switzerland, IPCC, 151, ISBN: 978–92–9169–143–2 .

136. Palmer, D., R. Gottschalg, T. Betts, E. Koumpli, and I. Cole (2018) A GIS–based method for identification of wide area rooftop suitability for minimum size PV systems using LiDAR data and photogrammetry. Energies, 11, 3506. https://doi.org/10.3390/en11123506.

137. Paudyal, B. R., and S. R. Shakya, (2016) Dust accumulation effects on efficiency of solar PV modules for off grid purpose: A case study of Kathmandu. Solar Energy, 135, 103–110. https://doi.org/10.1016/j.solener.2016.05.046.

138. Perovich, D (2007) Light reflection and transmission by a temperate snow cover. Journal of Glaciology, 53, 201–210. Doi: 10.3189/172756507782202919, 2007.

139. Płaczek–Popko, E (2017) Top PV market solar cells 2016. Opto–Electronics Review, 25, 55–64. DOI: https://doi.org/10.1016/j.opelre.2017.03.002.

140. Platts (2011) World electric power plants database. New York: The McGraw–Hill Companies; 2011.

141. Postel, S. L (2000) Entering an era of water scarcity: the challenges ahead. Ecol Appl 10, 941–948.

142. Postel, S. L., G. C. Daily, and P. R. Ehrlich (1996) Human Appropriation of Renewable Fresh Water. Science 271, 785 (1996).

143. Powers. L., J. Newmiller, and T. Townsend (2010) Measuring and modeling the effect of snow on photovoltaic system performance. 35th IEEE Photovoltaic Specialists Conference, Honolulu, HI, 2010, 000973–000978, 2010. Doi: 10.1109/PVSC.2010.5614572.

144. Principe, J., and W. Takeuchi (2018) Assessment of solar PV power potential over Asia Pacific region with remote sensing considering meteorological factors. Journal of Renewable and Sustainable Energy, 11, 013502. Doi: https://doi.org/10.1063/1.5059335.

145. Rahmatmand, A., S. J. Harrison, and P/H. Oosthuizen (2019) Numerical and experimental study of an improved method for prediction of snow melting and snow sliding from photovoltaic panels. Applied Thermal Engineering, 158,113773. https://doi.org/10.1016/j.applthermaleng.2019.113773.

146. Raskin, P., P. Gleick, P. Kirshen, G. Pontius, and K. Strzepek, (1997) Water futures: assessment of long–range patterns and problems. Comprehensive assessment of

the freshwater resources of the world, Stockholm Environment Institute, Stockholm, Sweden.
147. REN21: Renewables 2019 Global Status Report. (REN21 Secretariat, 2019). Available at: https://www.ren21.net/reports/global–status–report/
148. REN21. Renewables 2013 global status report, ISBN 978–3–9815934–0–2.
149. Riggs, G. A. and D. K. Hall (2015) MODIS Snow Products Collection 6 User Guide. Available online: https://nsidc.org/sites/nsidc.org/files/files/MODIS–snow–user–guide–C6.pdf. [Accessed 05 Jan 2020].
150. Rodriguez, D.J., A. Delgado, P. DeLaquil & A. Sohns (2013). Thirsty energy. In Water Papers; World Bank: Washington, DC, USA. Available online: https://openknowledge.worldbank.org/handle/10986/16536
151. Ross, M (1995) Snow and Ice Accumulation on Photovoltaic Arrays: An Assessment of the TN Conseil Passive Melting Technology. Energy Diversification Research Laboratory, CANMET, Natural Resources Canada, Varennes, 1995.
152. Rost, S., D. Gerten, A. Bondeau, W. Lucht, J. Rohwer, & S. Schaphoff (2008) Agricultural green and blue water consumption and its influence on the global water system. Water Resources Research, 44. https://doi.org/10.1029/2007WR006331
153. Rübbelke, D., and S. Vögele (2011) Impacts of climate change on European critical infrastructures: The case of the power sector. Environmental Science & Policy, 14, 53–63.https://doi.org/10.1016/j.envsci.2010.10.007.
154. Ruiz–Arias, J., J. Tova–Pescador, D. Pozo-Vázquez and H. Alsamamra (2009) A comparative analysis of DEM-based models to estimate the solar radiation in mountainous terrain. International Journal of Geographical Information Science, 23, 1049– 1076.
155. Rutberg, M. J (2003). Modeling Water Use at Thermoelectric Power Plants [M.S thesis]. Massachusetts Institute of Technology, USA.
156. Said, S (1990) Effects of dust accumulation on performances of thermal and photovoltaic flat–plate collectors. Applied Energy, vol. 37, 73–84.
157. Said, M., and B. Nimmo (1979) Effects of dust on the performance of thermal and photovoltaic flat plat collectors in Saudi Arabia: Preliminary results. Alternative Energy Sources, 2, 145–152.
158. Salinas, S. V., C. B. Ning and S. C. Liew (2009) Characterization of aerosol physical and optical properties from a combination of ground–based and hand–held Sun–photometer 186 data of Singapore. 2009 IEEE International Geoscience and Remote Sensing Symposium, Cape Town, 2009.
159. Sampaio, P. G. V., and M. O. A Gonzalez (2017) Photovoltaic solar energy: Conceptual framework. Renewable & Sustainable Energy Reviews, 74, 590-601. https://doi.org/10.1016/j.rser.2017.02.081, 2017.
160. Sayigh, A (1978) Effect of dust on flat plate collectors. Sun, mankind's future source of energy. Proceedings of the international solar energy society congress, New Delhi, 1978.

161. Schwingshackl, C., M. Petitta, J. Wagner, G. Belluardo, D. Moser, M. Castelli, M. Zebisch and A. Tetzlaff (2013) Wind effect on PV module temperature: Analysis of different techniques for an accurate estimation. Energy Procedia, 40, 77–86.
162. Service, R. F (2005) Is It Time to Shoot for the Sun? Science, 309, 548– 551
163. Shen, Y., T. Oki, N., Utsumi, N, S. Kanae, & N. Hanasaki (2008) Projection of future world water resources under SRES scenarios: water withdrawal, Hydrological Sciences–Journal–Des Sciences Hydrologiques, 53. http://doi/pdf/10.1623/hysj.53.1.11
164. Shiklomanov, I. A (2000). International Water Resources Association Appraisal and Assessment of World Water Resources. Water International, 25, 250–8060. https://doi.org/10.1080/02508060008686794
165. Siddiqi, A. & A. Diaz (2011) The water–energy nexus in Middle East and North Africa. Energy Policy, 39 (6), 4529–4540.
166. Simic, A., R. Fernandes, R. Brown, P. Romanov, and P. William (2004) Validation of VEGETATION, MODIS, and GOES + SSM/I snow–cover products over Canada based on surface snow depth observations. Hydrol. Process, 18, 1089–1104. DOI: 10.1002/hyp.5509 2004.
167. Skoplaki, E., A. G. Boudouvis and J. A. Palyvos (2008) A simple correlation for the operating temperature of photovoltaic modules of arbitrary mounting," Solar Energy Materials & Solar Cells, 92, 1393–1402.
168. Simmons, M. R., Twilight in the Desert, Wiley, Hoboken, NJ, 2005.
169. Singh, R. and R. Banerjee (2015) Estimation of rooftop solar photovoltaic potential of a city. Solar Energy, 115, 589–602. https://doi.org/10.1016/j.solener.2015.03.016
170. Solarbuzz (2002) Solarbuzz module prices, available at www.solarbuzz.com.
171. Solomon, S., G. K. Plattner, R. Knutti& P. Friedlingstein (2009) Irreversible climate change due to carbon dioxide emissions. Proceedings of the National Academy of Sciences of the United States of America, 106, 1704–1709.
172. Sørensen, B (1999) Long term scenarios for global energy demand and supply. Four global greenhouse mitigation scenarios, Roskilde University, pp: 213.
173. Spang, E. S., W. R. Moomaw, K. S. Gallagher, P. H. Kirshen, and D. H. Marks (2014) The consumptive water footprint of electricity and heat: a global assessment Environ. Res. Lett., 2014, 9.
174. Taylor, R. G., B. Scanlon, P. Döll, M. Rodell, R. van Beek, Y., Wada, L., Longuevergne, M. Leblanc, J.S. Famiglietti, M. Edmunds, L. Konikow, T.R. Green, J. Chen, M. Taniguchi, M. F. P. Bierkens, A. MacDonald, Y. Fan, R.M. Maxwell, Y. Yechieli, J.J. Gurdak, D.M. Allen, M. Shamsudduha, K. Hiscock, P. J.–F. Yeh, I. Holman, and H. Treidel (2013) Groundwater and climate change, Nature Clim. Change, 3, 322–329. Doi: 10.1038/nclimate1744.
175. The Atlantic Council. A Marshall plan for energy and water supply in developing countries; 2005. Available online: /www.acus.org/programs–energy_–projects–marshall.aspS [Last Accessed on November 20, 2020].
176. Tertzakian, P. A., A thousand barrels a second: The coming oil break point and the challenges facing an energy dependent world, McGraw–Hill, New York, 2006.

177. Trancik, J. E (2014) Renewable energy: Back the renewables boom. Nature 507, 300–302.
178. Trancik, J.E., and D. Cross–Call (2013) Energy technologies evaluated against climate targets using a cost and carbon trade–off curve. Environ. Sci. Technol. 47, 6673–6680.
179. Trutnevyte, E., C. Guivarch, R. Lempert & N. Strachan (2016) Reinvigorating the scenario technique to expand uncertainty consideration. Climatic Change, 135, 373–379.
180. Turral, H., J. Burke, & J. M. Faurès (2011) Climate change, water and food security. Water Rep., 36, Food and Agric. Organ., Rome.
181. Tyagi, V. V., N.A. Rahim, N. Rahim, and J. A. Selvaraj (2013) Progress in solar PV technology: Research and achievement. Renewable and Sustainable Energy Reviews, 20, 443–461. Doi: https://doi.org/10.1016/j.rser.2012.09.028.
182. UBC ATSC 113 (2018) – Weather for Sailing, Flying & Snow Sports. Greg West and Rosie Howard
183. United Nations, Report of the United Nations Conference on sustainable development, Rio de Janeiro, Brazil, UN, (2012). Available online: https://sustainabledevelopment.un.org/index.php?page=view&type=111&nr=1358&menu=35
184. United Nations, Department of Economic and Social Affairs, Population Division (2018). The World's Cities in 2018—Data Booklet (ST/ESA/ SER.A/417).
185. United Nations Department of Economic and Social Affairs Population Division 2015
186. United Nations Water (2008). Status Report on Integrated Water Resources Management and Water Efficiency Plans. Available online: https://doi.org/10.1016/S1878– 7649(14)70566–2
187. U.S. Department of Energy, 2012. SunShot Vision Study. Technical Report. U.S. Department of Energy. Washington, DC.
188. United States Department of Energy (2004) How much land will PV need to supply our electricity? Available online: http://www.oilcrisis.com/apollo2/photovoltaics/HowMuchLandNREL.pdf
189. United Nations Development Programme (UNDP, 2006). Human Development Report 2006 Beyond scarcity: Power, poverty and the global water crisis. Available online: http://hdr.undp.org
190. United Nations, Report of the world summit on sustainable development, New York, UN, (2002).
191. Van den Broek, R (2000) Sustainability of biomass electricity systems. An assessment of costs, macro–economic and environmental impacts in Nicaragua, Ireland and the Netherlands, Utrecht University, pp: 215.
192. Vassolo, S., and P. Döll (2005) Global–scale gridded estimates of thermoelectric power and manufacturing water use. Water Resour Res, 41:W04010. Doi: http:// dx.doi.org/10.1029/2004WR00336.
193. Vera, I., & L. Langlois, (2007) Energy indicators for sustainable development. Energy, 32, 875–882.

194. Vörösmarty, C. J., P. Green, J. Salisbury, and R. B. Lammers (2000) Global water resources: Vulnerability from climate change and population growth. Science 289, 284–288.
195. Wada, Y., M. Florke, N. Hanasaki, S. Eisner, G. Fischer, S. Tramberend, Y. Satoh, M. T. H. van Vliet, P. Yillia, C. Ringler, P. Burek & D. Wiberg (2016) Modeling global water use for the 21st century: the Water Futures and Solutions (WFaS) initiative and its approaches. Geoscientific Model Development, 9, 175–222.
196. Wada, Y. and M. F. P. Bierkens (2014) Sustainability of global water use: past reconstruction and future projections, Environ. Res. Lett., 9, 104003, doi:10.1088/1748–9326/9/10/104003.
197. Wada, Y., L. P. H, Van Beek, & M. F. P. Bierkens (2011). Modelling global water stress of the recent past: on the relative importance of trends in water demand and climate variability. Hydrol. Earth Syst. Sci, 15, 3785–3808. https://doi.org/10.5194/hess–15–3785–2011
198. Wakim, F (1981) Introduction of PV power generation to Kuwait," Kuwait Institute for Scientific Research, Kuwait.
199. Waldman, J., S. Sharma, S. Afshari, & B. Fekete (2019) Solar–power replacement as a solution for hydropower foregone in US dam removals. Nat. Sustain 2, 872–878.
200. Yamazaki, D., D. Ikeshima, R. Tawatari, T. Yamaguchi, F. O'Loughlin, J. C. Neal, C. C. Sampson, S. Kanae, and P. D. Bates (2017), A high–accuracy map of global terrain elevations, Geophys. Res. Lett., 44, 5844–5853, doi: 10.1002/2017GL072874.
201. Wanielista, M., R. Kersten and R. Eaglin (1997) Hydrology Water Quantity and Quality Control. John Wiley & Sons. 2nd edition.
202. Ward, G.T (1955) Performance of a Flat–plate Solar Heat Collector. Proceedings of the Institution of Mechanical Engineers, 169, 1091–1112. doi:10.1243/PIME_PROC_1955_169_108_02
203. Watanabe, M., T. Suzuki, R. O'ishi Y. Komuro, S. Watanabe S. Emori T. Takemura M. Chikira, T. Ogura, M. Sekiguchi, K. Takata, D. Yamazaki, T. Yokohata, T. Nozawa, H. Hasumi H. Tatebe, and M. Kimoto (2010) Improved climate simulation by MIROC5: mean states, variability, and climate sensitivity. J Clim, 23, 6312– 6335. Doi: 10.1175/2010JCLI3679.1
204. Wiginton, L. K., H. T. Nguyen & J. M. Pearce (2010) Quantifying rooftop solar photovoltaic potential for regional renewable energy policy. Computers Environment and Urban Systems, 34, 345–357. https://doi.org/10.1016/j.compenvurbsys.2010.01.001
205. World Economic Forum (2019) The Global Risks Report 2019 14th Edition Insight Report. Available online: http://wef.ch/risks2019
206. World Economic Forum (2015) Global Risks 2015 10th Edition Insight Report. Available online: www.weforum.org
207. World Water Assessment Programme (2009) The UN World Water Development Report 3: Water in a Changing World. UNESCO, Paris, France, Earthscan, London, UK.
208. Worldwatch Institute, Washington, DC, 2005, Renewables 2005—Global Status Report, found at: http://www.worldwatch.org/press/news/2005/ 11/06/Journal of Cleaner Production, 161, 1171–1179.

209. Zhou, Q., N. Hanasaki & S. Fujimori (2018) Economic Consequences of Cooling Water Insufficiency in the Thermal Power Sector under Climate Change Scenarios. Energies, 11, 2686.
210. Zouine M, M. Akhsassi, N. Erraissi, N. Aarich, A. Bennouna and M. Raoufi (2018) Mathematical Models Calculating PV Module Temperature Using Weather Data: Experimental Study. Proc. 1st Int. Conf. Electron. Eng. Renew. Energy, 2018, 630–9. doi:10.1007/978–981–13–1405–6